Version 1.0
October 2004

HST Two-Gyro Handbook

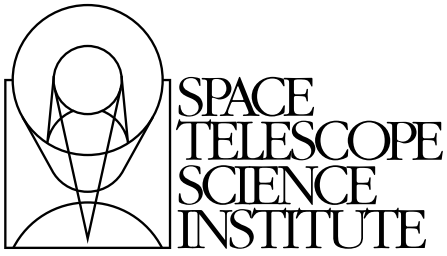

Space Telescope Science Institute
3700 San Martin Drive
Baltimore, Maryland 21218
help@stsci.edu

Operated by the Association of Universities for Research in Astronomy, Inc., for the National Aeronautics and Space Administration

User Support

For prompt answers to any question, please contact the Science and Instrument Support Department Help Desk.

- **E-mail:** help@stsci.edu
- **Phone:** (410) 338-1082
  (800) 544-8125 (U.S., toll free)

World Wide Web

Information and other resources are available on the STScI World Wide Web site:

- **URL:** http://www.stsci.edu/hst

Revision History

Version	Date	Editors
1.0	October 2004	Sembach, K.R., et al.

Citation

In publications, refer to this document as:
Sembach, K. R., et al. 2004, "HST Two-Gyro Handbook", Version 1.0, (Baltimore: STScI)

Send comments or corrections to:
Space Telescope Science Institute
3700 San Martin Drive
Baltimore, Maryland 21218
E-mail:help@stsci.edu

HST may be forced to switch from three-gyro to two-gyro mode operations during the course of Cycle 14. This will impact both scheduling efficiency and scientific performance. A number of changes have been instituted in both the proposal format and the review process to take this eventuality into account. HST web pages and documents, such as the Call for Proposals, the HST Primer, and the Instrument Handbooks, use the symbol at the left to indicate that the material contained therein may be affected by two-gyro operations. Readers should consult the Two-Gyro Handbook (this document) or the HST Two-Gyro Science Web Page for information about two-gyro mode operations.

Acknowledgments

The information in this Handbook is a brief summary of the experience gained by many individuals working on the HST two-gyro mode development at STScI and elsewhere. Some of the material contained herein is based upon documentation and information available at the HST Two-Gyro Phase I Design Review (February 2004) and Critical Design Review (July 2004). The material related to guiding performance and pointing jitter (Chapter 5) is an early synopsis of initial analyses of HST pointing control simulations performed by the HST Pointing and Control Systems group at Lockheed Martin Technical Operations Company. We thank all of the individuals and groups involved in these design reviews and simulations for their efforts. We especially thank Brian Clapp for his efforts in leading the simulation efforts.

The following people at STScI contributed to the written or graphical content of this handbook:

John Biretta, Tom Brown, George Chapman, Colin Cox,
Ron Downes, Rodger Doxsey, Mark Giuliano, Sangeeta Malhotra,
Ed Nelan, Merle Reinhart, Ken Sembach, Allison Vick

We thank Susan Rose and Jim Younger for their assistance with the hardcopy and web-based production of the Handbook. We also thank Stefano Casertano and Diane Karakla for helpful comments.

Table of Contents

PART I:

Introduction

The chapters in this part of the Handbook explain how to use this Handbook, where to go for help, special considerations for Cycle 14, and background information on the HST gyroscopes.

CHAPTER 1:

Introduction

In this chapter. . .

As the Hubble Space Telescope enters its fourteenth observing cycle, there is a possibility that only two gyroscopes may be available for observatory attitude control sometime during the cycle. HST operations and scheduling of observing programs depend upon the number of functioning gyros. The exact time when the reduction from three to two functioning gyros will happen is unknown, so preparations are being made to ensure that HST remains productive when this changeover occurs. This Handbook summarizes the important information necessary to understand the differences between operating HST with three gyros and two gyros, as well as the considerations necessary for planning observing programs that can be implemented if only two gyros are functioning.

1.1 Purpose

The *HST Two-Gyro Handbook* is the primary reference for issues related to HST observations conducted with an attitude control system having just two functional gyroscopes. The Handbook, which is maintained by scientists at STScI, serves the following purposes:

- It provides background information on the HST gyroscopes and their use.
- It provides technical information about the expected performance of the HST attitude control system in two-gyro mode.
- It provides a description of scheduling constraints and orbital visibility periods relevant for HST operations with only two gyroscopes.
- It describes the available scheduling/visibility tools and information required for the preparation of Cycle 14 Phase I proposals.
- It provides instrument-specific information for the preparation of Cycle 14 Phase I proposals, which is not presently contained in the individual Instrument Handbooks or the *HST Primer.*

1.1.1 Document Conventions

This document follows the usual STScI convention in which terms, words, and phrases that are to be entered by the user in a literal way into an HST proposal are shown in typewriter font (e.g., `ORIENT`, `ACS/HRC F814W`). Names of software packages, tasks, or commands are given in bold type (e.g., **calstis, TinyTIM, MultiDrizzle**).

1.1.2 Examples Used in this Handbook

To introduce observers to the scheduling and visibility tools available for Cycle 14, we have prepared several examples to illustrate the types of considerations necessary when planning constrained observations. The examples contained in Part II of this Handbook are:

1. Example 1: Time-series observations of the Hubble Deep Field and Hubble Ultra Deep Field.
2. Example 2: Time-series light curve observations of a supernova found in Example 1.
3. Example 3: Time-constrained observations of recurrent nova T Pyx.
4. Example 4: An orientation-constrained observation of the Vela supernova remnant.

Additional examples relating to science instrument performance can be found in the individual chapters in Part III of this Handbook.

1.2 Handbook Layout

The chapters of this Handbook are as follows:

- Part I - Introduction
  - Chapter 1 - *Introduction*.
  - Chapter 2 - *Special Considerations for Cycle 14*, includes information about the probability of entering two-gyro mode in Cycle 14, points to updates to the Phase I proposal process, and provides a list of the type of observing programs and observations that may be affected when HST enters two-gyro mode.
  - Chapter 3 - *The HST Gyroscopes*, includes some brief background information about the gyroscopes aboard HST.
- Part II - Two-Gyro Information for Observers
  - Chapter 4 - *Slewing and Pointing*, includes information about how HST will slew and point in two gyro mode, the differences between two- and three-gyro modes, and the pointing constraints imposed for both modes.
  - Chapter 5 - *Guiding and Jitter*, contains a description of how guiding is performed in two-gyro mode and the properties of the jitter expected while guiding.
  - Chapter 6 - *Observation Planning*, describes the scheduling and visibility constraints observers will encounter when HST enters two-gyro mode, provides examples of how two-gyro mode impacts observing programs, and discusses the types of scheduling information that observers will need to fill out their Cycle 14 Phase I proposals.
- Part III - Science Instrument Performance
  - Chapter 7 - *ACS Performance in Two-Gyro Mode*, contains information about how the Advanced Camera for Surveys will perform while guiding in two-gyro mode.
  - Chapter 8 - *WFPC2 Performance in Two-Gyro Mode*, contains information about how the Wide Field and Planetary Camera 2 will perform while guiding in two-gyro mode.
  - Chapter 9 - *NICMOS Performance in Two-Gyro Mode*, contains information about how the Near Infrared Camera and Multi-Object Spectrograph will perform while guiding in two-gyro mode.
  - Chapter 10 - *STIS Performance in Two-Gyro Mode*, contains information about how the Space Telescope Imaging Spectrograph will perform while guiding in two-gyro mode.

- Chapter 11 - *FGS Performance in Two-Gyro Mode*, contains information about how the Fine Guidance Sensors will perform while guiding in two-gyro mode.

• Part IV - Reference Material

- Appendix A - *Guide Star Magnitudes,* contains reference information about the brightness of guide stars used by HST since January 2000.
- Appendix B- *Quiescent F2G-FL Jitter Predictions,* contains reference information concerning the pointing jitter due to rate gyro noise and Fine Guidance Sensor photomultiplier tube noise.

1.3 Preparing Observing Proposals for Cycle 14

Use the *HST Two Gyro Handbook* together with the appropriate Instrument Handbooks and the *Hubble Space Telescope Call for Proposals for Cycle 14 (*CP) when assembling your Cycle 14 Phase I proposal. The CP provides policy and instructions for proposing; the individual Instrument Handbooks contain detailed technical information about the science instruments assuming three-gyro operations; and this handbook provides information necessary to assess the feasibility of observations and to calculate your Phase I observing time requests for two-gyro operations during Cycle 14. In addition, the *HST Primer* provides a basic introduction to the technical aspects of HST and its instruments, and explains how to calculate the appropriate number of orbits in three-gyro mode.

If your Phase I proposal is accepted, you will be asked to submit a Phase II proposal in which you specify the exact configurations, exposure times, and sequences of observations that should be performed. To assemble your Phase II proposal, you should use the appropriate Instrument Handbook(s) in conjunction with the *HST Two Gyro Handbook* and the *Phase II Proposal Instructions*. The *Phase II Proposal Instructions* describe the exact rules and syntax that apply to the planning and scheduling of observations in both two-gyro and three-gyro modes.

1.4 The Help Desk at STScI

STScI maintains a Help Desk that quickly provides answers to questions on any HST-related topic, including questions regarding two-gyro operations and the proposal process. The Help Desk staff have access to all of the resources available at the Institute, and they maintain a database of answers so that frequently asked questions can be immediately answered.

The Help Desk staff also provide STScI documentation, in either hardcopy or electronic form, including *Instrument Science Reports* and *Instrument Handbooks*. Questions sent to the Help Desk are answered within two working days. Usually, the Help Desk staff will reply with the answer to a question, but occasionally they will need more time to investigate the answer. In these cases, they will reply with an estimate of the time needed to reply with the full answer.

We ask that you please send *all* initial inquiries to the Help Desk. If your question requires an Instrument Scientist to answer it, the Help Desk staff will put one in contact with you. By sending your request to the Help Desk, you are guaranteed that someone will provide a response in a timely manner.

To contact the Help Desk at STScI:

- **Send E-mail:** help@stsci.edu
- **Phone:** 1-410-338-1082
  Toll-free in the U.S.: 1-800-544-8125

The Space Telescope European Coordinating Facility (ST-ECF) also maintains a Help Desk. European users should generally contact the ST-ECF for help; all other users should contact STScI. To contact the ST-ECF Help Desk:

- **Send E-mail:** stdesk@eso.org

1.5 Two-Gyro Resources at STScI

STScI has assembled a team of scientists, engineers, and computer programmers who are supporting the development, implementation, and on-orbit testing of two-gyro mode. This team is responsible for ensuring that HST remains highly productive after entering two-gyro mode. A key component of this work is to provide information to the astronomical community for the preparation of observing proposals that can be executed when HST enters two-gyro mode. This Handbook has been written in parallel with the development and testing of two-gyro mode. As a result, it contains our current expectations about how this mode will work. Any changes will be communicated via the Two-Gyro Science web site.

1.6 The STScI Two-Gyro Web Site

Information for the planning and scheduling of HST observations with two functioning gyros can be found on the HST Two-Gyro Science (TGS) web page at the following URL:

http://www.stsci.edu/hst/HST_overview/TwoGyroMode

This web page includes information that falls into the following categories:

- **What's New?:** This is where new and important information will be posted.
- **Target Visibility and Orientation Tools:** These tools should be used by observers when they prepare their Cycle 14 Phase I proposals. The tools provide information that observers will need to describe the impact of two-gyro mode on their observing plan.
- **Verification of Scheduling Constraints:** The information in this section tells observers how to use APT to verify that they have correctly characterized the scheduling constraints for the observations in their Phase I proposals.
- **Sky Availability Movie:** This narrated movie described the differences in sky availability between two-gyro and three-gyro modes.
- **Two-Gyro Science Overview:** The information in the navigational bar of the page includes an overview of two-gyro mode, scheduling and science implications, and useful links to related pages.

Proposers are strongly encouraged to check this web site frequently. Relevant information will be revised and updated throughout the Cycle 14 Phase I proposal submission period. The final web site updates will be made on 15 December 2005, or as specified in Section 14.2 of the *Call for Proposals*. Other information, not specific to two-gyro operations, can generally be accessed through the top-level STScI web page:

http://www.stsci.edu/.

CHAPTER 2:

Special Considerations for Cycle 14

In this chapter. . .

HST may be forced to switch from three-gyro to two-gyro mode operations during the course of Cycle 14. This will impact both scheduling flexibility and scientific performance. A number of changes have been instituted in both the Phase I proposal format and the review process to take this eventuality into account. This chapter highlights some of the changes to the Phase I proposal and the types of observations that may be affected if HST enters two-gyro mode in Cycle 14.

2.1 Probability of Entering Two-Gyro Mode

Expectations for when HST might enter two-gyro mode are somewhat uncertain because of the limited amount of lifetime data available for the types of mechanical gyros HST uses. A model has been developed that includes random gyro failures as well as a gyroscope wear-out function. The coefficients in this model are poorly known due to small number statistics. There have been some changes made in the assembly procedures for the gyros which should improve their lifetime, although no statistics are available for these units. The model based on HST flight experience predicts that two-gyro mode will be entered in spring of 2006, partway through Cycle 14. A brief summary of the predicted failure probabilities is given in Table 2.1, assuming a baseline set of dates on which the four currently functioning gyros are still operational. The probabilities in this table should be considered estimates only, as past performance does not necessarily translate into future survival.

Table 2.1: Probabilities for HST Gyro Failure

Reference Date on which the 4 Gyros Currently Operating are Still Functional	50% Probability Date[1]		Probability at End of Cycle 14 [1]	
	Drop to < 4 Gyros	Drop to < 3 Gyros	4 Gyros	3 Gyros
01-May-2004	Feb 2005	Mar 2006	4%	36%
01-Oct-2004	May 2005	May 2006	6%	42%
01-Mar-2005	Sep 2005	Jul 2006	9%	50%

1. Probabilities are based on a model of the gyro failure, including data for all pre-SM3A gyros and post-SM3A gyros as of 01-Aug-2001. Cycle 14 runs from 01-Jul-2005 to 30-Jun-2006.

2.2 Cycle 14 Phase I

The Cycle 14 *Call for Proposals* (*CP*) describes the policies and decision making processes applicable to two-gyro operations in Cycle 14. Observers should refer to that document for information about the types of input to be requested from observers and how that input will be used in the proposal process. We outline here some of the changes in the Phase I proposal process that are directly relevant to two-gyro mode. The changes include:

1. *Increased page allocations* to describe how GO and snapshot observing programs are affected by two-gyro operations (see *CP*, Sections 7.1.3 and 9.3). Proposers need to address the specific issues called

out in the *CP*. The description should include, among other things, answers to questions such as:

- What is the impact of two-gyro mode operations on the scientific goals of the proposal?
- How would the proposal be modified to accommodate two-gyro observations?

2. S*pecification of the number of primary and parallel orbits for two-gyro mode*, which must now be entered on the Phase I form for GO proposals (see *CP*, Section 8.6.2). The number of orbits entered for two-gyro mode may differ from the value entered for three-gyro mode. If the proposal is a snapshot proposal, the number of targets entered will apply to both three-gyro and two-gyro situations.
3. *Specification of orientation and timing special requirements* for each observing block (see *CP*, Section 8.15.12). This information is necessary for all constrained two-gyro observations since orientation and timing constraints may strongly affect the schedulability of the observations. The information must be supplied in two places:
   - In the "Two-Gyro Mode Observations" text section contained in the PDF attachment portion of the Phase I proposal (see *CP*, Section 9.3).
   - In the two-gyro mode keywords in the "Observation Summary" section of the APT form (see *CP*, Section 8.15.12). All scheduling keywords must be specified for two-gyro mode if applicable, regardless of proposal size. In past cycles, scheduling keywords were required only for large programs requesting ≥100 orbits in three-gyro mode.

2.2.1 Assessment of Proposals and Two-Gyro Information

The *Call for Proposals* describes the proposal selection procedures to be used by the time allocation committees. Section 6.2 of the *CP* contains specific information about how two-gyro considerations will be used in the proposal rankings. Section 6.3 of the *CP* outlines the selection criteria relevant for all proposals.

2.3 Phase II Submissions

Successful GO and SNAP proposers must submit a Phase II program that provides complete details of the proposed observations. Information related to the preparation of Phase II two-gyro programs will be provided to successful proposers when they receive their award notification.

2.4 Types of Observations That May Be Affected

Observers should be aware that observations with either orientation or timing constraints may prove difficult to implement if HST enters two-gyro mode because of the additional pointing restrictions necessary for attitude control and observatory safety. Roughly half the sky is visible at any point in time in two-gyro mode, compared to >90% of the sky in three-gyro mode. Descriptions of how one checks the schedulability of a target and its orbital visibility can be found in Section 6.2 of this Handbook.

Whenever possible, observers should try to minimize the number of special requirements placed on their observations. This will result in improved schedulability and long range planning, greater flexibility in the three-gyro to two-gyro transition, and more efficient use of observing time. Descriptions and examples of how orientation and timing constraints can affect the scheduling of an object and its orbital visibility period can be found in Chapter 6 of this Handbook. Proposers are strongly encouraged to check the Two-Gyro Science web page for additional information throughout the proposal process.

The following types of observing programs and observations may be affected by scheduling or visibility constraints when HST enters two-gyro mode.

- Any observation with either an orientation or timing constraint. The following types of programs may be particularly difficult to schedule if they contain a large number of constraints:
  - Large GO programs (*CP*, Section 3.2.2).
  - Long-term GO programs (*CP*, Section 3.2.3).
  - Treasury GO programs (*CP*, Section 3.2.4).

- Time critical observations (*CP*, Section 4.1.5), particularly if a time-series must be obtained or if the time interval in which a TOO (*CP*, Section 4.1.2) must be observed is small.
- Coordinated observations (*CP*, Section 9.5), particularly if the coordination with another observatory involves timing constraints.
- Coordinated parallel observations (*CP*, Section 4.2) using instrument modes for which the orientation must be specified.
- Continuous viewing zone observations (*CP*, Section 4.1.1), which will still be available in two-gyro mode but may be more difficult to schedule.
- Solar System observations (*CP*, Section 4.1.3). Fast-moving objects, such as comets, requiring gyro-only pointing or single FGS guiding cannot be scheduled in two-gyro mode.

CHAPTER 3:

The HST Gyroscopes

In this Chapter...

3.1 Gyroscope Overview[1]

HST has six rate-sensing gyroscopes. Under normal operating procedures, three of the six gyros must be functioning to provide sufficiently accurate pointing to achieve guide star acquisitions and science data collection. The gyroscopes aboard HST sense whenever the attitude of the observatory is changing, whether during large angle slews from one target to another or during small pointing changes as a result of subtle forces acting upon the observatory. Each gyroscope senses the motion about a single axis. The relative orientations of the gyro axes within HST are different so that the torques exerted on the gyroscopes by attitude changes affect each gyro differently. As a result, any combination of three gyros can be used to define a set of three orthogonal axes around which changes in the roll, pitch, and yaw of the observatory may be measured.

There are many different types of gyroscopes available, but only gas bearing gyros are capable of providing the combination of extremely low noise, excellent stability, and high sensitivity to motions that is required for HST observations. Each gyro has a wheel spinning at a constant rate of 19,200 rotations per minute on gas bearings. The wheel is mounted in a sealed cylinder, which floats in a thick fluid. Electricity is carried to the motor that spins this wheel by thin wires, or flex leads, approximately the width of a human hair. The wires are immersed in the fluid along with the

1. Some of the information in this chapter was reproduced from the *Hubble Space Telescope Gyroscopes Hubble Facts sheet* available from the GSFC HST Program Office.

wheel. Changes in the gyroscope rates induced by movement of HST are captured by onboard electronics. This information is then fed to Hubble's central computer where it is analyzed. The HST pointing is changed through the use of several reaction wheel assemblies. Each assembly contains spinning wheels, which when spun at varying rates, create the appropriate torques required for the desired movement.

The gyroscopes are packaged in pairs, in devices called rate sensing units (RSUs). Each RSU weighs approximately 24.3 pounds and is 12.8 x 10.5 x 8.9 inches in size. The individual gyroscopes weigh approximately 6 pounds and are 2.75 x 6.5 inches in size. Figure 3.1 shows an exploded view of one of the HST gyroscopes. Figure 3.2 shows a gyro after assembly.

Figure 3.1: Exploded View of a Gas Bearing Gyroscope

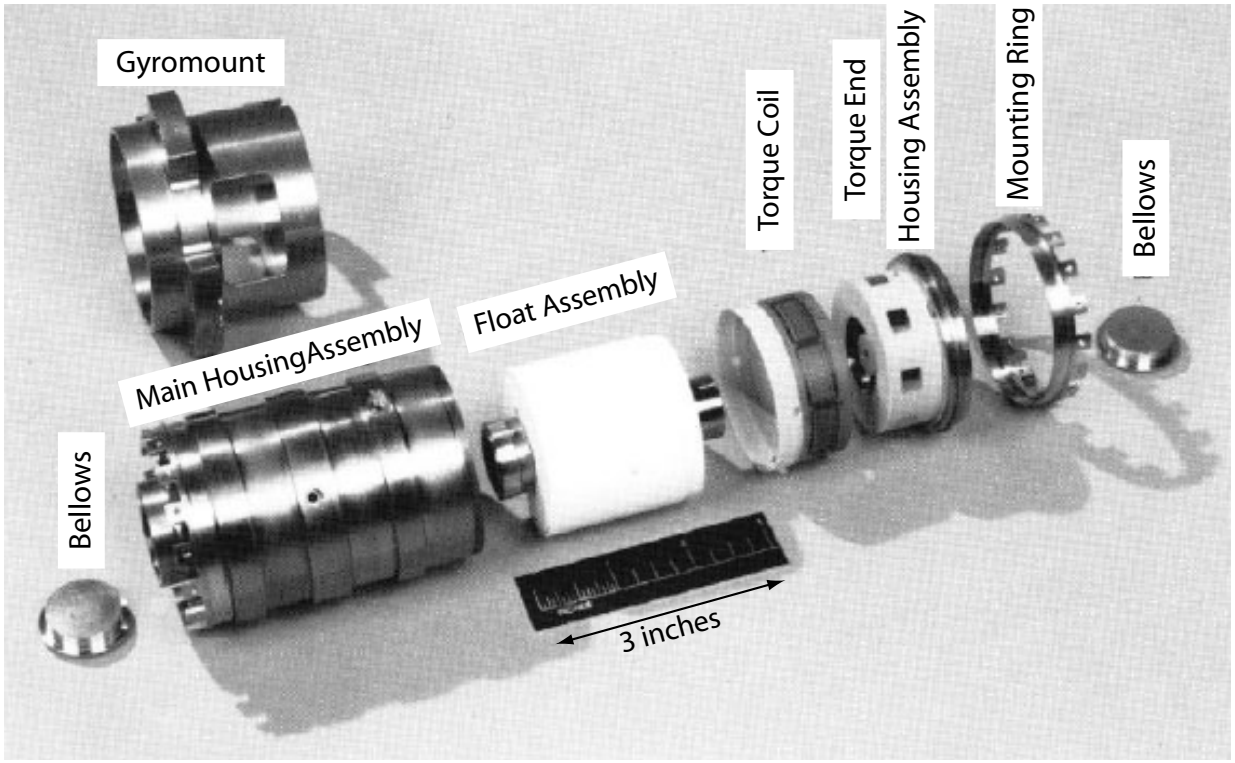

Figure 3.2: Assembled Gyroscope

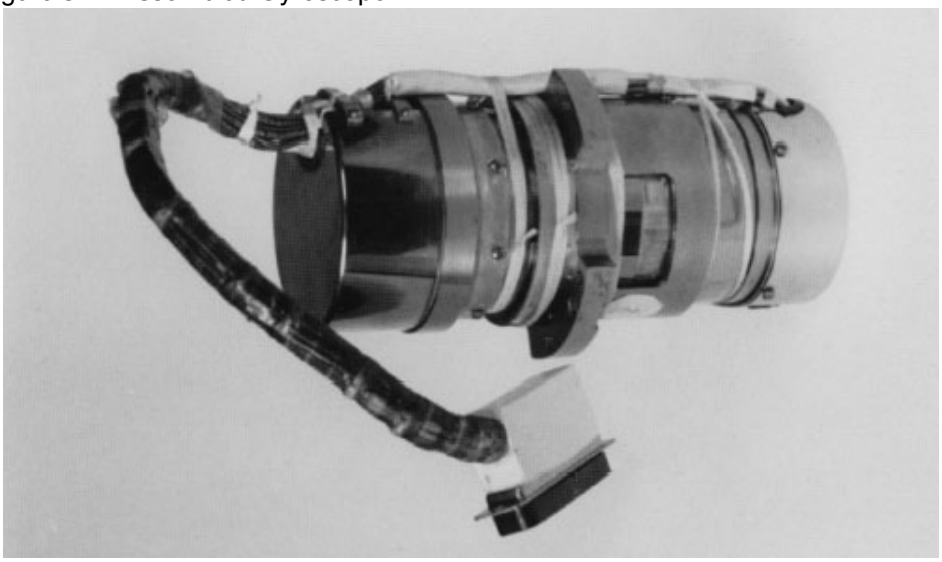

Figure 3.3: Schematic of the Hubble Space Telescope after Servicing Mission 3B

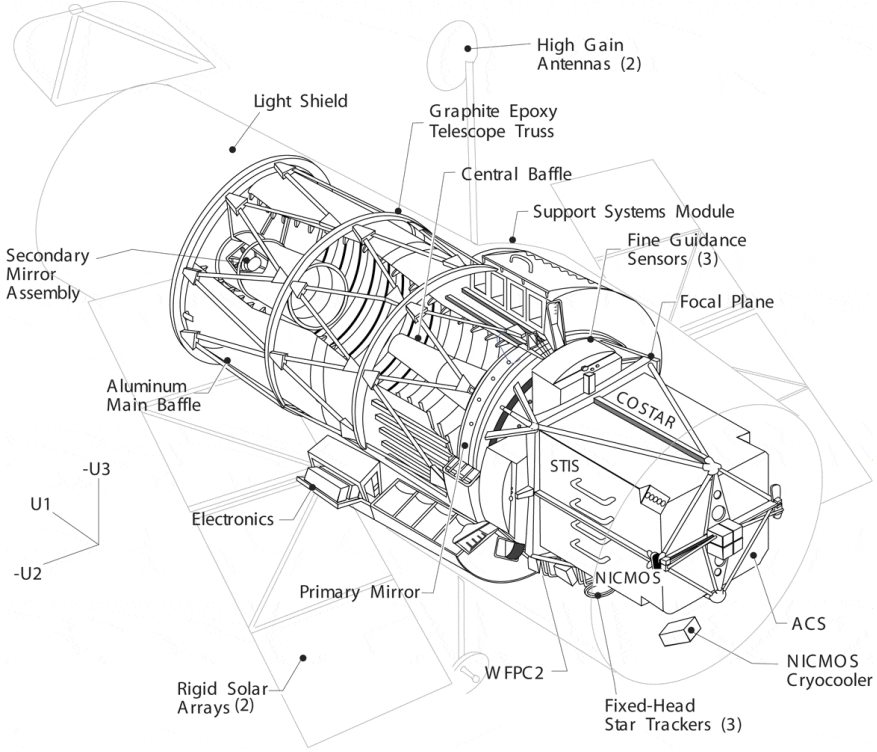

Major components are labelled, and definitions of the **U1**, **-U2**, **-U3 (V1**, **V2**, **V3)** spacecraft axes are indicated.

The HST gyroscopes are attached to the focal plane structure at the aft end of the observatory on the same side as the fixed-head star trackers (FHSTs). Figure 3.3 shows the HST field of view following SM3B in the standard HST coordinate system. The RSUs are accessed by opening the large cargo bay doors on the **U3** side of the observatory.

3.2 Previous Gyroscope Replacements

Four of the six original HST gyroscopes were replaced during the first servicing mission (SM1) in December 1993 by astronauts aboard Space Shuttle flight STS-61. In the years after this servicing mission, the HST gyroscopes failed at a higher-than-expected rate. On 13 November 1999, the fourth of six gyroscopes aboard HST failed, leading to a halt of science observations and entry into safe mode. In anticipation of this event, servicing mission 3, which NASA had been planning for several years, was split into two separate missions: SM3A and SM3B. During SM3A (STS-103, December 1999), astronauts replaced all six gyroscopes (three RSUs) with a full complement of improved gyroscopes.

In the time since SM3A, two of the six gyroscopes have failed. The first gyroscope (Gyro #5) failed on 28 April 2001, and the second (Gyro #3) failed on 29 April 2003. One gyro (Gyro #6) has been turned off to extend its lifetime; it will be switched back on when one of the three gyroscopes currently providing attitude control fails. Gyroscopes #1, #2, and #4 are currently in use.

The gyroscopes aboard HST have failed because of electronics problems, flex lead problems, and rotor restrictions. A manufacturing weakness with a hybrid electrical component prompted the replacement of the gyros on SM1. The flex lead failures that led to the SM3A replacements resulted from corrosion of the thin electrical wires immersed in the fluid inside the gyroscopes. The problem has been addressed in part by using pressurized nitrogen rather than pressurized air containing oxygen during the fluid fill portion of the gyroscope assembly. Some of the gyroscopes that would have been installed during SM4 would also have had silver plated leads to reduce corrosion. The failures occurring in the current on-orbit gyros appear to be due to some sort of rotor restriction. The restrictions may be caused by patches of lubricant that have built up in the air bearings of the gyros or by small particles that have become lodged between the bearing surfaces. The restrictions prevent the bearings from turning smoothly. The HST Project is currently investigating the use of diamond-like coatings on the bearing surfaces to reduce rotor restrictions. This is the same type of coating used in the NICMOS cryocooler turbine.

Clearly, replacing or adding new gyroscopes would be a priority for any future servicing mission designed to prolong the life of HST.

PART II:

Two-Gyro Information for Observers

The chapters in this part of the Handbook describe HST slewing and pointing in two-gyro mode, guiding and jitter in two-gyro mode, and the procedures for assessing the schedulability and visibility periods for astronomical targets to be observed in two-gyro mode.

CHAPTER 4:

Slewing and Pointing

In this chapter . . .

In this Chapter we discuss the slewing and pointing procedures required in two-gyro mode and compare/contrast these with those needed in three-gyro mode.

4.1 Overview

Slewing of HST is much the same in two-gyro mode as in three-gyro mode, with a few important differences. The primary difference between the two modes is the accuracy of the pointing at the ends of slews. In three-gyro mode, the telescope is generally pointed to within 50-100 arcseconds of the target after a 180 degree slew. In two-gyro mode, the pointing error at the end of a slew of any duration can be as large as 10 degrees because the rate change for one axis of control must be supplied by the HST magnetometers rather than by a gyroscope. For this reason, it is necessary to have a different sequence of activities at the ends of slews in two-gyro mode.

The slew rates in two- and three-gyro modes differ slightly. In three-gyro mode, the maximum maneuver rate is ~11 degrees per minute of time with a typical rate of ~6 degrees per minute. In two-gyro mode the maneuver rate is expected to be ~85% of these values. Two-gyro pointing control and constraints are described in the following sections.

4.2 Two-Gyro Coordinate Conventions

To more easily understand the control of the telescope with two gyros, it is convenient to define a reference frame for the gyroscope control directions and the "missing" control axis. Figure 4.1 is an illustration of an orthogonal coordinate system with two gyros (Gyro A and Gyro B). The first axis of the system is defined by the Gyro A measurement axis. The second axis is defined by the cross product of the two measurement axes of Gyro A and Gyro B. This axis is called the G_X axis. The semi-major axis of the jitter ellipse is the direction associated with rotations about the G_x axis. Information for the G_X axis must be supplied by one of the HST pointing control system sensors other than the two functioning gyros, such as the Fine Guidance Sensors. The third axis is defined by the cross product of the second (G_X) and first (G_A) axes. This axis lies in the gyro plane in a direction that is 90° from the G_A axis.

Figure 4.1: Orthogonal Two-Gyro Coordinate System

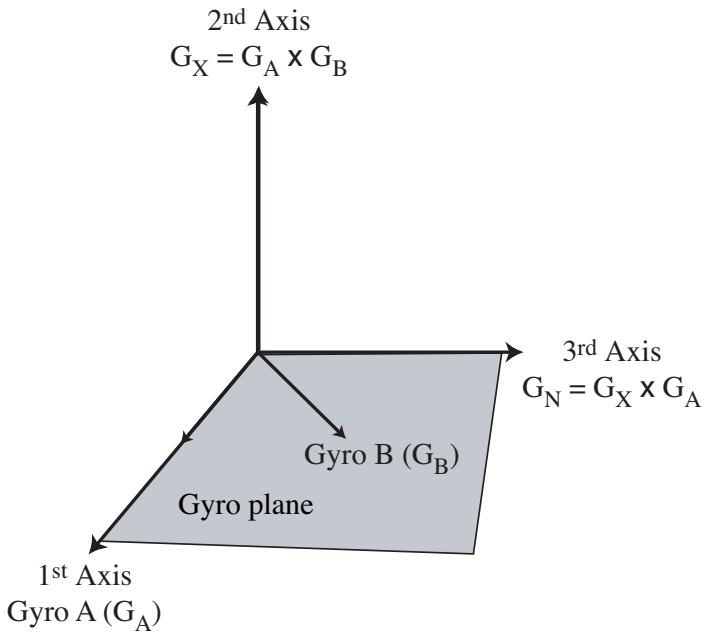

4.3 Pointing Control with Two Gyros

A major rework of the HST attitude control software was necessary to prepare HST for two-gyro operations. This extensive redesign was done by engineers and software experts at the Goddard Space Flight Center. The various control modes described below are part of the updated onboard attitude control system and are invoked automatically when needed.

4.3.1 Magnetic Sensing System and Two Gyros (M2G)

The M2G mode uses two gyros in combination with information about the Earth's magnetic field orientation to provide pointing control. The Magnetic Sensing System (MSS) on HST consists of two magnetometers. The magnetometers measure the strength and direction of the Earth's magnetic field. Together with a model for the magnetic field, they can be used to supply pointing control information for the G_X axis. The typical pointing accuracy in M2G mode is 2-5 degrees but can be as poor as ~10 degrees when the G_X axis is aligned with the Earth's magnetic field. This mode is used during large-angle slews and FHST and FGS occultations. It may also be entered when onboard attitude determinations (OBADs) fail, as guide star acquisitions will not be attempted.

Attitude is estimated in M2G mode through a combination of rates provided by the two gyros and the attitude derived from the cross product of the magnetic field model and the magnetic field measured by the MSS. The time derivative of the magnetic field is measured in the vehicle reference frame by the MSS. The data for this changing B-field is filtered heavily to avoid spurious results. It is then compared to the expected value of the B-field derivative calculated from the magnetic field model. This comparison allows the error about B to be calculated if the alignment of the Earth's magnetic field and HST are favorable.

M2G mode has the following sub-modes:

1. *Attitude Hold Mode*: This mode is used when gyro plane errors are expected to be small (e.g., after two successful onboard attitude determinations). The G_X axis is controlled by the MSS, while the gyro plane is controlled with the gyro rate information. This mode can be entered from the T2G mode after a successful OBAD.

2. *Maneuver Mode*: This mode is used to perform large-angle vehicle maneuvers. The G_X axis is controlled by the MSS, while the gyro plane is controlled with the gyro rate information in conjunction with additional information from the MSS. This mode can be entered only from the M2G attitude hold or M2G coarse attitude hold modes.

3. *Coarse Attitude Hold Mode*: This mode is used when significant gyro plane errors are expected (e.g., after an onboard attitude determina-

tion failure). The G_X axis is controlled by the MSS, while the gyro plane is controlled with the gyro rate information in conjunction with additional information from the MSS. This mode can be entered from the M2G maneuver mode or from the T2G mode after an unsuccessful OBAD.

4.3.2 Fixed-Head Star Trackers and Two Gyros (T2G)

The T2G mode uses two gyros in combination with one or more of the fixed-head star trackers (FHSTs) to provide pointing control necessary to perform attitude determinations and to reduce the pointing uncertainty to less than 1 arcminute. HST has three FHSTs that are located at the aft end of the observatory. They are attached to the focal plane structure close to the gyroscopes. One FHST points along the **-V3** axis (see Figure 5.2). The other two are tipped backwards and tilted relative to the **-V1** direction, pointing toward the rear of the observatory. The FHSTs have 8 x 8 degree fields of view and are sensitive to stars brighter than $m_V \sim 6$, with a typical centroiding accuracy of 10-15 arcseconds. The use of FHST information is required throughout the T2G mode.

Upon entering T2G mode from M2G mode, an FHST is used to lock onto the position of any star, and this information is fed into the control law to damp the vehicle rates about the G_X axis. After the rates have damped and while the FHST remains locked onto the star, a second FHST can be used to collect information about the star positions in its field of view. The star maps are compared to an onboard star catalog to determine the attitude of the observatory. This onboard attitude determination may be followed by a maneuver to correct the pointing, and a second OBAD is performed to ensure that the pointing has been refined sufficiently.

The rate damping in T2G mode following an M2G mode sequence is expected to take less than ~120 seconds. The attitude error following small (≈0.5 degree) maneuvers is expected to be ≤15 arcseconds. The attitude error following an extended period of attitude hold is expected to be ≤30 arcseconds.

T2G mode has three sub-modes:

1. *Rate Damping Mode*: This mode uses information from the FHSTs to damp the rates and to provide pointing stability in the G_X axis. It is the entry point into T2G mode from M2G mode. It is also the only mode that can be entered from zero gyro sunpoint (ZGSP) safemode.
2. *Attitude Hold Mode*: This mode determines and holds the observatory attitude after the rates have been damped. One or more OBADs with the FHSTs may occur while in this mode. It is the sole entry point into the F2G mode. It can be entered from the T2G rate damping mode or from the F2G mode. It can also be re-entered from the T2G maneuver mode after a vehicle maneuver.

3. *Maneuver Mode*: This mode is used to perform the maneuvers required for attitude corrections following an OBAD in the T2G attitude hold mode. After the maneuver, control is returned to the T2G attitude hold mode.

4.3.3 Fine Guidance Sensors and Two Gyros (F2G)

The F2G mode uses information from the HST Fine Guidance Sensors (FGSs) in combination with two gyros to provide the fine pointing control required for guide star acquisitions and science observations. Just before entering F2G mode, an FGS is used to find and track a star. Upon entering F2G mode, the FGS is used in coarse track mode to control the attitude along the G_X axis and dampen the rates remaining from the T2G activities. A second FGS then searches for a guide star, enters coarse track mode, and proceeds to fine lock. Once in fine lock, it provides information for the G_X axis. After the jitter is low enough, the first FGS transitions into fine lock and reduces the jitter even further so that the guide star acquisition and science observations can be performed.

The F2G mode has two sub-modes:

1. *F2G-CT*: This is the F2G coarse track mode. This mode is used to damp the gyro rates remaining from T2G mode in preparation for entry into F2G fine lock mode.
2. *F2G-FL*: This is the F2G fine lock mode. Science observations are obtained in this mode after the guide star acquisition is completed. The expected jitter in this mode is <30 milli-arcseconds. Control in this mode is performed using the dominant (brighter) guide star.

An abort from either F2G sub-mode results in the attitude control system dropping back into T2G mode. From here, it may be necessary to drop into M2G mode if FHST visibility is insufficient to remain in T2G mode.

4.3.4 A Typical Sequence of Events for an Acquisition

The general sequence of events that must occur for an HST science observation to be made (slew, guide star acquisition, and science observation) are the same in three-gyro mode and two-gyro mode, but the implementation of these events is considerably different. Figure 4.2 depicts these events in graphical form. The sequence for both modes begins with a slew to the target.

In three-gyro mode, a short FHST update may sometimes be required between the end of the slew and the start of the guide star acquisition process. This update can use any FHST and can occur at any point before the acquisition. When the FGSs come out of occultation, the guide star

acquisition occurs and is followed immediately by the science observation(s), which may include a target acquisition. The science observation can continue until the target is occulted. During occultation, the telescope pointing drifts by less than ~5 arcseconds. On subsequent orbits, a guide star re-acquisition occurs and is followed by another science observation.

In two-gyro mode, the slew is performed in M2G mode under the control of two gyros and the MSS. T2G mode is entered when an FHST becomes available, and the resulting M2G gyro rates are damped while the observatory waits for a second FHST to become available. Once this occurs, the FHSTs are used to locate stars for an onboard attitude determination and to correct the pointing, which may be off by as much as 10 degrees. (OBADs are indicated by the "map" blocks in Figure 4.2.) A second OBAD is required to check the correction, and this information is used to refine the pointing even further. While waiting for the FGSs to become unocculted, the FHSTs are used to stabilize the pointing. When an FGS is available, the guide star acquisition process commences and F2G mode is entered to reduce the pointing uncertainties and jitter even further. The science observation begins at the end of the guide star acquisition. During occultation the control system drops back to M2G mode, and the whole process, from M2G through F2G, must be repeated for the next orbit.

Figure 4.2: Typical Sequence of Events for an Observation

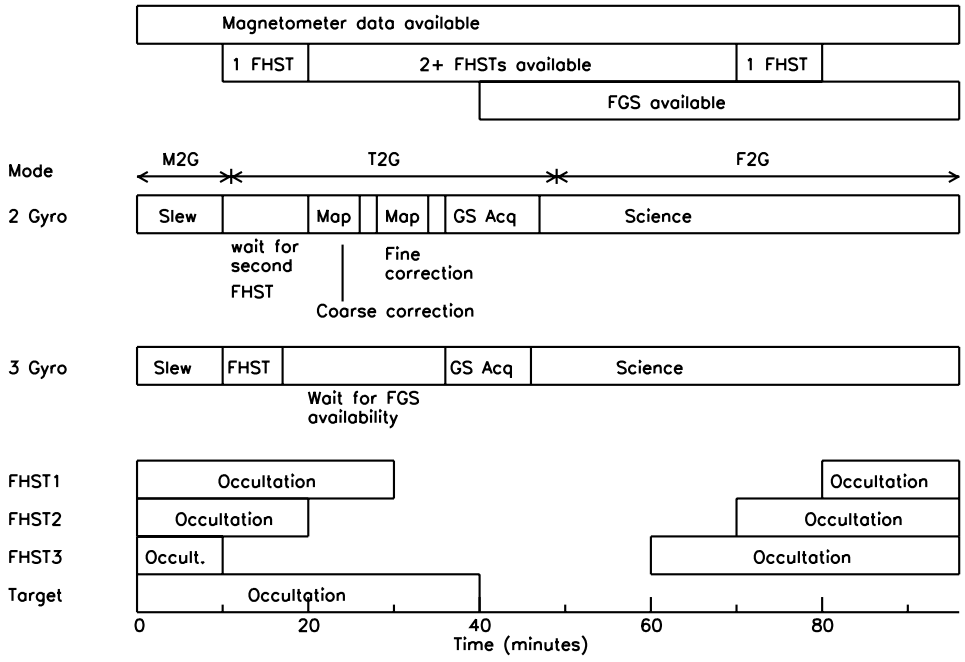

4.3.5 Gyro-only Pointing

Observing without the use of guide stars (gyro-only pointing) is occasionally allowed in three-gyro mode (see Section 3.2.3 of the *HST Primer*). In two-gyro mode, gyro-only pointing will not be allowed for external science observations. It may still be used for external Earth-calibration exposures or internal calibration exposures.

4.4 Pointing Constraints

The need to use a sequence of MSS, FHSTs, and FGS observations to provide attitude control information for the G_X axis in two-gyro mode results in a set of pointing constraints that is more stringent than in three-gyro mode. The pointing uncertainty of as much as 10 degrees in M2G mode requires more stringent Sun-avoidance constraints. The need to have FHST coverage throughout T2G mode also results in reduced scheduling possibilities since multiple FHSTs must be unocculted by the Earth at the appropriate times. This latter constraint is the primary reason for the reduced schedulability of targets in directions ahead of the Sun (see Chapter 6). A summary of pointing constraints in both three-gyro mode and two-gyro mode is provided in Table 4.1.

Table 4.1: Pointing Constraints Summary

Pointing Constraint	Three-Gyro Mode	Two-Gyro Mode
Sun angle range allowed	50˚-180˚	60˚-180˚
Off-nominal roll angle allowed	5˚ for V1-Sun angle 50˚-90˚; increasing to 30˚ at V1-Sun angle = 178˚; unlimited at V1-Sun-angle = 178˚-180˚	5˚ for V1-Sun angle 60˚-115˚; increasing to 20˚ at V1-Sun angle = 179˚; unlimited at V1-Sun-angle = 179˚-180˚
V1 Moon constraint (FGS HV on)	>9.5˚	Same as three-gyro mode
Earth avoidance (FGS guiding, dark limb)	>6˚	Same as three-gyro mode
Earth avoidance (Science obs, dark limb)	>6˚	Same as three-gyro mode
Earth avoidance (FGS guiding, bright limb)	>13.5˚	Same as three-gyro mode
Earth avoidance (Science obs, bright limb)	>20˚	Same as three-gyro mode
SAA avoidance	Instrument dependent	Same as three-gyro mode

CHAPTER 5:

Guiding and Jitter

In this chapter . . .

In this chapter we describe guiding in two-gyro mode and the pointing jitter that is expected while guiding. The jitter expectations are based upon high-fidelity simulations conducted by the HST Pointing Control Systems Group at Lockheed Martin Technical Operations Company. The information in this chapter will be checked against data from on-orbit tests planned in early 2005.

5.1 Guiding

The general procedures for acquiring guide stars in preparation for science observations are outlined in the *Slewing and Pointing* chapter of this Handbook. Here, we concentrate on a few key issues that are relevant for guiding while science observations are taking place.

5.1.1 Guide Star Acquisitions

Guide star acquisitions in two-gyro mode will take slightly longer than those routinely performed in three-gyro mode. The typical two-gyro guide star acquisition time is expected to be approximately 7 minutes, compared to approximately 6 minutes for three-gyros. This slight increase in acquisition time is required to perform the additional procedures necessary to stabilize the HST pointing sufficiently to enter F2G fine lock mode (see Chapter 4).

Unlike three-gyro mode, the pointing errors accumulated during occultations by the Earth in two-gyro mode are expected to be sufficiently large to prevent the types of guide star re-acquisitions that are currently performed in three-gyro mode. Therefore, full guide star acquisitions will be performed every orbit in two-gyro mode.

Single guide star acquisitions have sometimes been necessary when two suitable guide stars could not be acquired by the FGSs. While this type of acquisition is possible in three-gyro mode, single guide star acquisitions will not be allowed in two-gyro mode. If a pair of suitable guide stars cannot be acquired in two-gyro mode during the guide star acquisition, the pointing control system will drop into a coarser pointing mode (see Section 4.2.5).

Table 5.1 summarizes some of the relevant guide star acquisition differences between three-gyro and two-gyro mode.

Table 5.1: Guide Star Acquisitions

Activity	Three-Gyro Mode	Two-Gyro Mode
Guide star acquisition (initial orbit in visit)	~6 min	~7 min
Guide star acquisition (orbits following initial orbit in visit)	~5 min (re-acquisition)	~7 min
Single guide star acquisition	Allowed	Not Allowed
Dual guide star acquisition with only 1 star successfully acquired	Observation proceeds successfully in many cases	Acquisition fails; revert to T2G or M2G mode

5.1.2 Guide Star Magnitudes

Unlike three-gyro mode, pointing performance and maintenance of guide star lock in two-gyro mode are expected to depend on the magnitudes of the guide stars chosen. Figure 5.1 shows a histogram of the magnitudes of all guide stars used by HST from January 2000 through August 2004. The average guide star magnitude in this time period was $m_V = 12.1$, with a median magnitude of $m_V = 12.3$. These estimates include magnitudes for

both dominant and secondary guide stars (when available). Some guide stars were used multiple times. On average, 25% of the guide stars were brighter than $m_V = 11.3$, and 25% were fainter than $m_V = 13.1$. Less than 1% of the guide stars used were fainter than $m_V \geq 14.0$. Appendix A contains additional information about the brightness distribution of the guide stars for each FGS in this time period.

Figure 5.1: HST Guide Star Magnitudes (Jan. 2000 - Aug. 2004)

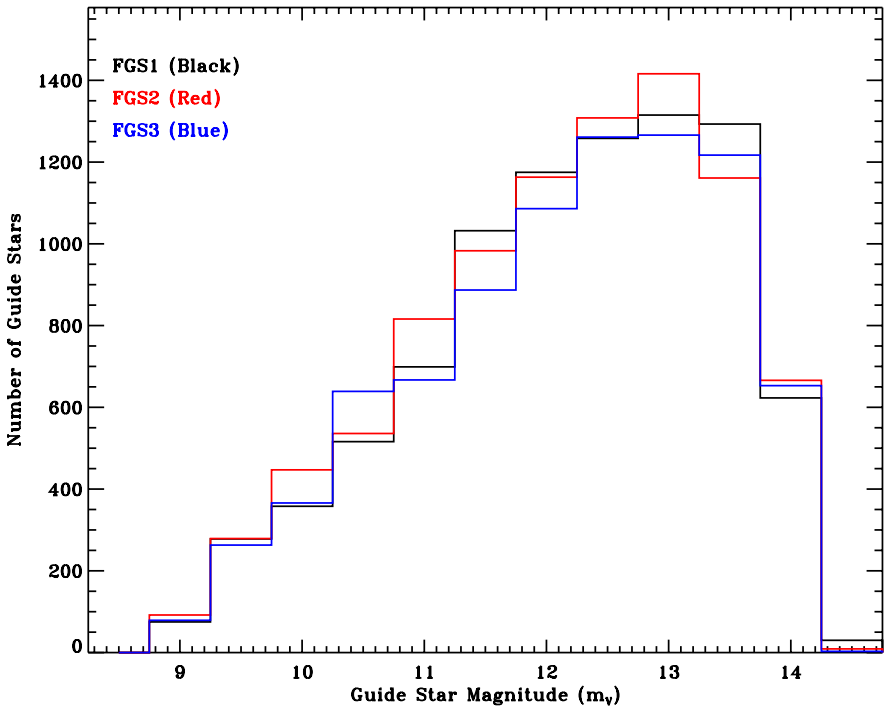

5.1.3 Guiding Performance

The guiding performance in two-gyro mode (F2G-FL) is expected to be degraded slightly compared to three-gyro mode. Initial indications from ground simulations are that the jitter ellipse (see Section 5.2) will be less than 20 mas in size. Several on-orbit tests are planned for February 2005 to quantify the guiding performance more accurately so that updates will be available in time for Cycle 14 Phase II proposal preparations.

An important consideration for faint ($m_V \geq 14.0$) guide stars is the possibility that HST may lose lock under special circumstances. The primary concern is that the FGSs used to guide are also providing pointing information to the attitude control system. Loss of lock is expected to occur only if substantial disturbances occur while guiding on faint stars. The gyro pair available in two-gyro mode will affect the probability of loss of lock since the various types of disturbances change the pointing in preferred directions. Simulations of the jitter caused by different disturbances (see below) and the past history of guide star magnitudes (see Appendix A)

indicate that loss of lock will occur infrequently, and perhaps only if multiple disturbances are present simultaneously. If loss of lock does occur, science data collection will cease, and it may or may not be possible to resume science observations during the impacted visit. Loss of lock results in the pointing control dropping into T2G mode (if FHST visibility is available) or even into M2G mode (if no FHSTs are available at the time of loss of lock).

5.2 Jitter Overview

5.2.1 Jitter Description

The HST gyroscopes are oriented with respect to each other so that three functioning gyroscopes can be used to provide three-axis stability for the telescope. Small high-frequency motions of the observatory caused by noise in the gyros and fine guidance sensors, mechanical vibrations, disturbances in the pointing induced by thermal and mechanical effects, gravity gradients across the observatory, and atmospheric drag introduce small changes in the telescope pointing while it is in fine guiding mode obtaining science data. As a result, the HST pointing is constantly changing over very small angular scales that are set by the pointing control law in the attitude control system.

The magnitude and shape of telescope jitter in the **V2**-**V3** plane[1] is expected to be different in two-gyro mode than it currently is in three-gyro mode. Typical root-mean-square (RMS) pointing jitter of less than ~5 mas over 60-second intervals is currently achieved in three-gyro mode. For two-gyro mode, we have adopted a 30 mas x 10 mas jitter ellipse for the discussions of the impact on the science instruments in Part III of the Handbook and in the science instrument exposure time calculators available for Cycle 14 Phase I proposal preparations. We provide more information about the sources, frequencies, and magnitude of the jitter predicted by simulations below.

5.2.2 Jitter Orientation

Plotted on the plane of the sky (the **V2-V3** observatory plane) as a function of time, the present three-gyro telescope pointing while guiding

1. The **V1**, **V2**, and **V3** coordinate system is sometimes referred to in other HST documentation as the **U1**, **U2**, **U3** coordinate system, in which **V1** = **U1**, **V2** = **-U2**, and **V3** = **-U3** (see Figure 5.2). The plane of the sky lies in the **V2**-**V3** plane. Observatory roll occurs about the **V1** axis; pitch occurs about the **V2** axis; and yaw occurs about the **V3** axis.

with the fine-guidance sensors is described by a nearly circular distribution of points with a typical RMS pointing jitter of <5 mas. Reducing the number of gyros from three to two results in a loss of gyro information for one axis. With two gyros, the circular jitter distribution becomes an ellipse since there is less precise control in the direction orthogonal to the plane defined by the two functioning gyros. As of the writing of this document, Gyros #1, 2, and 4 are operating, and Gyro #6 is functional but turned off. Table 5.2 lists the angle of the G_X axis on the plane of the sky for each possible pair of remaining gyros. The component of jitter about the G_X axis in each direction is also listed. For reference, Figure 5.2 contains a map of the HST field of view showing the relative positions of the science instruments projected onto the **V2**-**V3** plane.

Table 5.2: Two-Gyro Jitter Ellipse Orientations

Gyro Set	Component of G_X			Angle of G_X Axis on Plane of Sky[1]
	(V1 Direction)	(V2 Direction)	(V3 Direction)	
1 & 2	0.0	1.0	0.0	0.0°
1 & 4	0.5303	-0.7820	-0.3275	-22.7°
1 & 6	-0.5303	-0.7820	0.3275	22.7°
2 & 4	-0.8005	0.3387	-0.4994	55.6°
2 & 6	0.8005	0.3387	0.4994	-55.6°
4 & 6	-0.6678	0.0	-0.7443	90.0°

1. Angle is measured from the **V3** axis counterclockwise in the **V2-V3** (sky) plane (see Figure 5.2).

Figure 5.2: HST Field of View Following SM3B

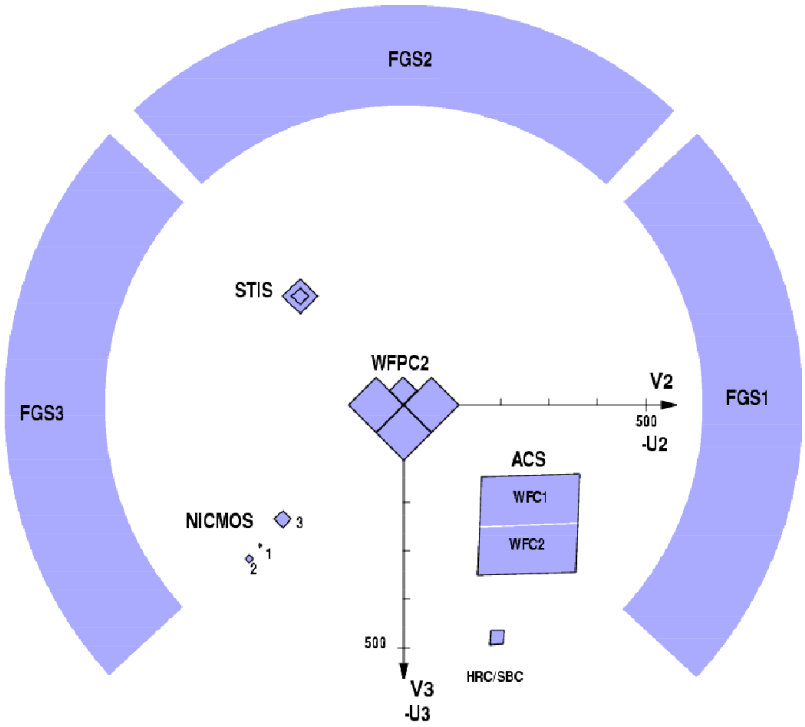

5.2.3 Sources of Jitter

There are numerous sources of jitter in the HST pointing, but many of these sources have little impact on the total jitter budget. The dominant sources include thermal gradients across the solar arrays, high gain antenna (HGA) gimbal articulations, occasional disturbances about the **V2** axis believed to be caused by rotations of the SSM equipment shelf, reaction wheel zero-speed crossings, rate gyro noise, and FGS photomultiplier tube (PMT) noise. Very small contributions (<2 mas) arise from ACS filter wheel motions and SSM thermal gradients.

In two-gyro mode, jitter contributions from the combination of rate gyro noise and FGS PMT noise may be more prominent than the rate gyro noise alone in three-gyro mode. The noise introduced into the attitude control law by the Fine Guidance Sensors used to provide pointing control information about the G_X axis is particularly important when fainter guide stars are used because of reduced signal-to-noise in the FGS measurements. Information about the jitter caused by rate gyro noise and FGS PMT noise can be found in Appendix B.

Approximate values for the jitter introduced by various sources are listed in Table 5.3. These values are expected to be conservative (generous) estimates of the jitter based upon simulations used to predict the response

of HST to disturbances encountered on-orbit. Descriptions of the primary sources of jitter in this table can be found in Section 5.3.

Table 5.3: Sources of Jitter in the Two-Gyro F2G-FL Jitter Budget

Jitter Source		Jitter (mas, 60-sec RMS)	Comment
Solar Array (SA3) Thermal Gradients		8.92	Frequent
V2 Disturbances		4.13	Frequent
High Gain Antenna (HGA) Gimbal Articulations	Low-rate TDRSS tracking	3.35	Usually present
	High-rate slews	8.02	Intermittent
Reaction Wheel Zero-Speed Crossings	Hot attitude	2.50	Frequent
	Cold attitude	6.00	
FGS PMT + Rate Gyro Noise		3.90	Always present
ACS Filter Wheels		<2.0	Minimal contribution
SSM Thermal Gradients		1.59	Minimal contribution

5.2.4 Jitter Frequencies

The HST pointing is most susceptible to disturbances with frequencies between 0.01 and 0.5 Hz, or periods between 100 and 2 seconds. Higher frequency disturbances damp very quickly. Some sources of jitter (aero and gravity torques, for example) have very low frequencies. The FGS and gyros provide pointing information at a rate of 40 Hz. The pointing control law implemented in the F2G-FL mode has a closed-loop post-filtered bandwidth of ~1 Hz for the entire system, including the G_X axis and gyro plane. Therefore, it should be possible to observe and correct for many sources of jitter, even in two-gyro mode.

5.3 Disturbances and Primary Sources of Jitter

There are several types of disturbances that contribute to the jitter expected in two-gyro mode. Below we discuss the most important disturbances listed in Table 5.3.

5.3.1 Solar Array (SA3) Disturbances

Thermal gradients across the third set of HST solar arrays, which were installed during SM3B, lead to several different motions of the solar arrays as they release accumulated stresses. The most important motion is an in-plane bending occurring at a frequency of ~1 Hz. The solar array disturbances occur irregularly; they are not traceable to terminator crossings but are related to the thermal changes caused by the motion of HST around the Earth.

SA3 disturbances last 1-2 seconds and have a variety of amplitudes. Trending of past SA3 events by the HST PCS Group yields the expected frequency of disturbances summarized in Table 5.4. Like the V2 disturbances, the SA3 disturbances are not likely to cause significant data quality degradation unless the event occurs during a short (<10 second) science exposure. Both two-gyro and three-gyro observations are susceptible to these events.

The simulations conducted to date indicate that loss of lock may be an issue in two-gyro mode if SA3 disturbances with amplitudes greater than ~100 mas are encountered. This can be exacerbated if the SA3 disturbance occurs at the same time as disturbances cause by other sources (e.g., high gain antenna gimbal articulations). Loss of lock resulting from SA3 disturbances is most problematic for gyro combination 4-6 (the G_X axis has a significant component in the **V3** direction) and least problematic for gyro combination 1-2 (the G_X axis is purely in the **V2** direction). The probability of losing lock during an SA3 disturbance in two-gyro mode increases as the magnitudes of the guide stars increase. SA3 disturbances with amplitudes greater than ~300 mas will likely cause loss of lock for any gyro pair with guide star magnitudes $m_V > 14$. Even for bright guide stars (e.g., $m_V < 10$), loss of lock may still occur for gyro pairs 2-4, 2-6, and 4-6 if the SA3 disturbance has an amplitude greater than ~270 mas. Such events are relatively rare (~1 every 20 days). Combining the expected sensitivity of the different gyro pairs to loss of lock, past guide star magnitude distributions (see Appendix A), and the SA3 disturbance frequencies in Table 5.4, the HST PCS Group predicts ~1 loss of lock per day in two-gyro mode.

Table 5.4: SA3 Disturbance Frequency

Disturbance (mas)	Events/day
43.4	11
80.1	3.32
117.6	1.62
155.9	0.62
194.6	0.23
232.4	0.1
271.4	0.05
310.5	0.02
348.1	<0.01
384.5	<0.01

5.3.2 V2 Disturbances

V2 disturbances are brief (less than ~ 1 second) impulsive disturbances believed to be caused by the rapid motion of the Support Systems Module (SSM) Equipment Shelf about the **V2** axis. The motion of the shelf appears to be caused by the release of stresses accumulated in the mechanical structure of the shelf over time. The movement of the shelf itself does not correspond to a movement of the telescope, but the shelf motion does induce a subsequent telescope pointing change.

The HST gyros and FHSTs are mounted to the equipment shelf. When the shelf moves, the gyros sense the motion, and the control law reacts to the perceived motion of the telescope by commanding the reaction wheels to correct for the motion. The FGSs, which are guiding on stars, detect this commanded motion and feed information into the attitude control loop to move the boresight to the proper position necessary to return the stars to their original positions. After this corrective motion, the telescope is once again pointed properly, but the equipment shelf remains rotated relative to its position before the V2 disturbance.

V2 disturbances typically occur in groups of ~5 events, with spacings of a few minutes. The peak-to-peak excursions of the disturbances range from ~25 mas to ~200 mas. The most probable events are those with 50-55 mas amplitudes. Table 5.5 lists the number of expected V2 disturbances per day as a function of amplitude. V2 disturbances are more common for large off-nominal roll angles.

Table 5.5: V2 Disturbance Frequency

Disturbance (mas)	Events/day
55	10.0
60	7.6
65	4.2
70	2.6
75	1.7
80	1.3
85	0.98
90	0.76
95	0.63
100	0.49
105	0.36
110	0.25
115	0.17
120	0.12
200	<0.01

HST is susceptible to V2 disturbances in two-gyro mode as well as three-gyro mode. However, the sensitivity to these disturbances in two-gyro mode will depend strongly on which pair of gyros is operating because the disturbances occur only about the **V2** axis. Gyro combination 1-2 has a G_X axis oriented along the **V2** direction. Therefore, the gyros cannot detect a rotation of the equipment shelf about the V2 axis. As a result, no command would be given to induce telescope motion, and no subsequent command would need to be issued to correct the telescope pointing. Other gyro combinations can sense the shelf rotation; combination 4-6 is the most sensitive since the **V2** axis is completely within the gyro plane. In this case, the behavior of the telescope pointing and the resulting jitter induced by the disturbance would be similar to that encountered in three-gyro mode.

Using the past history of V2 disturbance amplitudes measured on-orbit, the simulations predict that V2 disturbances will not cause loss of guide star lock, even for faint guide stars. These disturbances will not significantly affect data quality of long exposures because the disturbance duration is brief. However, V2 disturbances could severely degrade the quality of short (<10 second) exposures if the exposures occur during the brief disturbance intervals; this is rather unlikely in most cases, but

observers should be aware of this possibility. This cautionary note applies for observations in both two-gyro and three-gyro mode.

5.3.3 High Gain Antenna Motions

HST has two high gain antennae (HGA) that are used to provide communications with the Tracking and Data Relay Satellite System (TDRSS). The antennae are used to receive commanding instructions and to return engineering and science data. Each steerable HGA sits at the end of a boom extending along the **V3** axis and is gimbaled to provide tracking capability as HST orbits the Earth. The gimbal articulations required to position the two HST antennae properly for communications with the TDRSS satellites contribute to the HST jitter budget in two-gyro mode. The magnitude of the jitter depends upon the antenna tracking mode.

Low-rate tracking during communication with the TRDSS satellites or during preparations for communication contributes about 3.0-3.5 mas of jitter (RMS value over a 60 second time interval). The jitter induced by this "ephemeris tracking" is caused primarily by translational bending of the booms along the **V1** and **V2** axes. It occurs almost constantly since the antennae are often in this tracking mode.

High-rate tracking can also introduce jitter. There are two general types of high-rate tracking - "hardware splines" and "jitter splines". Hardware splines occur at a tracking rate near the hardware limit of 30 degrees per minute. They occur roughly 25 times per week for periods of 5-16 minutes, and they are used only during vehicle slews. They are not currently used during guiding in three-gyro mode and will not be used in the two-gyro F2G mode either. Jitter splines are more common (~60 times per week). About half have tracking rates of <2 degrees per minute, and half have rates of 6-12 degrees per minute. They range in duration from about 10 minutes to 8 hours, with an average duration of about 1.5 hours. The total fraction of time spent in jitter spline mode is about 50%. The simulations described below include the worst case high-rate tracking jitter expected - about 8 mas RMS averaged over a 60 second time interval.

5.4 HSTSIM Jitter Simulations

HSTSIM is a high-fidelity, non-linear time domain HST pointing performance simulator developed and maintained by the Pointing Control Systems Group at Lockheed Martin Technical Operations (LMTO) Company. It includes realistic models for the HST hardware (FGS, FHSTs, gyroscopes, etc.) as well as models of orbital dynamics, the Earth's magnetic field, and sources of attitude disturbances (e.g., high gain antenna moves, V2 and SA3 disturbances, and aerodynamic and gravity gradients).

The information in this section is based on the disturbance data analysis and simulations conducted in the summer of 2004 by Brian Clapp and the PCS Group at LMTO.

5.4.1 Integrated Jitter Predictions

HSTSIM models were run for the full range of possible gyro pairs in two-gyro mode. A three-gyro model was also constructed for the currently operating 1-2-4 gyro set. The HSTSIM jitter predictions for three-gyro guiding mode are shown in Figure 5.3, and the predictions for the F2G-FL mode with the 1-4 gyro combination are shown in Figure 5.4. These models incorporate sample disturbances of the type described above, including an SA3 disturbance with an amplitude of 80 mas, thirteen V2 disturbances with amplitudes of 60-120 mas, and HGA tracking disturbances. The timelines shown are not meant to mimic a particular on-orbit combination of disturbance events, but rather are designed to explore the sensitivity of the possible gyro combinations to a variety of different types of disturbances. Clearly, multiple disturbances can be combined to produce larger amounts of jitter.

Figure 5.3: Three-Gyro Jitter Simulation Example with Disturbances

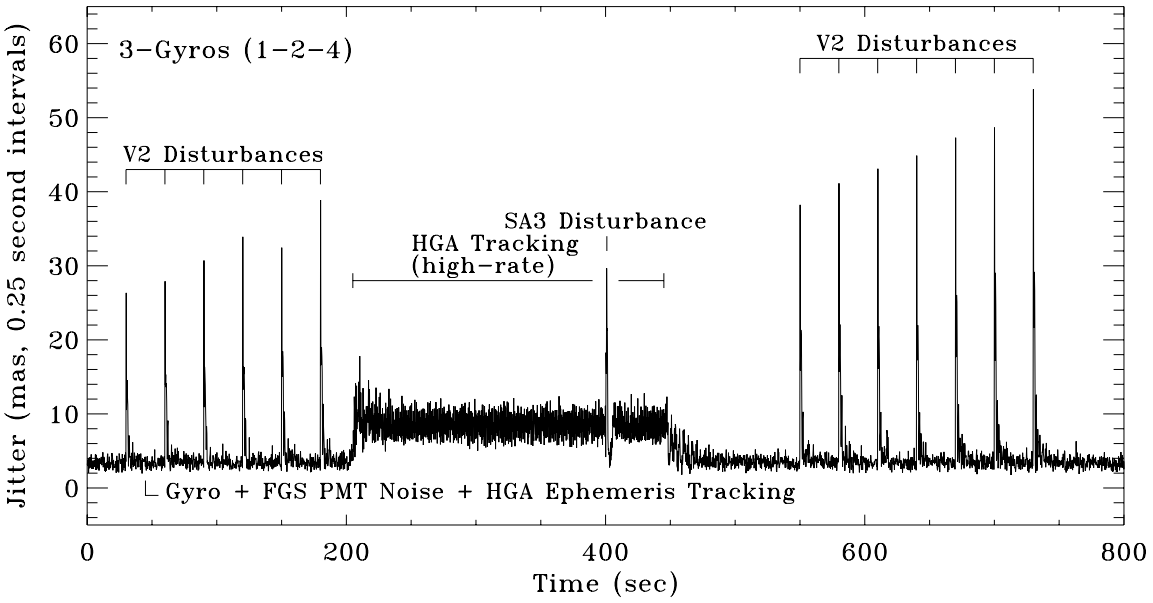

Figure 5.4: F2G-FL Two-Gyro Jitter Simulation Example with Disturbances

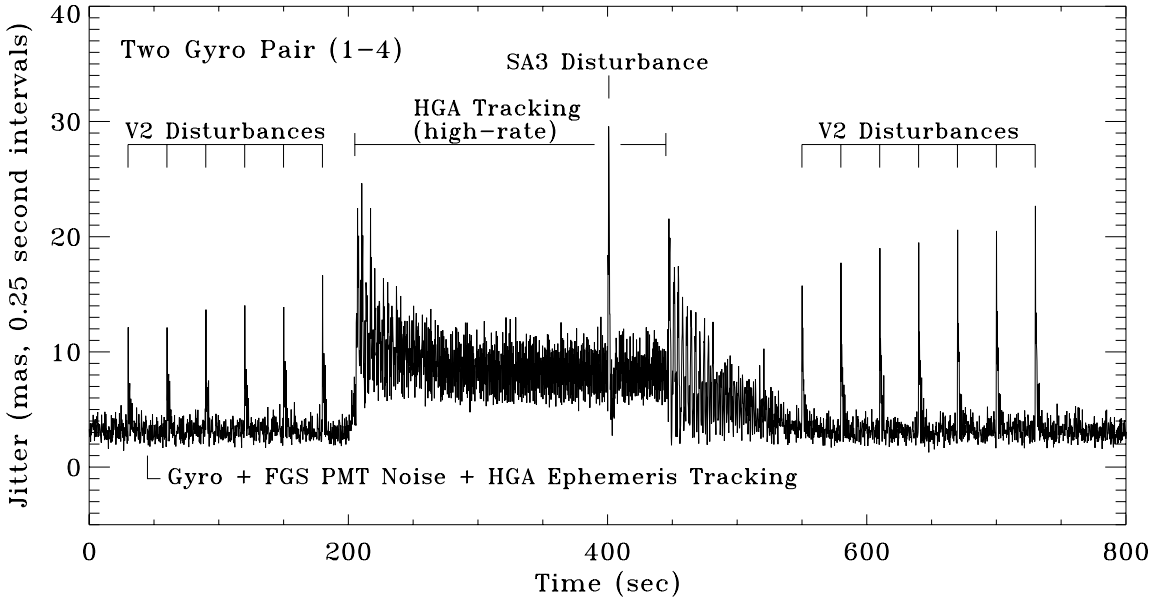

Sample jitter ellipses in the **V2**-**V3** plane are shown in Figure 5.5 for the 1-4 and 2-6 gyro pairs. The data in the upper middle panel corresponds to the jitter time series shown in Figure 5.4 for gyro pair 1-4 with a 13^{th} magnitude guide star. The large excursions caused by V2 disturbances are evident in all six panels. Note the slight increase in the jitter as the guide star magnitude increases. The increase in this jitter ellipse axis results from the increased FGS PMT noise in the simulations with the fainter guide stars. The points in these panels have been binned into 0.25 second jitter averages to make it easier to see these effects. Data from the full 800 second simulations are shown.

Figure 5.5: Jitter Ellipses for Two Possible Pairs of Gyros

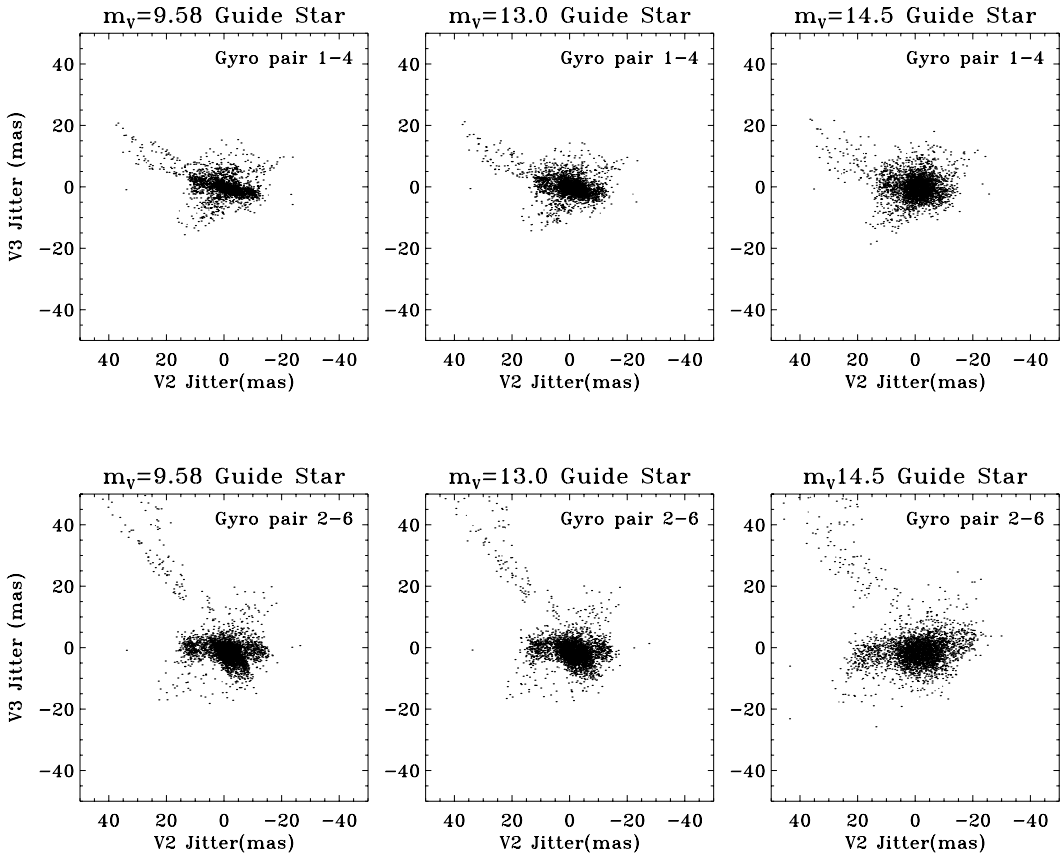

Table 5.6 summarizes the expected jitter in two-gyro mode based upon the HSTSIM predictions. For each possible two-gyro combination and three different FGS guide star magnitudes, the table lists the maximum root-mean-square (RMS) jitter measured in any 60 second interval during the F2G-FL portion of the simulations. The assumptions used in these predictions are the same as those described for the simulation data above. The corresponding values for three-gyro mode are listed at the bottom of the table. Note that these are the maximum values expected; typical jitter values for times between SA3 and V2 disturbances will be considerably less. In all instances, except the loss of lock case for the m_V = 14.5, gyro 1-4 combination, the predicted jitter is well under the 30 mas x 10 mas jitter assumed in the HST instrument descriptions in Part III of this Handbook.

Table 5.6: Two-Gyro and Three-Gyro Jitter Predictions (Including Disturbances)

Gyro Set	Angle of G_X Axis on Plane of Sky[1]	Maximum Boresight Jitter (mas, 60-second RMS) [2]		
		m_V = 9.58	m_V = 13.0	m_V = 14.5
Two-Gyro F2G-FL Results				
1-2	0.0	9.55	9.76	10.40
1-4	-22.7	10.65	10.86	11.65
1-6	22.7	11.72	11.91	13.06
2-4	55.6	12.20	12.30	15.97
2-6	-55.6	12.39	12.47	17.41
4-6	90.0	12.26	12.49	18.93[3]
Three-Gyro Results				
1-2-4	N/A	9.73	9.73	9.75

1. Angle is measured from the **V3** axis counterclockwise in the **V2-V3** (sky) plane (see Figure 5.2).
2. These values are the maximum jitter encountered during any 60 second interval in the F2G-FL portion of the simulation.
3. Loss of lock occurred during SA3 disturbance concurrent with high-rate HGA track.

5.5 On-Orbit Verification Tests

On-orbit tests of the F2G mode pointing and jitter are currently planned for February 2005. During those tests, HST will be operated as if it were in two-gyro mode. The tests will assess the magnitude and shape of the pointing jitter in this mode and its impact on the performance of the science instruments. They will also help to determine if changes to the attitude control law, which could modify the jitter amplitudes, need to be made. If necessary, the current jitter predictions in this Handbook will be revised after these tests.

CHAPTER 6:

Observation Planning

In this Chapter we discuss the specific considerations related to planning observations with HST in two-gyro mode. This includes assessing the schedulability and visibility periods of fixed targets, determination of continuous viewing zone opportunities, special considerations for moving targets, and the tools available to proposers planning the two-gyro portions of their Phase I proposals.

6.1 Introduction

Observers will face some changes in the way they design and describe their observing programs in response to the HST *Call for Proposals* in Cycle 14 and future cycles. The most obvious changes involve new information that must be supplied in the Phase I proposals to address the possibility that HST may have only two functioning gyros available for some fraction of Cycle 14. The availability of only two gyros impacts how the observations are scheduled, the visibility periods available for scientific observations, and instrument performance. This chapter describes the scheduling constraints encountered during two-gyro operations and provides information necessary for observers to successfully complete their Phase I proposal submissions. Instrument performance in two-gyro mode is described in Part III of this Handbook.

6.2 All-Sky Availability of Fixed Targets

6.2.1 Overview

The schedulability of an HST observation depends upon many factors and differs considerably between three-gyro and two-gyro operations. To highlight some of these differences, it is useful to compare the accessible regions of the sky in the two modes on 5 December 2005.

Figure 6.1: Sky Availability on 5 December 2005

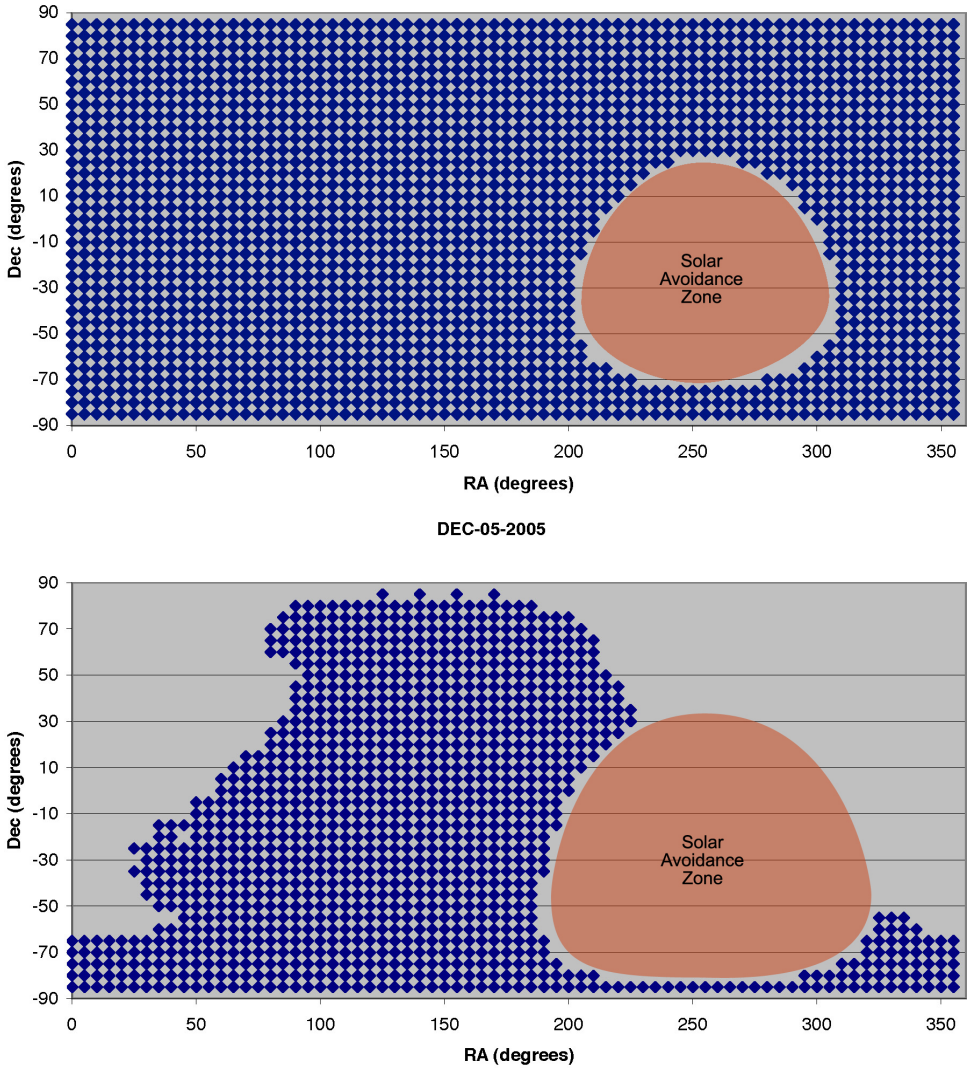

Caption: Sky availability for 5 December 2005 in both three-gyro mode (top panel) and two-gyro mode (bottom panel).

Figure 6.1 shows the sky availability for a single day in Cycle 14 assuming attitude control with either three gyros (top panel) or two gyros

(bottom panel). Blue regions indicate areas of the sky that can be observed on that date. Grey areas of the sky are not observable at that time. The unobservable region of sky is much larger in two-gyro mode than in three-gyro mode because of constraints imposed to achieve guide star acquisitions and to ensure the safety of the observatory. On any given day there is a region of the sky that cannot be observed in either two-gyro or three-gyro mode because of solar avoidance constraints. In three-gyro mode, all regions of the sky outside the solar avoidance zone (50 degree radius) are accessible on any day. The solar avoidance zone for two-gyro mode is larger, with a 60 degree radius. A large region of the sky ahead of the solar avoidance zone (at larger right ascensions than the Sun) is also unobservable in two-gyro mode because of constraints imposed by the process of correcting slew errors and achieving fine guiding lock. Thus, in two-gyro mode most targets can only be observed when they are on the trailing side of the Sun as it moves along the ecliptic. Over the course of year, all areas of the sky are available in two-gyro mode, but the total time available in any given direction is less than in three-gyro mode.

6.2.2 All-sky Availability Movie

A short narrated movie showing the sky availability during the course of a year can be found on the web at:

http://www.stsci.edu/hst/HST_overview/TwoGyroMode/2GyroMovies/2gyro.html

This movie compares the three-gyro and two-gyro availabilities in one-week increments in a format similar to the figure above. It shows the variable nature of the sky availability in two-gyro mode and the features discussed previously. It also shows that the availability near the equatorial poles is periodic and alternating. This availability pattern at high declinations is tied to the precession of the HST orbit.

6.2.3 Number of Available Days During the Course of a Year

It is useful to consider how many days per year a target of fixed position can be observed by HST. The top panel of Figure 6.2 shows the number of days in Cycle 14 that any position in the sky is observable by HST with its present three-gyro pointing capabilities. This plot is essentially an encapsulation of the contents of the sky availability movie described above. The color-coding of this figure indicates the number of days for which at least one orbit (defined here to be a contiguous time block of at least 30 minutes) is available to observe a fixed target. In this figure, the allowable Sun angle range is 50-180 degrees. The fewest number of schedulable days occurs over a small swath of sky near the ecliptic, with availability increasing toward the equatorial poles. The minimum number of days

available is approximately 260. A large portion of the sky at greater than 50 degrees ecliptic latitude has at least one schedulable orbit over the entire cycle duration. Be aware that this plot does not convey the information necessary to judge uninterrupted availability as occurs in the continuous viewing zones (CVZs). CVZ opportunities depend on a variety of additional factors that are described elsewhere (see the *HST Primer* and Section 6.6).

Figure 6.2: All-Sky Target Schedulability in Cycle 14

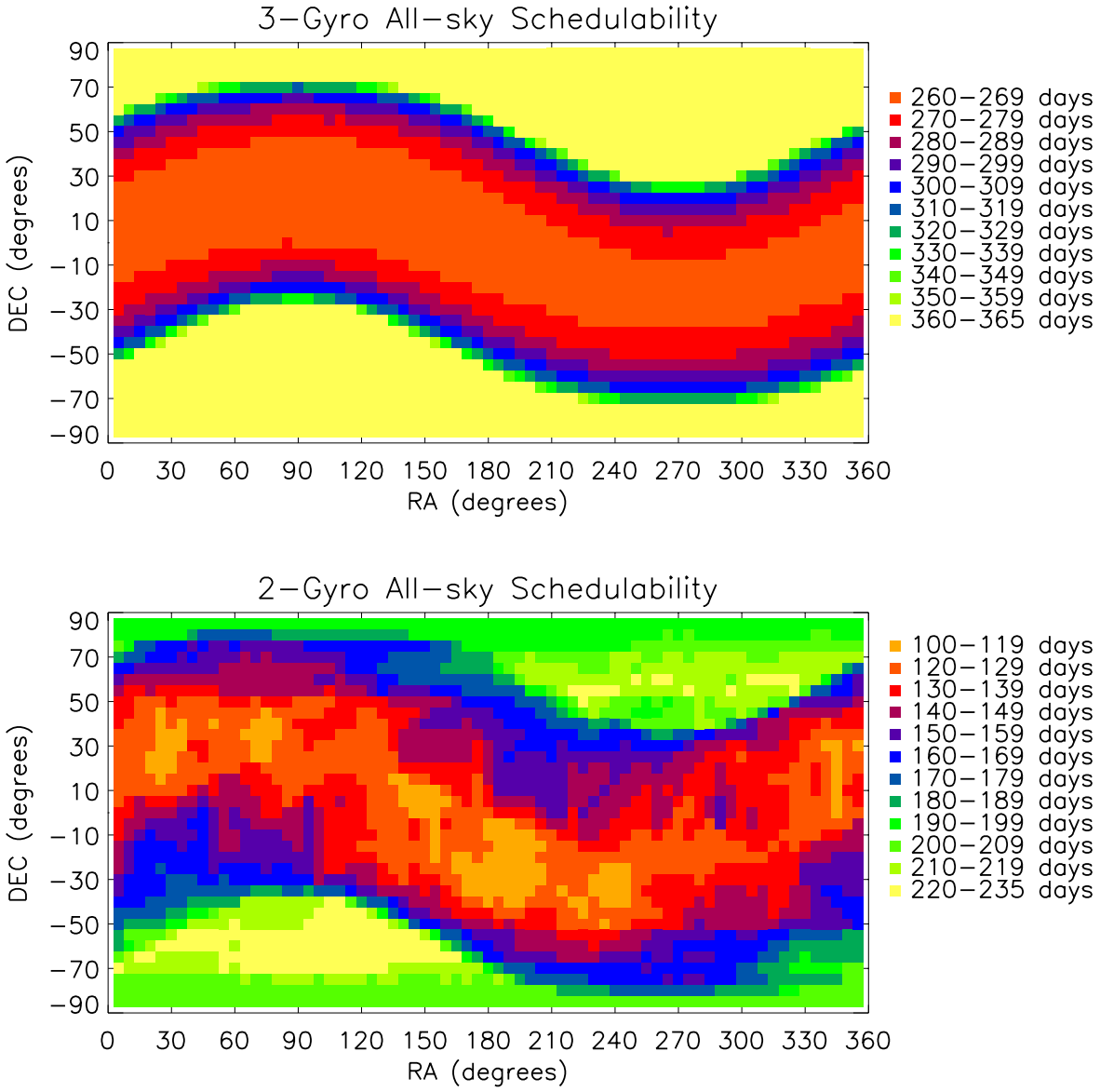

The bottom panel of Figure 6.2 shows the number of days in Cycle 14 that any position in the sky is observable with HST operating in two-gyro mode. Here, the allowable Sun angle range is restricted to 60-180 degrees.

Note that the absolute level of the color scaling is different than it is in the three-gyro case shown in the top panel. There are several things worth noting about this panel when comparing it to the three-gyro results. First, and most importantly, the total number of schedulable days at all positions in the sky decreases substantially in two-gyro mode. The minimum number of days that any given direction can be scheduled is 104, and the maximum is 234. Second, the smooth progression in availability seen in the top panel becomes slightly less regular, with pockets of reduced availability occurring across the sky. The overall trend for greater availability increasing toward the equatorial poles remains, but even some high declination pointings have fewer than half as many schedulable days as in three-gyro mode.

A comparison of the all-sky fixed target schedulability for two-gyro and three-gyro operations can be found in Figure 6.3. This figure shows the percentage of the sky as a function of number of observable days having at least one ≥30 minute orbit available for observations. Despite the dramatic reduction in visibility with two gyros, only a small percentage of the sky (3%) is observable for less than 120 days in two-gyro mode.

Figure 6.3: Comparison of Three-Gyro and Two-Gyro Target Schedulability

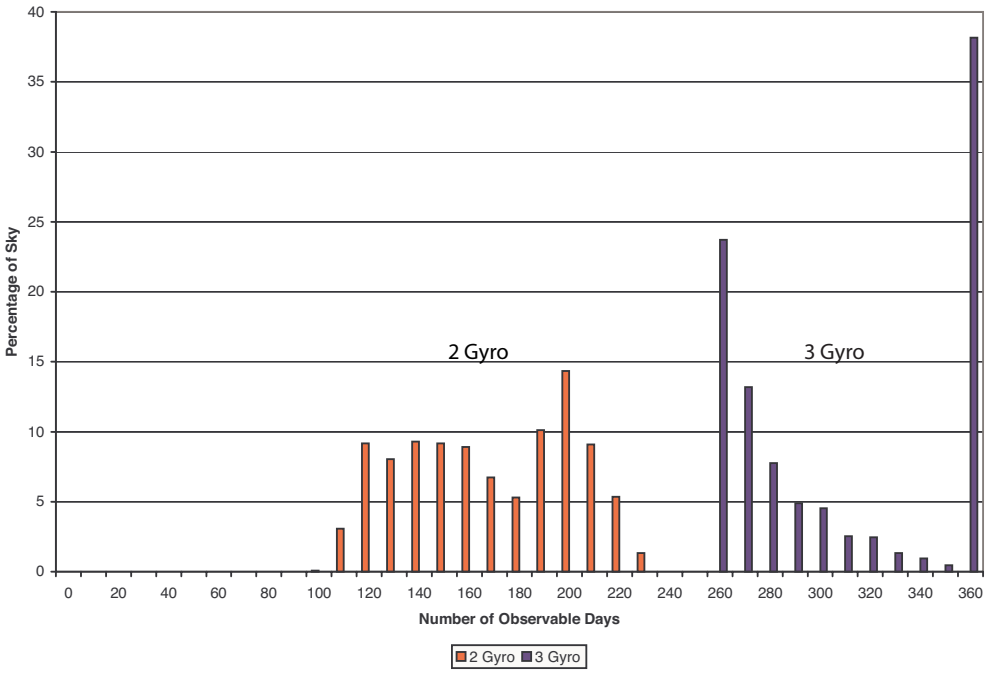

6.3 Assessing the Schedulability and Visibility Periods of Fixed-Targets

6.3.1 Overview

The primary observational constraints on the schedulability of most fixed targets in two-gyro mode are the position of the target in the sky, the required orientation (roll angle) of the observatory, and the required timing of the observation. Orientation constraints are usually specified with the `ORIENT` special requirement and often involve a restricted range of allowable roll angles that correspond to a particular time period that HST is able to achieve this orientation. Timing requirements may be specified either implicitly through the `ORIENT` special requirement or explicitly through timing special requirements (e.g., `BETWEEN, AFTER`, etc.). In some cases, an observation may not be schedulable in two-gyro mode because of the restrictions imposed by orientation and/or timing special requirements.

Whenever possible, observers should try to minimize the number of special requirements placed on their observations. This will result in improved schedulability and long range planning, greater flexibility in the three-gyro to two-gyro transition, and more efficient use of observing time.

The operational definition of orbital visibility period for two-gyro operations is the same as it is for three-gyro operations. Orbital visibility is the unocculted time available during the orbit for guide star acquisitions, target acquisitions, science exposures, calibration exposures (e.g., wavecals), and instrument overheads. The amount of time needed for acquisitions in two-gyro mode (7 minutes) is slightly larger than that required in three-gyro mode (6 minutes); see Section 5.1.

Figure 6.4 provides a graphical description of the general decision process involved in determining the schedulability and orbital visibility periods for fixed targets observed in two-gyro mode. The decision process for unconstrained observations involves minimal effort, whereas constrained observations require more careful consideration of the times of year that an observation can be scheduled. We discuss both types of observations below.

Figure 6.4: Two-Gyro Scheduling and Visibility Decision Tree

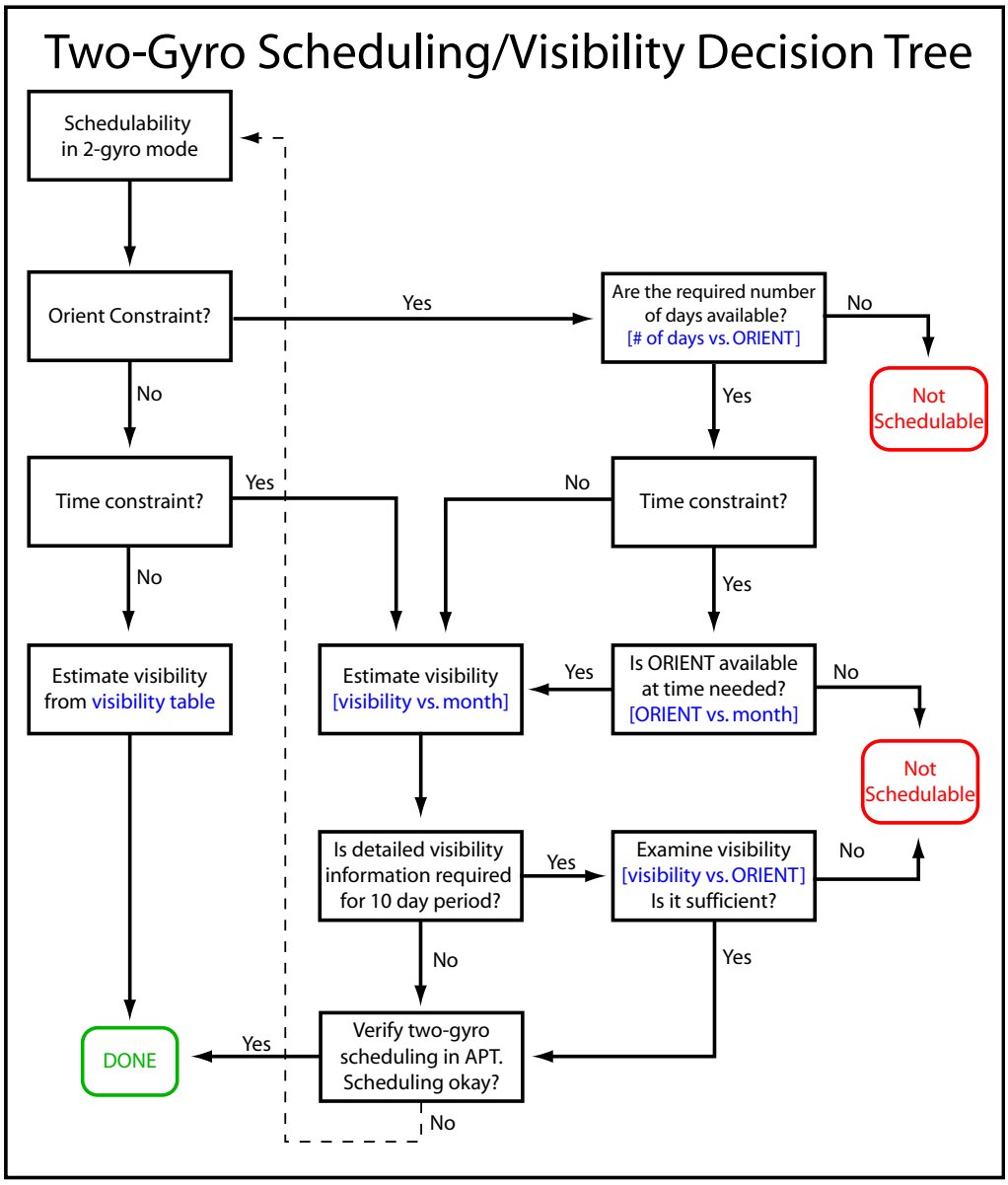

6.3.2 Unconstrained Fixed-Target Observations

If the observer does not need to specify the orientation of the observatory or the time of year of the observation, then the impact on scheduling is minimized and the observation will be schedulable at some time during the year, as is now the case for three-gyro operations. The orbital visibility of an unconstrained fixed-target is determined primarily by its declination. Table 6.1 lists both the three-gyro and two-gyro orbital visibility periods as a function of declination. These average values are sufficient for Phase I orbit calculations.

Table 6.1: Standard Fixed-Target Visibility Periods

|Declination| (degrees)	Orbital Visibility[1]		LOW Visibility[2] (minutes)
	Three-Gyro (minutes)	Two-Gyro (minutes)	
0–5	55	54	47
5–15	55	54	47
15–25	55	54	48
25–35	56	55	48
35–45	57	56	48
45–55	59	58	45
55–65	60	59	45
65–75	61	60	43
≥75	62	61	42

1. The orbital visibility periods in this table are the typical unocculted orbital visibility times available for guide star acquisitions and instrument-related activities.
2. LOW visibility refers to low-sky observations specified with the LOW special requirement. These approximate times apply to both two-gyro and three-gyro modes, but may be reduced by a few minutes for two-gyro mode once all of the two-gyro scheduling constraints are finalized with on-orbit tests.

6.3.3 Constrained Fixed-Target Observations

If an observer's science goals require specification of either the orientation of the observatory and/or the timing of the observation, determinations of the schedulability and orbital visibility period are slightly more complicated. An on-line tool to help observers determine when a fixed target can be scheduled during Cycle 14 is available on the Two-Gyro Science web page at:

http://www.stsci.edu/hst/HST_overview/TwoGyroMode/AllSkyInformation

Observers enter the coordinates of their targets into the web form, and the tool provides several graphical products that can be used to assess when and for how long the targets are visible. The calculations used to construct this output were performed on a 5˚x5˚ grid on the sky. The output returned is appropriate for the grid point nearest the input coordinates. Thus, any input position is within 3.5 degrees of a grid point. This sampling is sufficient to provide accurate scheduling and visibility information for any position on the sky for the Phase I proposal process. The models used as input to produce this information rely upon realistic representations of the constraints expected for two-gyro and three-gyro operations. For clarity,

Moon avoidance constraints are not included in these results; this does not alter the schedulability of a fixed-target or its orbital visibility significantly. Complete models including all constraints will be available for Phase II proposal processing.

The products returned by the web tool include: 1) A plot and table of the total number of days per year that each orientation is available; 2) A plot and table of when each orientation is available during Cycle 14 and the first half of Cycle 15; and 3) A plot and table of the target visibility as a function of date during Cycle 14 and the first half of Cycle 15. The first two plots contain information about the schedulability of the target, and the third contains the information necessary to determine how much time per orbit is available for the observation. Additional detailed information will also be available for constrained observations as discussed below.

In the discussions that follow, we consider two locations in the sky to provide an overview of the typical considerations required for low declination and high declination observations with orientation and/or time constraints. We show results for a low-latitude fixed-target at $\alpha = 0^\circ$, $\delta = 0^\circ$, and a high latitude target at $\alpha = 0^\circ$, $\delta = +70^\circ$.

Number of Available Days as a Function of Orientation

The number of days that a particular HST orientation (roll angle) can be achieved differs markedly between two-gyro and three-gyro operations. Plots of the number of days available in Cycle 14 as a function of orientation are shown for the low-latitude location in Figure 6.5 and the high-latitude location in Figure 6.6. In these plots, the availability with three-gyro operations is shown as a red histogram, while availability with two-gyro operations is shown as a blue histogram. An available day is defined to be one in which at least one orbit with 30 minutes of continuous visibility exists after the guide star acquisition. Some days may have only short visibility periods, while other days may have many orbits with acceptable visibility. No distinction based on number of orbits per day is made here. A portion of the table returned by the web tool for the low latitude example is provided in Table 6.2.

All roll angles are available at some time during the year in three-gyro mode. The number of days of availability may be quite limited for some orientations, especially at low declinations as a result of Sun angle constraints. The range of available orientations expands at higher latitudes, with the number of days of availability increasing for some orientations and decreasing for others. In two-gyro mode, the number of days available for a given orientation is always less than or equal to the number of days available in three-gyro mode, and in some cases it is identically zero.

Figure 6.5: Orientation Availability for a Low-Latitude Target Near $\alpha = 0^{\circ}$, $\delta = 0^{\circ}$

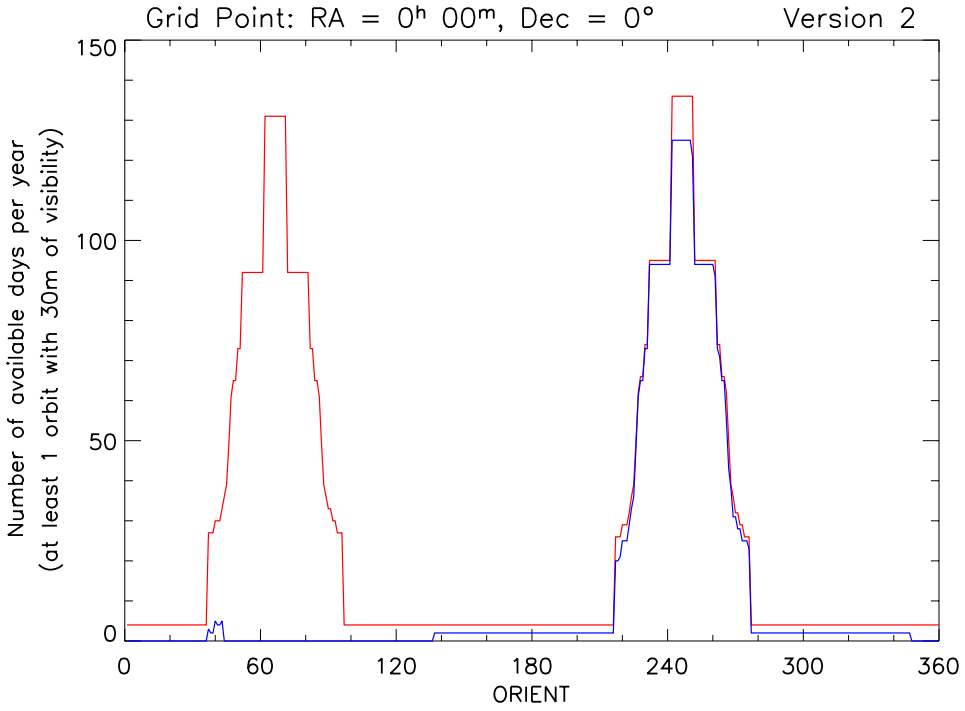

Caption: Number of days per year that a particular orientation is available for a target at $\alpha = 0^{\circ}$, $\delta = 0^{\circ}$. The red curve shows the three-gyro results. The blue curve shows the two-gyro results.

In the low latitude example in Figure 6.5, there are two primary zones of availability over restricted ranges of orientations and a baseline floor of availability at all orientations for observations conducted in three-gyro mode. The range of accessible orientations is reduced greatly by the constraints imposed by two-gyro operations. In particular, the prominent zone of availability between orientations of ~40 degrees and ~100 degrees in three-gyro mode disappears completely as does the floor of limited availability at all orientations. The prominent zone of availability between ~220 degrees and ~280 degrees also shrinks slightly in size in two-gyro mode. The loss of one of the primary zones of availability strongly affects the scheduling of the observation, but since the zones are separated by 180 degrees the impact on many science programs should be minimal unless the absolute sign of the roll angle is important or observations at roll angles separated by 180 degrees are required. In two-gyro mode, an observation of a target at this position that required an orientation of <137 degrees or >347 degrees would not be schedulable; observations in the two low-visibility wings (137-216 degrees, 277-347 degrees) are highly constrained.

Table 6.2: Sample Tabular Output for the Two-Gyro Data Shown in Figure 6.5

Grid Point: RA = 0h 00m, Dec = 0

Orientation Angle	Number of Days Available
:	:
:	:
210	2
211	2
212	2
213	2
214	2
215	2
216	2
217	20
218	20
219	21
220	25
:	:
:	:

Figure 6.6: Orientation Availability for a High-Latitude Target at $\alpha = 0^{\circ}$, $\delta = +70^{\circ}$

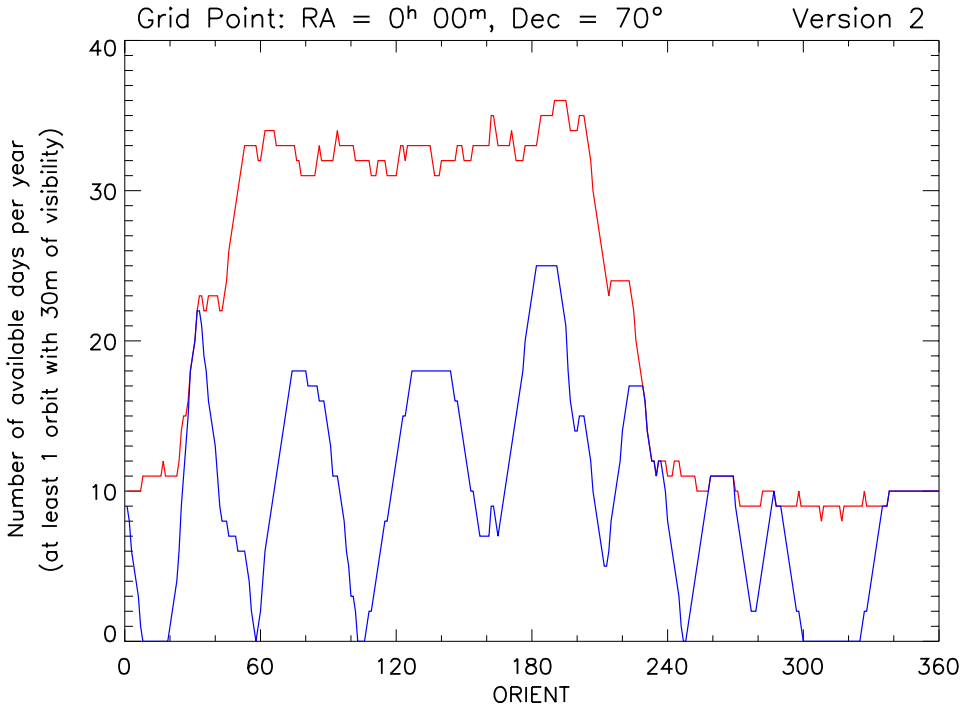

Caption: Number of days per year that a particular orientation is available for a target at $\alpha = 0^{\circ}$, $\delta = 70^{\circ}$. The red curve shows the three-gyro results. The blue curve shows the two-gyro results.

In the high latitude example in Figure 6.6, most orientations are available for five or more days in two-gyro mode, with some notable exceptions occurring over restricted ranges in orientation where the availability dips to zero. The two-gyro availability is typically a factor of

2–3 times less than in three-gyro mode, except over limited orientations where the two-gyro availability is similar to the availability in three-gyro mode.

Availability of Roll Angles in Cycle 14

If a sufficient number of days exists to observe a target, the next step in determining its schedulability is to check when the target could be scheduled. If there are roll angle (`ORIENT`) constraints, the observer should check when the particular orientation is available by examining the web tool plot illustrating `ORIENT` versus time. Example plots are shown in Figure 6.7 and Figure 6.8, and a sample of the tabular output is shown in Table 6.3. The time axis on these plots extends for 18 months from the start of Cycle 14 so that observers can judge whether observations that may begin in Cycle 14 could be concluded in the first half of Cycle 15. The blue regions of the figures indicate what orientations are available for the specified date if only two gyros are available and there is at least one orbit with 30 minutes of visibility after the guide star acquisition. The gold regions indicate less than 30 minutes of two-gyro visibility for some ORIENTs on that date. The red contours, which encompass the blue and gold regions and may extend to other regions of the figures as well, bracket the orientation availability in normal three-gyro operations. Note that most orientations are available only for limited periods of time, even when HST has a full complement of gyros. In two-gyro mode, the orientation availability is reduced.

There are several features of these plots to point out. Consider first the low-latitude pointing in Figure 6.7. The February-May time period is unavailable because of Sun avoidance restrictions. The Sun-leading region of the sky (October-February) is accessible in three-gyro mode but not in two-gyro mode. The extended range of orientations available in late September 2005 and 2006 with three gyros occurs because the target is located in the anti-Sun direction at this time. Half of this time disappears when only two gyros are available.

Figure 6.7: Low-Latitude Target Roll Angles Available During Cycle 14

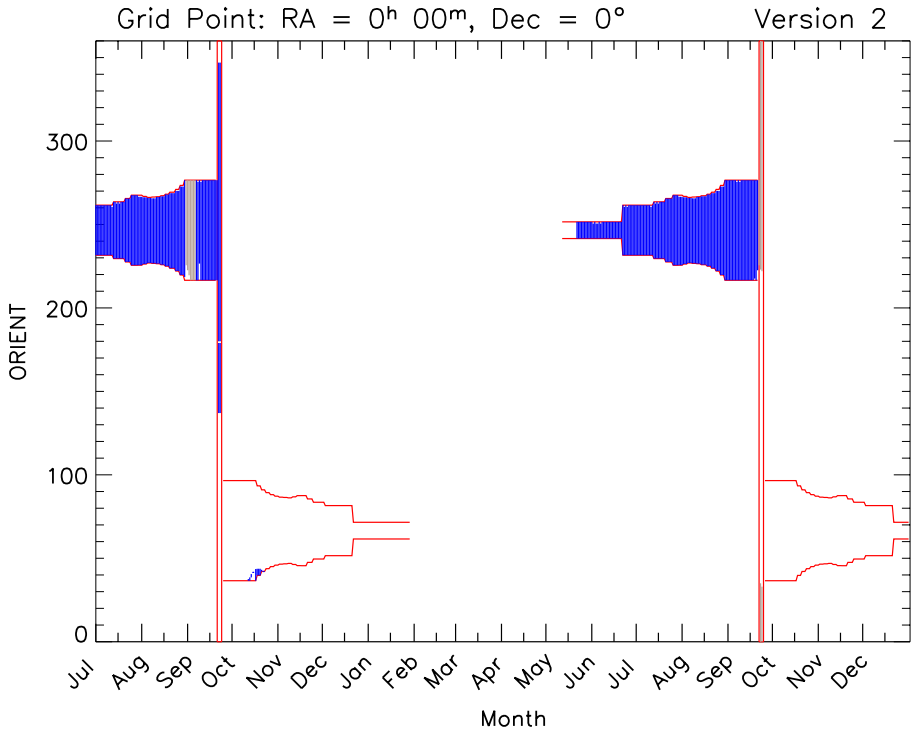

Caption: Roll angles (ORIENTs) available in two-gyro mode for a pointing in the direction $\alpha = 0^\circ$, $\delta = 0^\circ$ are shaded in blue for times when at least one orbit with 30 minutes of visibility exists. Gold regions indicate that orbits with less than 30 minutes of visibility exist. The ranges of roll angles available in three-gyro mode are shown as red contours. The time period covered on the x-axis includes Cycle 14 and the first half of Cycle 15 (1 July 2005 to 31-Dec-2006).

Table 6.3: Sample Tabular Output for the Two-Gyro Data Shown in Figure 6.7

```
Grid Point: RA = 0h 00m, Dec = 0

Date          Available Orientations
    :               :
    :               :
18 Sep 2005   216.6 - 276.6
19 Sep 2005   216.6 - 276.6
20 Sep 2005   216.6 - 276.6
21 Sep 2005   216.6 - 276.6
22 Sep 2005   137.0 - 179.0     180.0 - 347.0
23 Sep 2005   137.0 - 179.0     180.0 - 347.0
12 Oct 2005    36.6 -  37.6
13 Oct 2005    36.6 -  38.6
14 Oct 2005    38.6 -  40.6
15 Oct 2005    41.6 -  41.6
    :               :
    :               :
```

For the high latitude pointing in Figure 6.8, the availability of roll angles follows a smooth progression in time for three-gyro mode. This progression in two-gyro mode is broken into several time intervals

separated by periods where the object is unobservable. These breaks in availability occur primarily because precession of the HST orbit causes the Earth to block the FHSTs, which are needed for guide star acquisitions. Note that the availability of some orientations in two-gyro mode is the same as it is in three-gyro mode because the combination of Sun angle and off-nominal roll constraints is no more stringent than in three-gyro mode.

Figure 6.8: High-Latitude Target Roll Angles Available in Cycle 14

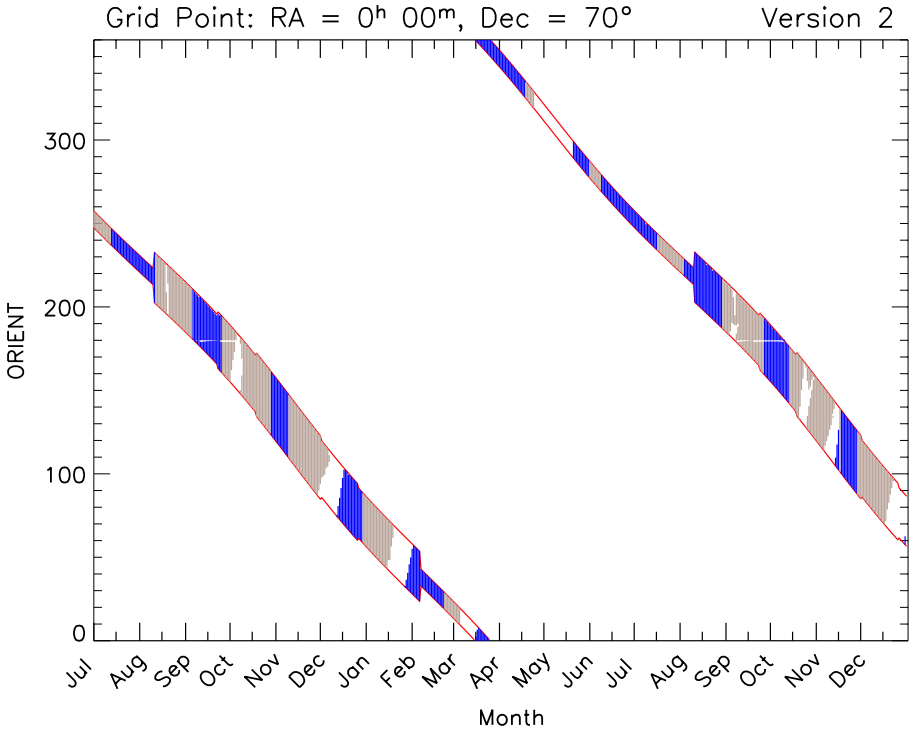

Caption: Roll angles (`ORIENT`s) available in two-gyro mode for a pointing in the direction $\alpha = 0^{\circ}$, $\delta = 70^{\circ}$ are shaded in blue for times when at least one orbit with 30 minutes of visibility exists. Gold regions indicate that orbits with less than 30 minutes of visibility exist. The ranges of roll angles available in three-gyro mode are shown as red contours. The time period covered on the x-axis includes Cycle 14 and the first half of Cycle 15 (1 July 2005 to 31-Dec-2006).

Target Visibility as a Function of Date

For constrained observations, the orbit visibility cannot be described in a simple table like that for unconstrained observations (Table 6.1). The web tool displays this information in graphical form in a plot of target visibility versus time for an 18 month period beginning at the start of Cycle 14. Plots for the low- and high-latitude sight lines are shown in Figure 6.9 and Figure 6.10. Sample tabular output for Figure 6.9 is shown in Table 6.4.

The target visibilities in these plots and accompanying tables have been reduced by the guide star acquisition time (6 minutes for three-gyro mode, 7 minutes for two-gyro mode) to allow for a more direct comparison of the amount of time available for instrument related activities (e.g., target

acquisition, exposure time, and instrument overheads). The visibility for the normal three-gyro case is shown as a red curve. The two-gyro visibility periods are indicated by blue points indicating the maximum visibility available, and by green lines indicating the full range of visibilities for the orientations available. In some instances, the maximum visibility depicted by the blue line may be identical to the minimum visibility in which case there is no green line, just a blue point. Note that in both examples the visibility on any given date is less in two-gyro mode than in three-gyro mode. This is due to the additional visibility constraints imposed by the more stringent two-gyro mode pointing restrictions.

Figure 6.9: Science Time Available for a Low-Latitude Target in Cycle 14

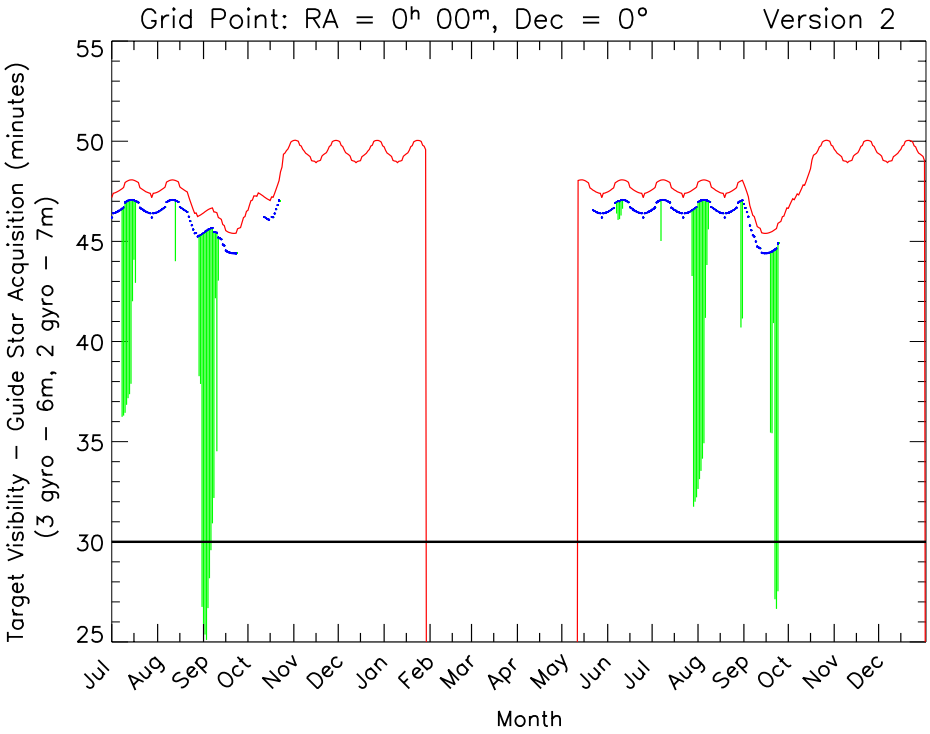

Caption: This plot shows the science time available per orbit for instrument-related activities for a pointing in the direction $\alpha = 0^\circ$, $\delta = 0^\circ$ after subtracting either 6 minutes (three-gyro mode) or 7 minutes (two-gyro mode) for guide star acquisition activities. The three-gyro results are shown in red. The blue points indicate the maximum science time available in two-gyro mode, while the vertical green lines illustrate the range of visibilities possible for allowed orientation angles. The time period covered on the x-axis includes Cycle 14 and the first half of Cycle 15 (1 July 2005 to 31-Dec-2006).

Table 6.4: Sample Tabular Output for the Two-Gyro Data Shown in Figure 6.9

Grid Point: RA = 0h 00m, Dec = 0

Date	Science Time Available (minutes) 2-Gyro (minimum)	2-Gyro (maximum)
:	:	:
:	:	:
05 Sep 2005	28.2	45.6
06 Sep 2005	29.6	45.7
07 Sep 2005	30.9	45.7
08 Sep 2005	32.2	45.5
09 Sep 2005	42.2	45.5
10 Sep 2005	34.5	45.4
11 Sep 2005	43.0	45.2
12 Sep 2005	45.2	45.2
13 Sep 2005	45.1	45.1
:	:	:
:	:	:

Figure 6.10: Science Time Available for a High-Latitude Target in Cycle 14

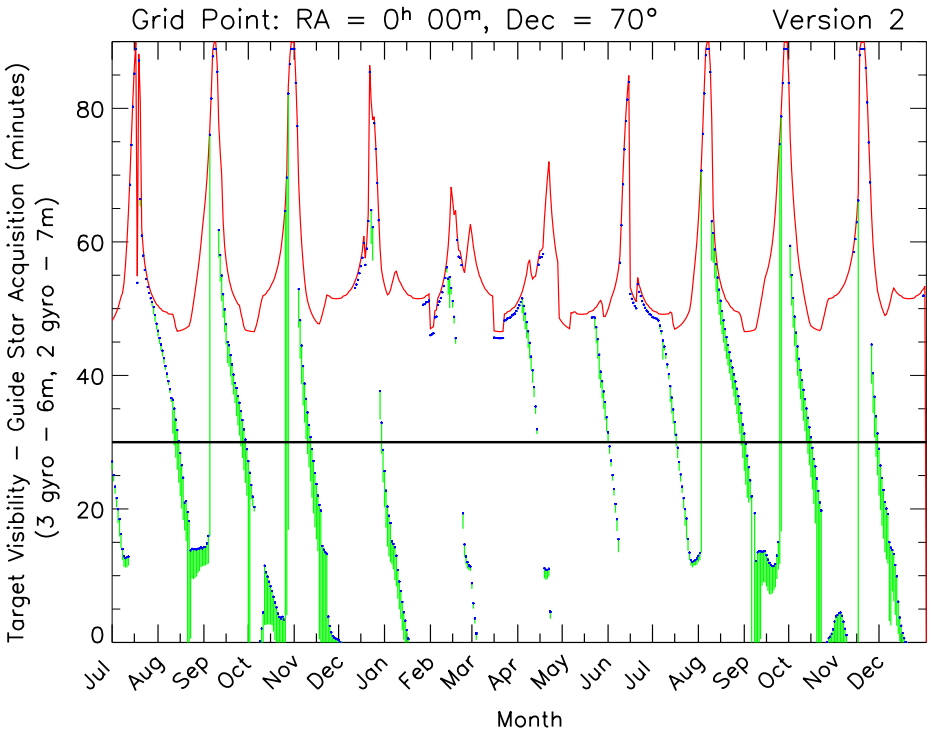

Caption: This plot shows the science time available per orbit for instrument-related activities for a pointing in the direction $\alpha = 0^{\circ}$, $\delta = +70^{\circ}$ after subtracting either 6 minutes (three-gyro mode) or 7 minutes (two-gyro mode) for guide star acquisition activities. The three-gyro results are shown in red. The blue points indicate the maximum science time available in two-gyro mode, while the vertical green lines illustrate the range of visibilities possible for allowed orientation angles. The time period covered on the x-axis includes Cycle 14 and the first half of Cycle 15 (1 July 2005 to 31-Dec-2006).

The horizontal black line at 30 minutes in Figure 6.9 and Figure 6.10 indicates the minimum acceptable science time (= target visibility - guide star acquisition time) that will be allowed for Phase I proposals in Cycle 14 without special scientific justification. Most observations can be scheduled at times when the science time exceeds this amount, and those few that cannot will likely have other restrictions that will preclude such observations. For example, in the high-latitude example, the visibility window on 1 September 2005 is only 12 minutes. Therefore, a target at this location in the sky will not be scheduled on this date.

In calculating the orbit visibility period in two-gyro mode for Cycle 14, observers should adopt the maximum visibility estimate indicated by the blue points in the visibility plots unless they have both `ORIENT` and timing restrictions, in which case they need to examine the more detailed visibility plots described in the next section. The HST scheduling system will make every effort to schedule observations when the visibility is optimized.

Detailed Target Visibility Considerations

In some cases it may be necessary to have a more detailed look at the target visibility for various orientations on a particular date to assess whether a highly constrained observation is feasible. The Detailed Visibility Tool on the Two-Gyro Science web page can be used to determine this information. The observer can enter the target coordinates and the desired date of the observation, and the tool will return a plot and table of the science time available as a function of orientation for the 11 day interval centered on the input date.

Figure 6.11 contains an example of the detailed visibility plot for the low-latitude sight line example on a set of dates centered on 10 July 2005. The resulting visibilities are color coded by date. The information is shown in tabular form in Table 6.5. Observers requiring a specific orientation on a specific date should specify the appropriate visibility indicated by these plots (or tables) in their Phase I proposals.

Figure 6.11: Detailed Visibility Plot for a Low-Latitude Target

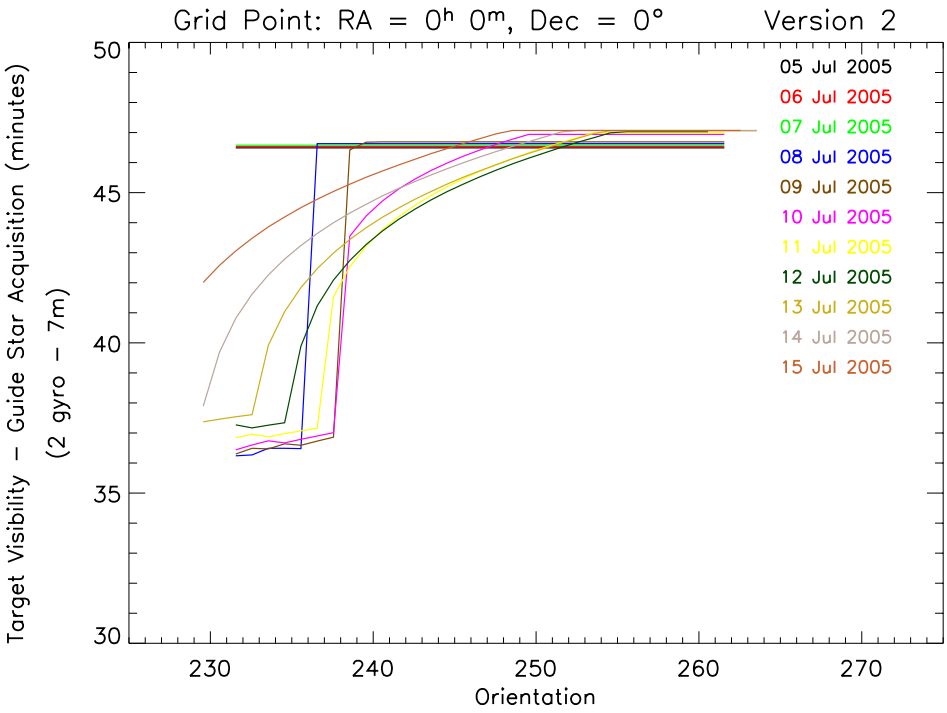

Caption: This plot shows the two-gyro mode science time available per orbit for instrument-related activities as a function of orientation for a pointing in the direction $\alpha = 0^{\circ}$, $\delta = 0^{\circ}$ after subtracting 7 minutes for guide star acquisition activities. The various curves shown correspond to the visibilities for the 11 days centered on 10 July 2005.

Table 6.5: Tabular Output for the Two-Gyro Data Shown in Figure 6.11

	Science Time Available (minutes)										
Year: 2005	Jul 05	Jul 06	Jul 07	Jul 08	Jul 09	Jul 10	Jul 11	Jul 12	Jul 13	Jul 14	Jul 15
Orientation											
230	0	0	0	0	0	0	0	0	37	38	42
231	0	0	0	0	0	0	0	0	37	40	43
232	46	47	47	36	36	36	37	37	38	41	43
233	46	47	47	36	36	37	37	37	38	42	43
234	46	47	47	36	36	37	37	37	40	42	44
235	46	47	47	36	37	37	37	37	41	43	44
236	46	47	47	36	37	37	37	40	42	43	45
237	46	47	47	47	37	37	37	41	42	44	45
238	46	47	47	47	37	37	42	42	43	44	45
239	46	47	47	47	46	44	43	43	43	44	45
240	46	47	47	47	47	44	43	43	44	45	46
241	46	47	47	47	47	45	44	44	44	45	46
242	46	47	47	47	47	45	44	44	44	45	46
243	46	47	47	47	47	45	45	44	45	45	46
244	46	47	47	47	47	46	45	45	45	46	46
245	46	47	47	47	47	46	45	45	45	46	46
246	46	47	47	47	47	46	45	45	46	46	47
247	46	47	47	47	47	46	46	46	46	46	47
248	46	47	47	47	47	47	46	46	46	46	47
249	46	47	47	47	47	47	46	46	46	47	47
250	46	47	47	47	47	47	46	46	46	47	47
251	46	47	47	47	47	47	47	46	46	47	47
252	46	47	47	47	47	47	47	47	47	47	47
253	46	47	47	47	47	47	47	47	47	47	47
254	46	47	47	47	47	47	47	47	47	47	47
255	46	47	47	47	47	47	47	47	47	47	47
256	46	47	47	47	47	47	47	47	47	47	47
257	46	47	47	47	47	47	47	47	47	47	47
258	46	47	47	47	47	47	47	47	47	47	47
259	46	47	47	47	47	47	47	47	47	47	47
260	46	47	47	47	47	47	47	47	47	47	47
261	46	47	47	47	47	47	47	47	47	47	47
262	46	47	47	47	47	47	47	0	47	47	47
263	0	0	0	0	0	0	0	0	47	47	47
264	0	0	0	0	0	0	0	0	47	47	0

6.3.4 Examples

In this section we provide some examples of how to determine the schedulability and visibility period for different types of observations in two-gyro mode.

Example 1: Time-series observations of the Hubble Deep Field (HDF) and Hubble Ultra Deep Field (HUDF).

Observer #1 wants to search for supernovae in the HDF and HUDF by repeating a set of ACS observations every ~45 days for as many consecutive 45-day intervals as possible. The fields are tiled with multiple

pointings, each of which has five 400 second integrations designed to fit in a single orbit in three-gyro mode. The total time required to tile either field is 15 orbits (~1 day). Orientation is not critical, as the field can be tiled in a manner that allows nearly full coverage of the field regardless of orientation. The HDF and HUDF are located at $\alpha = 12^h\ 32^m$, $\delta = +62°18'$ and $\alpha = 3^h\ 32^m$, $\delta = -27°\ 55'$, respectively.

Let's consider first the HDF. Using the on-line tool available at the Two-Gyro Science web site, we examine the scheduling and visibility plots available for the $\alpha = 12^h\ 40^m$, $\delta = 60°$ grid point. The plot of number of available days versus orientation shows that there are many days in Cycle 14 that the HDF is observable in two-gyro mode provided that the orientation is greater than ~130 degrees. Since Observer #1 does not have an orientation constraint, we skip the plot of orientation versus month and proceed directly to the plot of visibility versus month. From this plot (Figure 6.12), we see that good visibility is achievable for this program throughout much of the year. Prior to 23 September 2005, the field is not visible in two-gyro mode in Cycle 14.

Figure 6.12: Science Time Available per Orbit for the HDF in Cycle 14

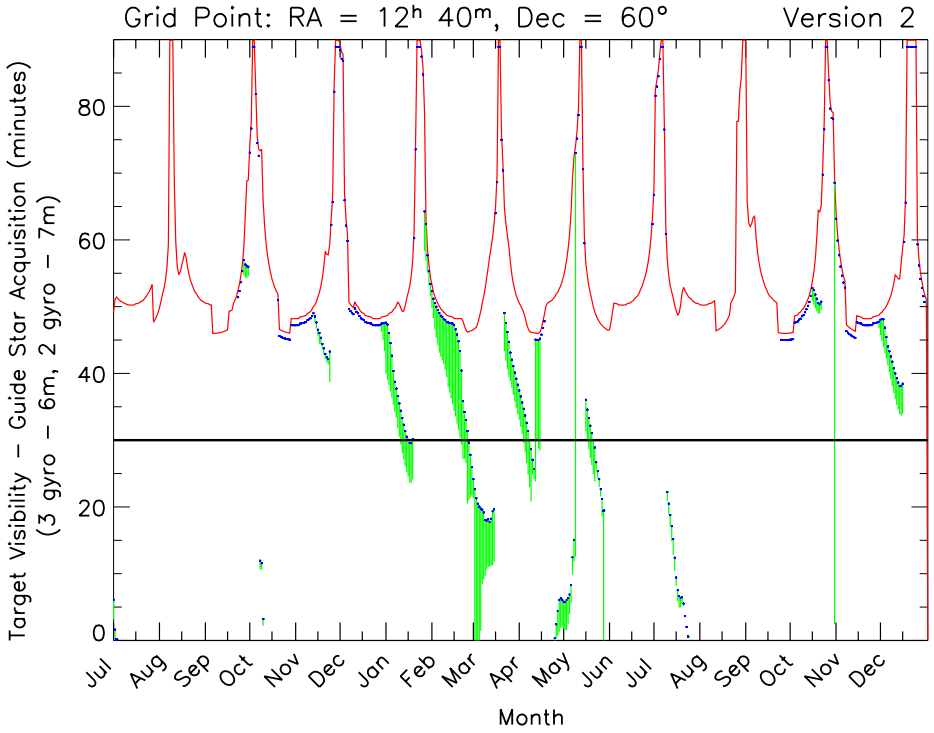

This program could be conducted with a set of 4 observing opportunities spaced ~45 days apart (e.g., 01-Nov-2005, 15-Dec2005, 01-Feb-2006, 16-Mar-2006). The science times available per orbit on these dates are listed in Table 6.6. A larger set of observations may be difficult to schedule since the next opportunity in this set (May 1) has very poor visibility. When dealing with visibilities that change rapidly over the course of a month, flexibility in time series spacing may improve the schedulability. For

example, in this case allowing a 56 day separation from March 15 to May 10, instead of the 45 day spacing between March 15 and April 29, would increase the visibility sufficiently to make another epoch of observations possible.

Table 6.6: Two-Gyro Science Time for the HDF on Selected Dates in Cycle 14

Observation Date	Science Time per Orbit (minutes)
01-Nov-2005	47
14-Dec-2005 15-Dec-2005 16-Dec-2005	49 48 48
31-Jan-2006 01-Feb-2006 02-Feb-2006	53 52 51
14-Mar-2006 15-Mar-2006 16-Mar-2006	19 20 64
29-Apr-2006 30-Apr-2006 01-May-2006	06 06 06

Now consider the HUDF. Using the on-line tool available at the Two-Gyro Science web site, we examine the scheduling and visibility plots available for the $\alpha = 3^h\ 40^m$, $\delta = -30^\circ$ grid point. The possibilities for scheduling a series of observations with a spacing of 45 days is much more limited. Starting the series as early as possible gives the greatest time coverage, but the program is still limited to ~3 observing opportunities (e.g., July 1, Aug. 15, Oct. 1) because the HUDF has very limited availability between November 2005 and June 2006. Table 6.7 and Figure 6.13 show the visibility periods. The short schedulability period in November 2005 has significantly reduced visibility windows (<23 min) and could be included in the series only with appropriate scientific justification. An additional window starting on December 3 is also possible.

Table 6.7: Two-Gyro Science Time for the HUDF on Selected Dates in Cycle 14

Observation Date	Science Time per Orbit (minutes)
01-Jul-2005	46
15-Aug-2005	47
01-Oct-2005	47
15-Nov-2005	20
03-Dec-2005	45

Figure 6.13: Science Time Available per Orbit for the HUDF in Cycle 14

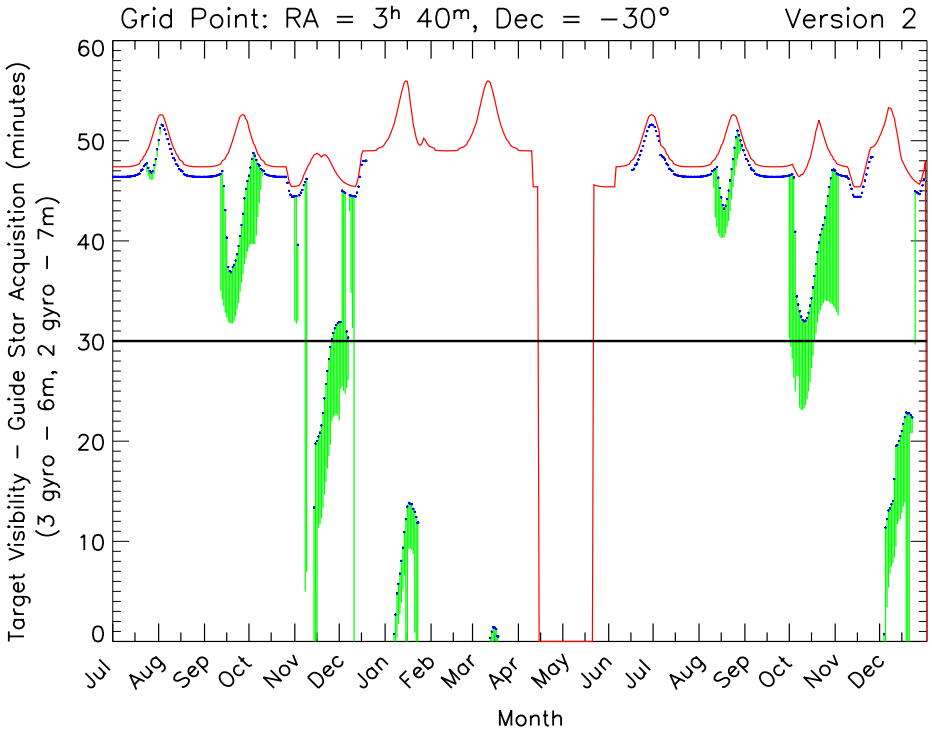

Example 2: Time-series light curve observations of a supernova found in Example 1.

Observer #1 finds a supernova in the HDF using the experiment outlined in Example 1 and wants to obtain the light curve of the supernova by obtaining photometric images of the supernova and surrounding field once a week for 7 weeks. The supernova was discovered after the second set of observations was obtained on 1 February 2006.

Using the visibility versus month plot generated for Example 1, Observer #1 notes that the orbital visibilities for the HDF and surrounding areas are good on February 8 and 15 (48 minutes). However, by February 22 the visibility has dropped to 36 minutes, and by March 1 it is only 24 minutes. Visibility does not improve sufficiently to observe this field until March 16, after which it is acceptable again until April 8. Thus, it is not possible to follow the supernova light curve throughout the entire 45 day period as hoped.

If the supernova had been found after the second epoch observations of the HUDF instead of the HDF, it would have been possible to follow the light curve for the full 45 day interval between 15 August 2005 and 1 October 2005 (see Figure 6.13).

Example 3: Time-constrained observations of recurrent nova T Pyx.

Observer #3 wants to observe the recurrent nova T Pyx ($\alpha = 9^h\ 05^m$, δ = -32° 23') during its next outburst, which should begin in early October 2005. The objective is to study the evolution of the ejected shell using images (3 orbits with at least 40 minutes of visibility) obtained as soon as possible after outburst, followed by images 7, 21, 49, 84, 112, 140, and 365 days later. There are no orientation constraints on the observations. Observer #3 estimates the science time available using the web tool plot of visibility versus month shown in Figure 6.14 for the nearby position at $\alpha = 9^h\ 0^m$, δ = -30° (see also Table 6.8).

Figure 6.14: Science Time Available for T Pyx in Cycle 14

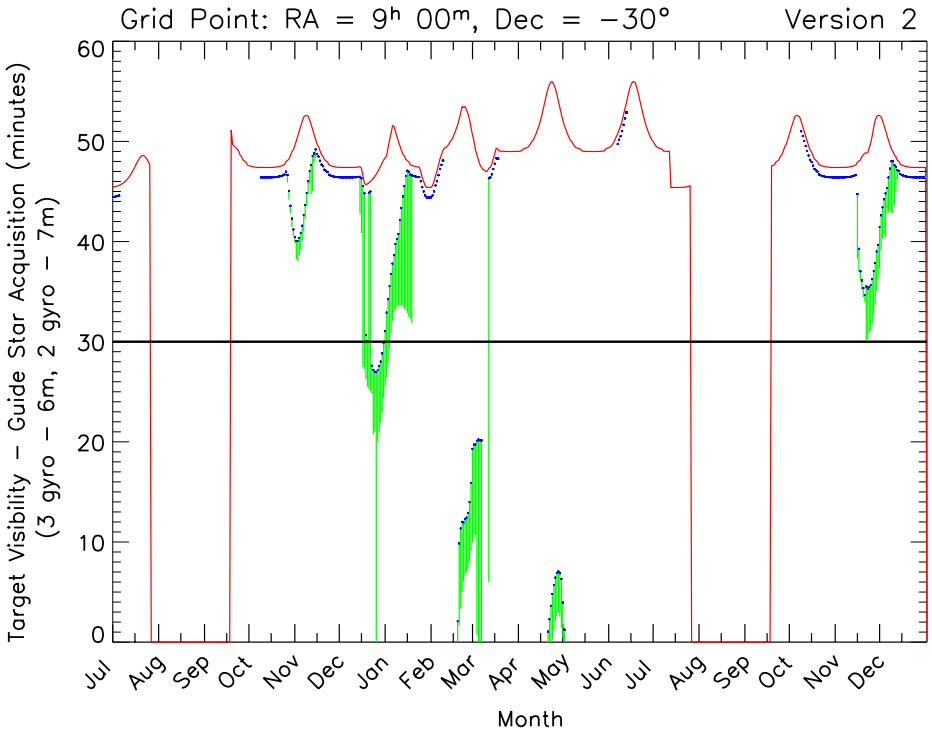

Examination of this plot provides the following information (assuming an October 9 start) for the relative timing of the observations and the amount of science time available per orbit.

Table 6.8: Two-Gyro Science Time Available for T Pyx on Selected Cycle 14 Dates

Observation Date	Relative Timing (days)	Science Time per Orbit (minutes)
09-Oct-2005	0	46
16-Oct-2005	7	46
30-Oct-2005	21	42
27-Nov-2005	49	47
01-Jan-2006	84	31
29-Jan-2006	112	44
26-Feb-2006	140	13
09-Oct-2006	365	51

Two of the observations have less than the 40 minutes of visibility needed for this particular science investigation, and are therefore not suitable choices for this time series. The day 84 observation would need to be moved back to December 22 (which puts it too close to the day 49 observation), or moved forward to January 9 (which puts it too close to the day 112 observation), to keep it. Since both dates are not useful, Observer #3 decides to drop this observation. The day 140 observation can be saved by moving it to day 154 (March 12), which has a visibility of 46 minutes. A possible revised series of observations is given in Table 6.9.

Table 6.9: Revised Two-Gyro Time Series for T Pyx in Cycle 14

Observation Date	Relative Timing (days)	Science Time per Orbit (minutes)
09-Oct-2005	0	46
16-Oct-2005	7	46
30-Oct-2005	21	42
27-Nov-2005	49	47
29-Jan-2006	112	44
12-Mar-2006	154	46
09-Oct-2006	365	51

However, while the outburst is expected around the beginning of October, it could occur later in the month, so it is necessary to check how a later outburst would impact the observations. With start dates of October 16, 23, and 30, the following sequences listed in Table 6.10 are possible.

Thus, if T Pyx goes into outburst anytime in October, the observations can be successfully obtained in two-gyro mode.

Table 6.10: Alternate Time Series for T Pyx in Cycle 14

Observation Date/Timing	Science Time per Orbit (minutes)	Observation Date/Timing	Science Time per Orbit (minutes)	Observation Date/Timing	Science Time per Orbit (minutes)
16-Oct-2005/0	46	23-Oct-2005/0	47	30-Oct-2005/0	42
23-Oct-2005/7	47	30-Oct-2005/7	42	06-Nov-2005/7	42
06-Nov-2005/21	42	13-Nov-2005/21	49	20-Nov-2005/21	48
04.Dec-2005/49	46	11-Dec-2005/49	46	16-Dec-2005/47	46
05-Feb-2006/112	46	15-Jan-2006/84	47	22-Jan-2006/84	47
12-Mar-2006/147	46	12-Mar-2006/140	46	12-Mar-2006/133	46
16-Oct-2006/365	48	23-Oct-2006/365	47	30-Oct-2006/365	46

Example 4: An orientation-constrained observation of the Vela supernova remnant.

Observer #4 wants to take an ACS image of a portion of the Vela supernova remnant near the position of the star HD 72089 ($\alpha = 08^h\ 29^m$, $\delta = -45^\circ\ 33'$). A roll angle of 70±5 degrees must be used to keep the bright star off the detector. A second observation to observe a different part of the remnant requires an orientation 90±5 degrees from the first observation.

Entering the coordinates of HD 72089 into the scheduling tool on the web yields the following plots of the number of days each orientation is available (Figure 6.15) and orientation versus month (Figure 6.16) for the nearby position at $\alpha = 8^h\ 20^m$, $\delta = -45^\circ$. It is apparent from these plots that an orientation of 70 degrees can be achieved in three-gyro mode in the March-April 2006 time frame, but that it cannot be achieved in two-gyro mode at any time in Cycle 14.

Realizing that the planned orientations are not viable, Observer #4 checks the availability of orientations 180 degrees from those originally envisioned. The inverse orientations at 250 degrees and 340 degrees are accessible in September 2005 and January 2006, respectively. Therefore, this observation is feasible in two-gyro mode as long as the requested orientations are changed to 250±5 degrees and 340±5 degrees. The availability of allowable orientations must be described appropriately in the Phase I proposal to reflect the fact that the allowed orientations and timings of the observations in two-gyro mode are more restrictive than in three-gyro mode.

Figure 6.15: Cycle 14 Orientation Availability in the Direction of the Vela SNR

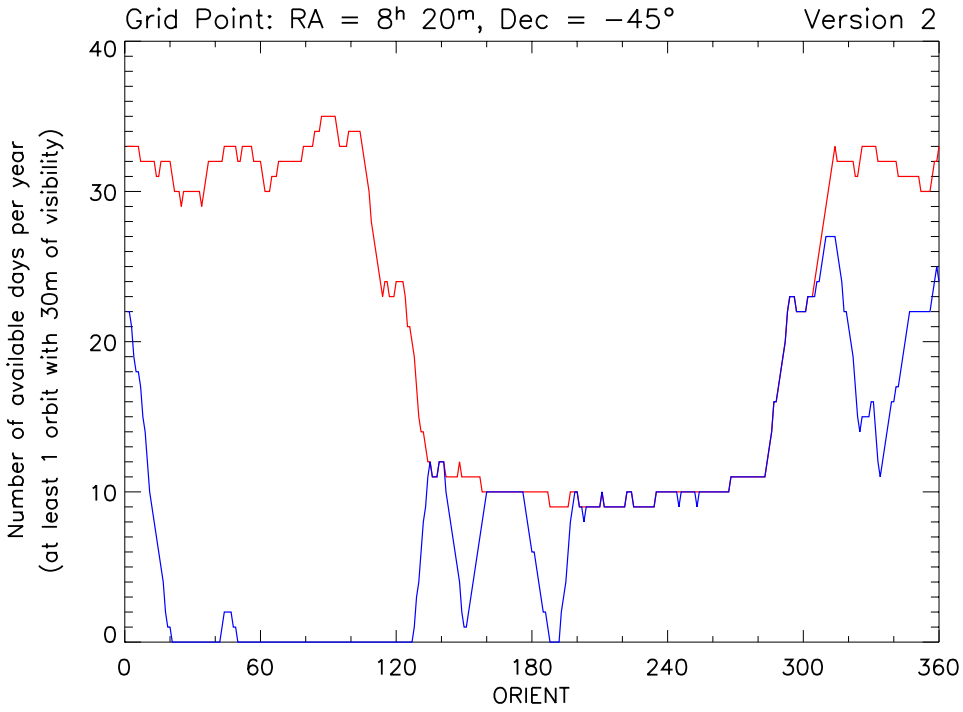

Figure 6.16: Cycle 14 Orientation Angles Versus Month Toward the Vela SNR

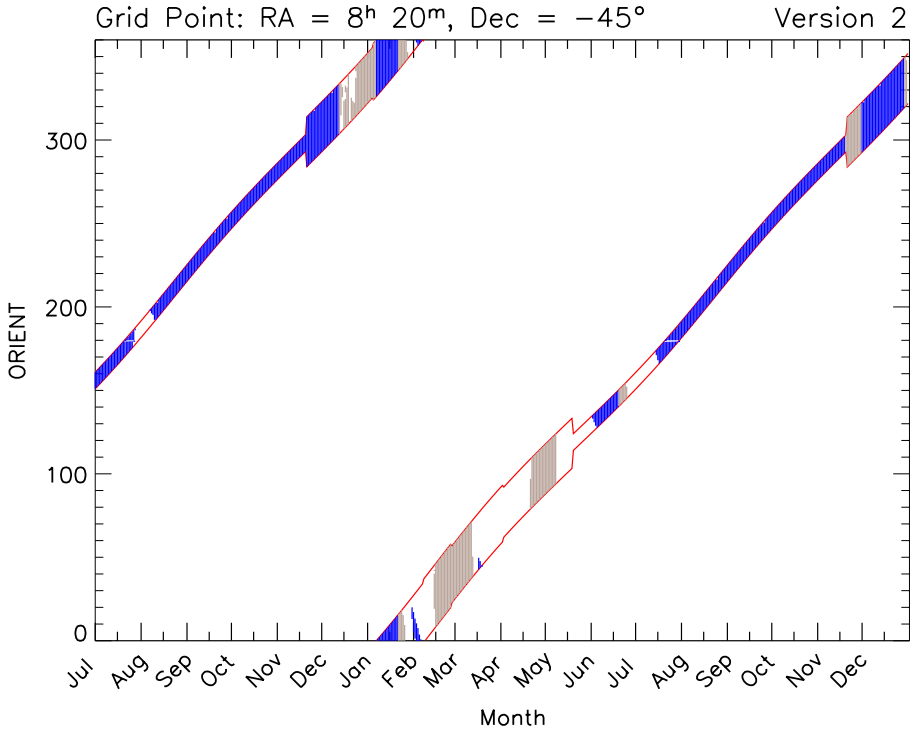

6.4 Verifying Scheduling Constraints for Phase I

The Astronomer's Proposal Tool (APT) package will contain software to check the schedulability of targets in Phase I proposal forms. When filling out the APT form for their Phase I proposals, Cycle 14 proposers will be asked to verify the availability of their targets in two-gyro mode. Note that this is the last step in the two-gyro scheduling/visibility decision tree shown in Figure 6.4. Observers should perform this check after they have entered their observation information based upon the tables and plots discussed in the previous sections of this chapter. Instructions for how do perform this check will be posted on the Two-Gyro Science web site.

6.5 Two-Gyro Orbit Calculations for Phase I

Orbit calculations for two-gyro observations are performed in a manner similar to those for three-gyro observations. The primary differences are:

- The visibility period for two-gyro observations should make use of the two-gyro visibility periods from the plots and tables described in this chapter. The tools for creating these plots and tables are available on the Two-Gyro Science web site.
- CVZ opportunities should be determined directly from the same plots in two-gyro mode instead of using the three-gyro CVZ tables if specific timing or orientation constraints are necessary for the observations.
- Guide star acquisition times in two-gyro mode are slightly longer than in three-gyro mode (see Table 5.1). Observers should assume a guide star acquisition time of 7 minutes for two-gyro mode.
- Exposure times for two-gyro observations should be calculated with the appropriate two-gyro exposure time calculators (ETCs) for each instrument. Links to these ETCs can be found on the main web page for each instrument.

Exposure time calculators (ETCs) for each science instrument have been updated to provide exposure time estimates for two-gyro mode observations. The updates incorporate changes to encircled energy distributions, spectral resolution, and other quantities related to the size of the jitter ellipse expected while guiding with two gyros. To be conservative, the assumed jitter ellipse for the two-gyro calculations is 30 mas x 10 mas, even though the guiding performance is expected to be better than this jitter estimate. The ETCs include a switch that allows the user to toggle between calculations for two-gyro and three-gyro modes. Additional exposure time calculation information, including specific examples, can be found in the individual instrument performance chapters in Part III of this Handbook.

6.6 Continuous Viewing Zones

The continuous viewing zones (CVZs) are regions of the sky where HST can observe without interruptions caused by target occultation by the Earth. These zones are approximately 24 degrees in size centered on the orbital poles, which are 28.5 degrees from the celestial poles. Thus, targets located in declination bands near ±61.5 degrees may be in the CVZ at some time during the 56-day HST orbital precession cycle. In three-gyro mode, there are typically 7 CVZ intervals per year with durations of 1 to 105 orbits. The interval duration depends upon the telescope orbit, target position, and constraints imposed by Sun and Earth limb avoidance. Note that South Atlantic Anomaly crossings limit the uninterrupted visibility of any target to no more than 5-6 orbits (see Section 2.3.2 in the *HST Primer*).

The CVZs in two-gyro mode will be the same size as those in three-gyro mode, but the durations may be shorter because of more restrictive pointing constraints. For a general idea of where the CVZs are located and how many orbits of CVZ time are available, observers should consult the web-based CVZ tables at

`http://www.stsci.edu/hst/proposing/docs/cvz-information/`

For more detailed information about whether constrained two-gyro observations qualify for CVZ time, observers should consult the visibility tables and plots discussed above. Only those observations for which the orbital visibility (= science time available + 7 minutes) is 96 minutes should be considered CVZ candidates.

Depending upon the on-orbit performance of the HST pointing, it is possible that a guide star acquisition will be required at the beginning of every HST orbit, even those that would otherwise qualify as CVZ orbits. In this case, there would be short intervals for which collection of science data would be interrupted while the acquisitions were occurring.

6.7 Moving Targets

We expect that there will be no significant impact on moving target observations beyond the increase in jitter discussed in Section 5.2. Gyro-only tracking and guide star handoffs for moving target observations will not be available in two-gyro mode. Proposers wanting to observe moving targets should consult the Two-Gyro Science web page for updates, which will be posted as information about observing moving targets in two-gyro mode becomes available.

PART III:

Science Instrument Performance

The chapters in this part of the Handbook describe the impact of two-gyro operations on science instrument performance. The content in these chapters has been provided by the ACS, WFPC2, NICMOS, STIS, and FGS instrument teams at STScI. This information should be used to plan observations, compare performance in two-gyro and three-gyro modes, and assess the feasibility of science programs. Cycle 14 proposers are encouraged to check the Two Gyro Science Web Site for updates on jitter characterization and the effects of jitter on instrument performance. The performance of the science instruments in three-gyro mode is discussed in the individual Instrument Handbooks

CHAPTER 7:

ACS Performance in Two-Gyro Mode

In this chapter. . .

This chapter contains information about the performance of the Advanced Camera for Surveys (ACS) when HST is guiding in two-gyro mode. Observers should use the information in this chapter to assess and justify the feasibility of their proposed ACS observations. For information about the three-gyro performance of ACS and planning observations in three-gyro mode, see the ACS Instrument Handbook.

7.1 ACS Point Spread Function

A potential impact of operating in two-gyro mode is a blurring of the point spread function (PSF) caused by pointing jitter. In the following discussions, we proceed with the assumption of a 30 mas x 10 mas RMS jitter ellipse, which we believe represents a “worst case” jitter. The exact

amount of jitter will likely depend on the details of the observation. For example, in two-gyro mode the Fine Guidance Sensors will be used to provide short-timescale tracking information, and hence photon noise in the guiders may be important. Observations with bright guide stars are likely to experience less jitter than the conservative numbers used here. The orientation of the G_X axis will also depend on which gyros remain functional, and of course, is not known at this time. Chapter 5 describes the expected properties of the jitter.

7.1.1 A Comparison of Pointing Jitter and Pixel Sizes

The pointing jitter acts as a convolution of the PSF, and its primary effect is to move counts out of the PSF central pixel into surrounding pixels. In an effort to roughly assess its impact on ACS observations, we list several relevant parameters in Table 7.1.

The WFC operates at long wavelengths and has large pixels, and hence the convolution of the Airy disk (35-70 mas) with the pixel size (50 mas) is comparable to the long axis of the two-gyro jitter ellipse (71 mas x 24 mas FWHM). We expect that the impact for WFC observations will be relatively minor, with the PSF central pixel intensity being reduced by roughly $\sqrt{2}$.

The HRC has smaller pixels (27 mas) and is capable of operating at shorter wavelengths, so we expect larger impacts. In the red, the convolution of the Airy disk (50-70 mas) and pixel size are again comparable to the jitter FWHM so intensity reduction factors of $\sim\sqrt{2}$ might be seen. In the blue the jitter FWHM is twice the combined pixel and Airy disk size, so reduction factors of ~2 may be seen. The same result applies to the SBC because the jitter FWHM is about twice the pixel size.

Many observers will be more concerned about the performance for aperture photometry, rather than these PSF central pixel estimates. However, for apertures more than about 2 pixels in radius, the jitter in two-gyro mode will have essentially no impact, as it affects mainly the PSF core.

These simple arguments, while instructive, ignore many complicating effects (optical aberrations and obscurations, electron diffusion in the detectors, etc.). More quantitative models are considered below.

Table 7.1: Various Parameters Affecting PSF Sharpness

Parameter		Size
Airy Disk FWHM at Wavelength:	115nm	9 mas
	200nm	17 mas
	400nm	33 mas
	800nm	66 mas
Pixel Size for Camera:	WFC	50 mas
	HRC	27 mas
	SBC	32 mas
Two-Gyro Jitter FWHM		71 mas x 24 mas

7.1.2 Model PSFs

The ACS Instrument Handbook gives model PSFs in Tables 4.9 and 4.10. We reproduce these model PSFs for both three-gyro and two-gyro modes in Table 7.2 (WFC), Table 7.3 (HRC), and Table 7.4 (SBC). The PSF is tabulated at several wavelengths for each camera. Each table gives the central 5 x 5 pixels of the PSF, and the numbers listed are the fraction of the total energy received in each pixel. These models have been generated using **TinyTIM**, taking into account the HST optical aberrations and obscurations as well as the CCD pixel response function (charge diffusion function). Field dependent geometrical distortions are also included. For two-gyro mode we have assumed a 30 mas x 10 mas (RMS) jitter. The major axis of the jitter ellipse has been arbitrarily placed along the x-axis of the undistorted pixel grid (the actual orientation will depend on the gyro pair in use).

For the WFC the impact of jitter is relatively modest, as the pointing jitter is comparable to the combined pixel and Airy disk size. For 30 mas x 10 mas RMS jitter, the central pixel of the WFC PSF is reduced from about 17% of the total counts to about 12% (Table 7.2). This calculation assumes the star is at the pixel center – the impact will be less if the star is located elsewhere on the pixel grid.

The impact on the HRC and SBC is larger, as the jitter ellipse is larger than both the pixel size (27 mas for HRC, 32 mas for SBC) and the size of the Airy disk – especially in the blue and ultraviolet. For example, for the HRC at 200 nm the central pixel is reduced from 18% in three-gyro mode to only 7% of the total counts in two-gyro mode (Table 7.3).

Table 7.2: ACS/WFC Model PSFs (5x5 pix) in Three-Gyro and Two-Gyro Modes

Three - Gyro					Two - Gyro				
WFC at 400 nm									
0.00	0.01	0.02	0.01	0.00	0.01	0.01	0.01	0.01	0.00
0.01	0.04	0.08	0.04	0.01	0.01	0.04	0.06	0.04	0.01
0.02	0.08	0.17	0.08	0.02	0.02	0.08	0.12	0.08	0.03
0.01	0.04	0.07	0.05	0.02	0.01	0.04	0.06	0.04	0.02
0.00	0.01	0.01	0.01	0.01	0.00	0.01	0.01	0.01	0.01
WFC at 80 0nm									
0.01	0.01	0.02	0.01	0.00	0.01	0.01	0.02	0.01	0.01
0.01	0.03	0.07	0.03	0.01	0.01	0.04	0.06	0.03	0.01
0.02	0.07	0.17	0.07	0.02	0.02	0.08	0.13	0.08	0.03
0.01	0.03	0.07	0.03	0.02	0.01	0.03	0.06	0.04	0.02
0.01	0.01	0.02	0.01	0.01	0.01	0.01	0.01	0.01	0.01

Table 7.3: ACS/HRC Model PSFs (5x5 pix) in Three-Gyro and Two-Gyro Modes

Three - Gyro					Two - Gyro				
HRC at t 200 nm									
0.01	0.01	0.01	0.01	0.01	0.01	0.01	0.01	0.01	0.01
0.01	0.03	0.05	0.03	0.01	0.02	0.04	0.04	0.03	0.01
0.01	0.05	0.18	0.04	0.01	0.03	0.06	0.07	0.06	0.02
0.01	0.02	0.05	0.02	0.01	0.01	0.02	0.04	0.03	0.02
0.00	0.01	0.01	0.01	0.01	0.00	0.01	0.01	0.01	0.01
HRC at 400 nm									
0.01	0.01	0.02	0.02	0.01	0.01	0.01	0.01	0.01	0.01
0.02	0.03	0.07	0.03	0.01	0.02	0.04	0.05	0.03	0.02
0.02	0.06	0.17	0.06	0.01	0.03	0.06	0.08	0.06	0.03
0.01	0.02	0.07	0.03	0.01	0.01	0.03	0.04	0.04	0.02
0.00	0.01	0.02	0.02	0.00	0.00	0.01	0.01	0.01	0.01
HRC at 800 nm									
0.00	0.01	0.02	0.01	0.00	0.01	0.01	0.01	0.01	0.01
0.02	0.04	0.05	0.03	0.01	0.02	0.03	0.04	0.03	0.01
0.01	0.05	0.07	0.05	0.01	0.02	0.04	0.05	0.04	0.02
0.01	0.03	0.05	0.04	0.01	0.01	0.03	0.04	0.03	0.02
0.00	0.01	0.02	0.01	0.00	0.01	0.01	0.01	0.01	0.01

Table 7.4: ACS/SBC Model PSFs (5x5 pix) in Three-Gyro and Two-Gyro Modes

Three - Gyro					Two - Gyro				
SBC at 120 nm									
0.01	0.01	0.01	0.01	0.00	0.01	0.01	0.01	0.01	0.01
0.02	0.03	0.04	0.02	0.01	0.02	0.03	0.03	0.02	0.01
0.01	0.05	0.18	0.03	0.01	0.02	0.06	0.08	0.05	0.02
0.01	0.01	0.04	0.02	0.00	0.01	0.02	0.03	0.02	0.01
0.00	0.00	0.01	0.01	0.01	0.00	0.01	0.01	0.01	0.01
SBC at 160 nm									
0.01	0.01	0.01	0.01	0.00	0.01	0.01	0.01	0.00	0.00
0.01	0.02	0.04	0.02	0.00	0.02	0.03	0.04	0.02	0.01
0.01	0.05	0.20	0.03	0.00	0.02	0.07	0.11	0.07	0.02
0.01	0.02	0.04	0.02	0.00	0.01	0.02	0.03	0.03	0.01
0.00	0.00	0.01	0.02	0.00	0.00	0.00	0.01	0.01	0.00

It is important to note that the PSFs given above correspond to the star landing precisely at the center of a pixel, which results in the largest possible fraction of counts in the central pixel of the PSF. In reality, the star will be randomly placed on the pixel grid, generally leading to a lower percentage of counts in the central pixel. For the extreme case of a star landing on the pixel corner, the peak flux is reduced by as much as a factor ~2, which is comparable or larger than the impact of two-gyro jitter. This effect is further discussed in Section 7.1.6.

7.1.3 Encircled Energy

Encircled energy distributions are plotted for the three ACS cameras in Figure 7.1 (WFC), Figure 7.2 (HRC), and Figure 7.3 (SBC). Each plot shows the distributions for both three-gyro and two-gyro modes at several representative wavelengths. The three-gyro curves are based on observed PSFs. The two-gyro curves were computed using **TinyTIM** model PSFs to estimate the general effects of jitter, which were then used to scale the observed three-gyro curves accordingly; this method allows us to accurately include effects such as far-red halos which are not reproduced well by the model PSFs. Differences between three-gyro and two-gyro mode are significant only in the PSF core (radii below ~0.2 arcseconds).

Figure 7.1: Encircled Energy for the ACS / WFC in Three- and Two-Gyro Modes

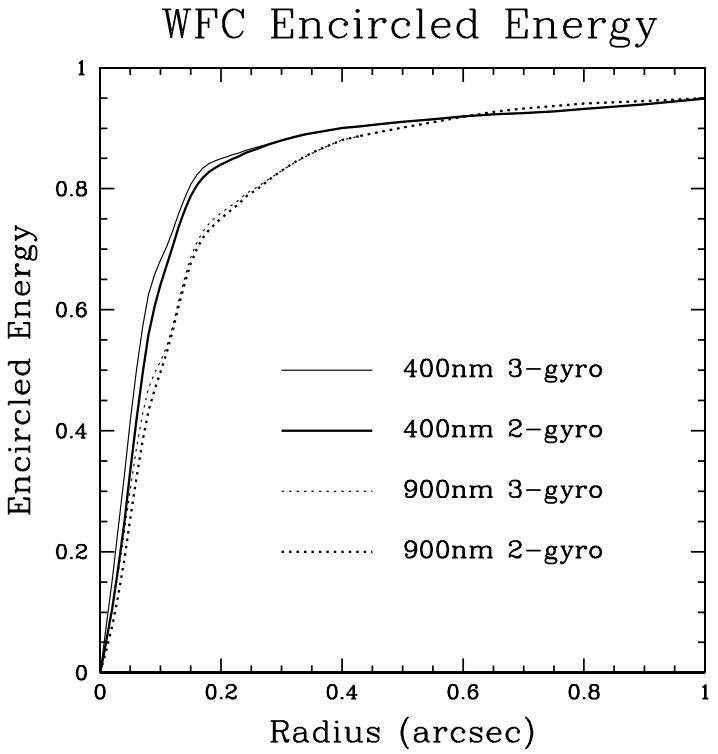

Figure 7.2: Encircled Energy for the ACS / HRC in Three- and Two-Gyro Modes

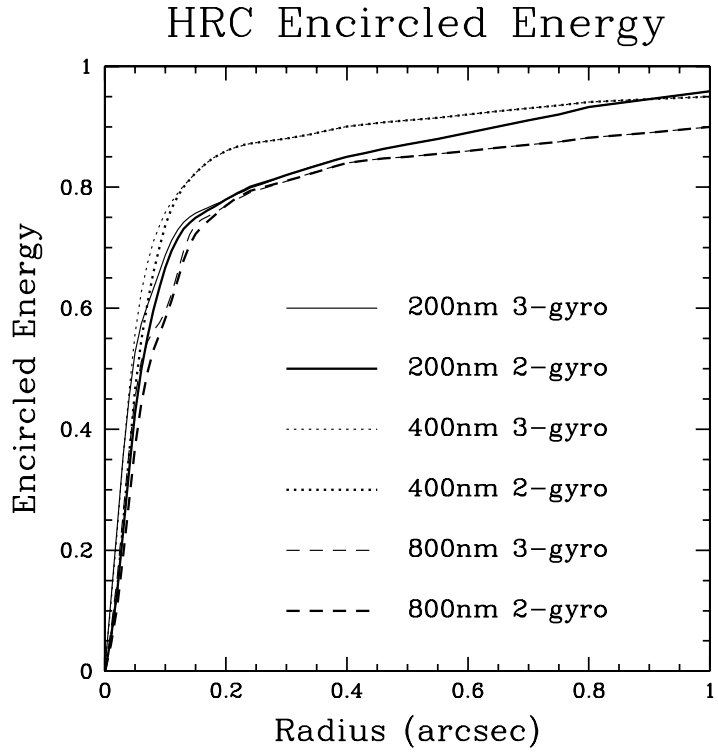

Figure 7.3: Encircled Energy for the ACS / SBC in Three- and Two-Gyro Modes

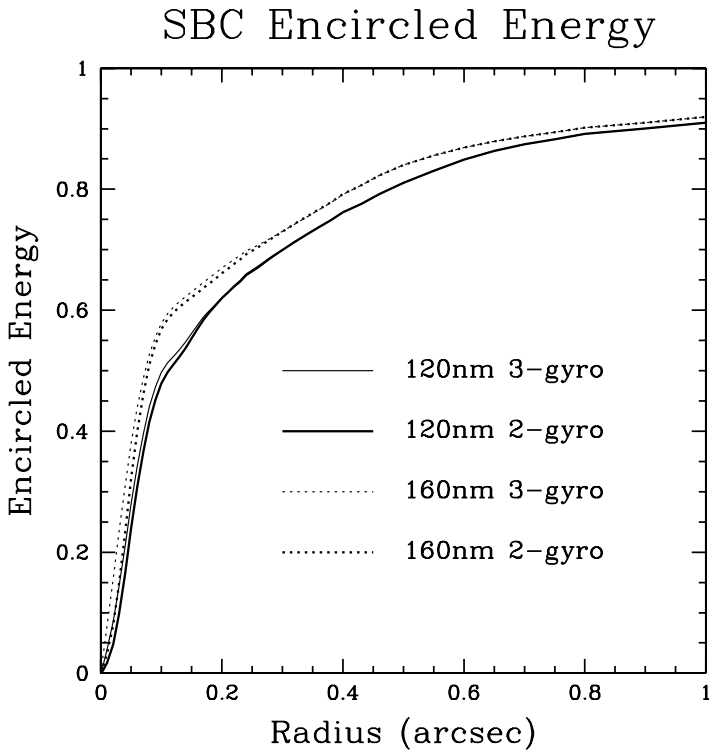

7.1.4 PSF Subtraction

Analysis techniques that depend on subtracting the PSFs of two target images will be impacted by the same effects that impact photometry. The PSF size is likely to depend on several factors, including guide star brightness and guiding disturbances. Additionally, the distribution of light within the PSF may also be variable from image to image – i.e., two images with the same PSF size (e.g., FWHM) could potentially have different light distributions depending upon which spacecraft events are contributing to the jitter in any given image. PSF subtraction will work best if both objects are within the same image, though it is often impossible to arrange this in practice.

The signal-to-noise ratio for PSF fits will be impacted by jitter in two-gyro mode. Section 7.4.2 below discusses this in detail.

7.1.5 Photometric Effects

Blurring of the PSF by pointing jitter will have obvious effects on photometric measurements. Both aperture photometry (where small apertures are used) and PSF fitting techniques will be impacted. Ideally, aperture corrections and model PSFs should be determined from the individual data frames, or at least should take into account the possibility that the PSF will vary from target to target, depending on factors that determine the pointing jitter.

7.1.6 Comparison to Other Effects That Degrade the PSF

It is instructive to compare the impact of two-gyro mode jitter to various other effects that already degrade the PSF in three-gyro mode. Table 7.5 illustrates the percentage reduction in PSF central pixel flux caused by various effects.

Table 7.5: Comparison of Various Effects That Degrade the PSF

Effect	Reduction in PSF Central Pixel Flux		
	WFC (600 nm)	HRC (600 nm)	SBC (160 nm)
Detector Charge Diffusion	43% - 59%	32% - 45%	-
PSF on Pixel Corner vs. Pixel Center	47%	19%	44%
OTA Breathing (+5 microns)	16%	10%	56%
Two-Gyro Jitter (30 x 10 mas RMS)	27%	42%	~50%

Charge diffusion within the CCD detector is a significant source of PSF blurring in both the WFC and HRC (Krist 2003). It is caused by diffusion of electrons within the CCD detector prior to readout, and can be significant as the CCD thickness is comparable to the pixel width (13-17 micron thickness vs. 15 x 15 micron pixels for WFC; 12-16 micron thickness vs. 21 x 21 micron pixels for HRC). The effect varies with wavelength, since different energy photons deposit electrons at different depths within the CCD. The CCDs are nearly opaque to blue photons, so these electrons, which are deposited on the CCD back surface, are farthest from the read-out electrodes (these are back-side illuminated devices). Therefore, charge diffusion is largest in the blue. In comparison, the CCDs are transparent to far-red photons, and hence these electrons can be deposited almost anywhere within the CCDs thickness. As a result, the detector diffusion effect is nearly twice as large in the blue as in the red.

The effect will obviously vary with local detector thickness as well, and the thickness of both the WFC and HRC vary significantly across the detector. In Table 7.5 we give results for both cameras near 600 nm, which represents a middle wavelength. The numbers given indicate the range of the effect measured at different locations on the detector. Charge diffusion effects have not been measured for the SBC, but are expected to be small.

The location of the PSF on the pixel grid will also significantly influence the sharpness of the PSF. The PSF will obviously be sharpest when the PSF is well-centered on a pixel, and will be least sharp when it lands at the intersection of four pixels (i.e., at a pixel corner). For the WFC and SBC, the pixels are large compared to the Airy disk, so this has a large effect – the central pixel intensity varies by a factor of ~2 between the pixel center and pixel corner cases. For the HRC, the Airy disk and pixels sizes are more closely matched, so the variation is smaller.

"Breathing" of the OTA refers to short-term focus changes caused by thermal transients. These occur as HST passes from orbit day to night, when the OTA is pointed at the bright Earth versus cold space. The typical variation amplitude is about 5 microns in OTA secondary mirror position, or about 0.055 waves RMS of defocus. We have estimated the impact of moving the OTA secondary mirror 5 microns farther from the primary mirror, and give the corresponding decrease in PSF central pixel flux in Table 7.5. At first glance it appears curious that there is a larger impact on the WFC than on the HRC, but the WFC normally operates slightly off optimal focus; adding breathing to this normal offset results in a larger effect.

Lastly, we list the decrease in PSF central pixel flux caused by the assumed 30 mas x 10 mas RMS jitter in two-gyro mode. As is apparent, the impact of two-gyro jitter is comparable to other effects that already degrade observations in three-gyro mode. For the WFC, jitter appears to have a smaller impact than both charge diffusion and PSF location. For the HRC charge diffusion and jitter have similar impacts, while for the SBC camera PSF location and breathing have impacts similar to two-gyro jitter. The conclusion from this is:

Two-gyro jitter, while undesirable, is expected to be no worse than other nuisance effects which already degrade the ACS PSF.

7.2 ACS Coronagraphy

Pointing jitter in two-gyro mode will probably have the largest impact on coronagraphy. Jitter will compromise the ability to accurately position targets behind the occulting mask. This is due to both the larger PSF and pointing jitter during target acquisitions. Once the target is in place, the PSF will vary both in size and in intensity distribution from exposure to exposure (depending on impulsive spacecraft events during the exposure) and from target to target (depending on guide star brightness and any other environmental factors). On-orbit tests of coronagraphic observing in two-gyro mode are planned for early 2005 to further study the feasibility of coronagraphic observations in two-gyro mode.

7.3 ACS Grism Observations

Blurring of the PSF may also impact the spectral resolution of ACS grism observations. The orientation of the jitter ellipse on the detector, and the impact on spectral resolution, will depend on which gyro pair remains operational. Even in the worst case scenario where the long axis of the jitter ellipse runs parallel to the dispersion, the impact of a 30 x 10 mas RMS jitter is relatively modest. For the WFC, the spectral resolution corresponds to ~2 detector pixels (100 mas FWHM), so the pointing jitter (71 mas FWHM) only degrades the resolution by about 20%. The impact is larger for the HRC and SBC for which the spectral resolution corresponds to ~65 mas FWHM, but even so the spectral resolution is only degraded by about 50%.

We note that the dispersion direction of the G800L grism relative to the spacecraft axes changes by about 36 degrees when it is used with the WFC instead of the HRC. This fact might be useful in minimizing the impact of jitter on spectral resolution.

There will be additional impacts on signal-to-noise ratio as the dispersed image is spread over more detector pixels by the jitter. This is discussed in the next section.

7.4 ACS Exposure Time / SNR Estimation

Blurring of the PSF in two-gyro mode will potentially impact the signal-to-noise ratio of observations since the counts are spread over slightly more pixels. To the extent that each pixel contributes noise due to sky backgrounds, dark current, and readouts, the signal-to-noise ratio will

be degraded. In this section we describe how this modifies signal-to-noise and exposure time calculations.

A modified version of the ACS Exposure Time Calculator web tool will be capable of handling two-gyro mode calculations. For most proposers, using the tool will be the easiest way to perform these calculations. The ACS Exposure Time Calculator (ETC) is available at:

http://www.stsci.edu/hst/acs/software/etcs/ETC_page.html.

7.4.1 SNR Estimation: Aperture Photometry

Most of the process of calculating signal-to-noise and exposure time remains unchanged in two-gyro mode. Only those aspects involving the encircled energy or flux in central pixel are modified. Tables 6.1 through 6.3 of the ACS Instrument Handbook give the parameters needed for signal-to-noise estimation in three-gyro mode. We show how those parameters, specifically the encircled energy and the flux in the central pixel, are modified between three-gyro mode and two-gyro mode in Table 7.6 (WFC), Table 7.7 (HRC), and Table 7.8 (SBC).

The two-gyro mode numbers have been calculated by scaling the observed three-gyro values with ratios derived using **TinyTIM** models to simulate both three-gyro and two-gyro PSFs.[1] The encircled energy values for the WFC and HRC assume the default 0.2 arcsecond radius aperture, and the SBC values assume the default 0.5 arcsecond radius aperture.

The encircled energy values are virtually unchanged between three-gyro and two-gyro modes. This is easily understood since the default aperture sizes are significantly larger than the assumed jitter (30 x 10 mas RMS or 71 x 24 mas FWHM).

There is virtually no difference between three-gyro and two-gyro signal-to-noise ratios for a given exposure if observers choose the default (or larger) aperture sizes.

Only in cases involving very small apertures with the HRC or SBC are there expected to be significant differences between the three-gyro and

1. This method was used since observed encircled energy tables were available for three-gyro mode, and these are thought to be more accurate than those derived from model PSFs. The PSF core is well-represented in the models, but there are also extended features due to optical reflections and scattering in the CCDs which the models do not reproduce very well. The models were used to derive scale factors between three-gyro and two-gyro cases, and these scalings were then applied to the observed three-gyro values.

two-gyro signal-to-noise results. The aperture sizes need to be significantly smaller than the defaults before the effects of two-gyro jitter become important.

On the other hand, the central pixel fluxes are reduced by factors of ~0.7 for the WFC, ~0.6 for the HRC, and ~0.5 for the SBC. The central pixel fluxes are often used to check for CCD saturation or SBC bright object problems. In these cases it is better to use the three-gyro central pixel fluxes than the two-gyro fluxes because we have assumed a worst-case jitter. It is likely the actual jitter will be less (see Chapter 5). The three-gyro calculation must be used for SBC bright object checking, for these same reasons.

Table 7.6: Comparison of Signal-to-Noise Estimation Parameters Between Three-Gyro and Two-Gyro Modes for the ACS WFC

Filter	Pivot λ (Å)	Three-Gyro Mode		Two-Gyro Mode	
		Encircled Energy[1]	Flux in Central Pixel	Encircled Energy[1]	Flux in Central Pixel
F435W	4322.8	0.79	0.22	0.78	0.15
F475W	4747.0	0.80	0.21	0.80	0.15
F502N	5022.5	0.80	0.21	0.80	0.15
F550M	5582.2	0.80	0.22	0.79	0.16
F555W	5358.0	0.81	0.22	0.81	0.16
F606W	5912.3	0.81	0.22	0.80	0.16
F625W	6307.1	0.81	0.22	0.80	0.16
F658N	6583.9	0.80	0.22	0.79	0.16
F660N	6599.4	0.80	0.22	0.79	0.16
F775W	7699.3	0.76	0.20	0.76	0.15
F814W	8061.1	0.65	0.20	0.65	0.15
F850LP	9054.3	0.76	0.15	0.75	0.11
F892N	8914.7	0.66	0.15	0.65	0.11
G800L	7530.7	0.76	0.17	0.76	0.13
CLEAR	6271.9	----	0.10	----	0.07

1. Default 0.2" radius aperture assumed.

Table 7.7: Comparison of Signal-to-Noise Estimation Parameters Between Three-Gyro and Two-Gyro Modes for the ACS HRC

Filter	Pivot λ (Å)	Three-Gyro Mode		Two-Gyro Mode	
		Encircled Energy[1]	Flux in Central Pixel	Encircled Energy[1]	Flux in Central Pixel
F220W	2256.6	0.75	0.18	0.75	0.08
F250W	2714.1	0.75	0.18	0.75	0.08
F330W	3361.7	0.79	0.16	0.79	0.07
F344N	3432.9	0.79	0.16	0.79	0.07
F435W	4310.3	0.81	0.17	0.81	0.09
F475W	4774.9	0.82	0.17	0.82	0.09
F502N	5021.0	0.82	0.17	0.82	0.10
F550M	5580.0	0.82	0.17	0.82	0.10
F555W	5357.5	0.83	0.14	0.83	0.08
F606W	5882.3	0.83	0.14	0.83	0.08
F625W	6289.7	0.83	0.14	0.83	0.09
F658N	6581.8	0.80	0.12	0.80	0.08
F660N	6581.3	0.80	0.12	0.80	0.08
F775W	7674.0	0.75	0.10	0.75	0.06
F814W	8121.0	0.75	0.10	0.75	0.06
F850LP	9207.7	0.71	0.09	0.70	0.06
F892N	8913.7	0.71	0.09	0.70	0.06
G800L	7586.3	0.75	0.07	0.75	0.04
PR200L	5639.9	0.75	0.16	0.75	0.09
CLEAR	5449.8	----	0.12	----	0.07

1. Default 0.2" radius aperture assumed.

Table 7.8: Comparison of Signal-to-Noise Estimation Parameters Between Three-Gyro and Two-Gyro Modes for the ACS SBC

Filter	Pivot λ (Å)	Three-Gyro Mode		Two-Gyro Mode	
		Encircled Energy[1]	Flux in Central Pixel	Encircled Energy[1]	Flux in Central Pixel
F115LP	1406.1	0.67	0.06	0.67	0.03
F122M	1273.8	0.68	0.07	0.68	0.03
F125LP	1437.5	0.68	0.07	0.68	0.03
F140LP	1527.0	0.70	0.10	0.70	0.04
F150LP	1610.7	0.71	0.12	0.71	0.05
F165LP	1757.9	0.73	0.15	0.73	0.06
PR110L	1429.4	0.86	0.26	0.86	0.12
PR130L	1438.8	0.86	0.28	0.86	0.13

1. Default 0.5" radius aperture assumed.

Example: What is the signal-to-noise ratio for a V=26.5 star of spectral class K0V observed with the WFC in F606W in 600 sec assuming a 0.05" radius aperture is used?

The signal-to-noise ratio will be given by

$$SNR = \frac{S \cdot \varepsilon_f}{\sqrt{S \cdot \varepsilon_f + B \cdot N_{pix}}}$$

where S is the total number of counts from the target, B is the effective number of background counts contributing noise per pixel, ε_f is fraction of counts encircled by the aperture, and N_{pix} is the number of pixels in the aperture. The number of target counts is given by

$$S = 2.5 \times 10^{11} \cdot t \cdot [\int Q(\lambda) T(\lambda) d\lambda / \lambda] \times 10^{-0.4(V + AB_v)}$$

where the exposure time t =600s, from ACS Instrument Handbook Table 6.1 the integral $\int Q(\lambda) T(\lambda) d\lambda / \lambda = 0.1578$, and from ACS Instrument Handbook Table 10.1 $AB_v = -0.12$. Thus,

$$S = 2.5 \times 10^{11} \cdot 600 \cdot 0.1578 \times 10^{-0.4(26.5 + (-0.12))} = 664$$

The effective number of background counts per pixel contains contributions from the sky, dark current, and read noise. These contributions can be estimated from ACS Instrument Handbook Tables 6.1

and 6.5, and are 0.1358 counts/s, 0.0032 counts/s, and 5 counts, respectively. We calculate an effective background count per pixel

$$B = 0.1358(600) + 0.0032(600) + (5)^2 = 108$$

The encircled energy for the 0.05" radius aperture can be determined from careful measurement and interpolation in Figure 7.1 and is found to be $\varepsilon_f = 0.38$ for three-gyro mode. The aperture contains $N_{pix} = 3.1$ pixels. Therefore, the signal-to-noise ratio in three-gyro mode is

$$SNR = \frac{S \cdot \varepsilon_f}{\sqrt{S \cdot \varepsilon_f + B \cdot N_{pix}}} = \frac{664 \cdot 0.38}{\sqrt{664 \cdot 0.38 + 108 \cdot 3.1}} = 10.4$$

In two-gyro mode $\varepsilon_f = 0.32$ and the result becomes

$$SNR = \frac{664 \cdot 0.32}{\sqrt{664 \cdot 0.32 + 108 \cdot 3.1}} = 9.0$$

Even for this very small aperture the difference between the three-gyro and two-gyro signal-to-noise ratios is modest in the WFC. The HRS would give SNR = 8.2 and 7.1, respectively, for this same situation in three-gyro and two-gyro modes.

7.4.2 SNR Estimation: PSF Fitting

PSF fitting is often used to derive photometric parameters, especially in crowded fields where aperture photometry is problematic. While this topic is not explicitly covered in the ACS Instrument Handbook, we briefly review the signal-to-noise calculation for PSF fitting (c.f., Biretta 2001). The signal-to-noise ratio for PSF fitting in the background-limited case is given by

$$SNR = \frac{S}{\sqrt{B}} \cdot \left(\sum (PSF)_{i,j}{}^2\right)^{1/2} = \frac{S}{\sqrt{B}} \cdot (sharpness)^{1/2}$$

where S is the number of detected photons from the source, B is average effective background counts contributing noise to each pixel (dark current, sky, read noise squared, etc.), and $(PSF)_{i,j}$ is the point spread function. We have assumed optimal weighting of the pixels in the image, with weights proportional to the PSF. The sharpness function can be defined as the sum of the PSF pixel values squared, which contains all the PSF-dependent information.[2] Three-gyro and two-gyro sharpness values

2. This sharpness factor can be thought of as the reciprocal number of pixels contributing background noise.

for the WFC, HRC, and SBC are given in Table 7.9, Table 7.10, and Table 7.11, respectively. For each case we give sharpness values for the star at both the pixel center and pixel corner.

From the values in the tables we can see that the signal-to-noise ratio for PSF fitting (background noise limited case) is typically reduced by 8% to 16% for the WFC in two-gyro mode. For the HRC the SNR loss can be as large as 40% in the blue, but is only ~14% at far-red wavelengths. For the SBC the SNR loss is between ~20% and ~40%.

Table 7.9: Sharpness Values for the ACS WFC in Three-Gyro and Two-Gyro Modes

Wavelength (nm)	Three-Gyro Mode		Two-Gyro Mode	
	Pixel Center	Pixel Corner	Pixel Center	Pixel Corner
400	0.084	0.063	0.059	0.054
600	0.080	0.063	0.057	0.053
800	0.069	0.064	0.051	0.050
1000	0.052	0.052	0.041	0.041

Table 7.10: Sharpness Values for the ACS HRC in Three-Gyro and Two-Gyro Modes

Wavelength (nm)	Three-Gyro Mode		Two-Gyro Mode	
	Pixel Center	Pixel Corner	Pixel Center	Pixel Corner
200	0.058	0.036	0.022	0.021
400	0.053	0.050	0.027	0.026
600	0.037	0.037	0.022	0.022
800	0.026	0.026	0.017	0.017
1000	0.015	0.015	0.011	0.011

Table 7.11: Sharpness Values for the ACS SBC in Three-Gyro and Two-Gyro Modes

Wavelength (nm)	Three-Gyro Mode		Two-Gyro Mode	
	Pixel Center	Pixel Corner	Pixel Center	Pixel Corner
115	0.040	0.028	0.020	0.019
120	0.044	0.031	0.021	0.020
130	0.052	0.035	0.024	0.022
140	0.060	0.039	0.027	0.025
150	0.070	0.044	0.030	0.027
160	0.079	0.049	0.033	0.030
170	0.089	0.054	0.035	0.032
180	0.099	0.059	0.038	0.034

Example: What is the signal-to-noise ratio for a V=26.5 star of spectral class K0V observed with the WFC in F606W in 600 seconds assuming PSF fitting with optimal weights?

The number of target counts is given by

$$S = 2.5 \times 10^{11} \cdot t \cdot [\int Q(\lambda) T(\lambda) d\lambda / \lambda] \times 10^{-0.4(V + AB_v)}$$

where the exposure time t =600s, from ACS Instrument Handbook Table 6.1 the integral $\int Q(\lambda) T(\lambda) d\lambda / \lambda = 0.1578$, and from ACS Instrument Handbook Table 10.1 $AB_v = -0.12$. Therefore,

$$S = 2.5 \times 10^{11} \cdot 600 \cdot 0.1578 \times 10^{-0.4(26.5 + (-0.12))} = 664$$

We will assume the exposure is background noise limited. The effective number of background counts per pixel contains contributions from the sky, dark current, and read noise. These contributions can be estimated from ACS Instrument Handbook Tables 6.1 and 6.5, and are 0.1358 counts/s, 0.0032 counts/s, and 5 counts, respectively. We calculate an effective background count per pixel

$$B = 0.1358(600) + 0.0032(600) + (5)^2 = 108$$

Since we do not know if the star will land on a pixel center or pixel corner, we will be conservative and use the pixel corner case. The signal-to-noise ratio in three-gyro mode is

$$SNR = \frac{S}{\sqrt{B}} \cdot (sharpness)^{1/2} = \frac{664}{\sqrt{108}} \cdot (0.063)^{1/2} = 16.0$$

and in two-gyro mode the result becomes.

$$SNR = \frac{664}{\sqrt{108}} \cdot (0.053)^{1/2} = 14.7$$

The difference between three-gyro and two-gyro modes is not dramatic for the WFC. This same calculation performed for the HRC yields SNR=12.7 for three-gyro mode and 9.8 for two-gyro mode. Here the difference is more significant due to the smaller HRC pixel size.

7.4.3 Examples from the ACS Instrument Handbook

We briefly review the examples in Section 6.6 of the ACS Instrument Handbook. Rather than repeating the entire text of each example, we merely summarize the nature of the calculation and how it would be modified in two-gyro mode.

Example 1: WFC Imaging a Faint Point Source

What is the exposure time needed to obtain a signal to noise of 10 for a point source of spectral type F5V, normalized to V=26.5, when using the WFC, F555W filter? Assume a `GAIN` of 1, a photometry box size of 11x11 pixels, and average sky values.

The three-gyro and two-gyro calculations will be identical since the photometry box is much larger (550 x 550 mas) than the jitter ellipse (30 x 10 mas RMS or 71 x 24 mas FWHM).

Consider what would happen if the photometry box were reduced to 5x5 pixels.

Again there is essentially no change. A 5x5 pixel box corresponds to a circular aperture of roughly 0.15 arcsecond radius. Examining Figure 7.1 we see that the 4000 Å encircled energy changes from about 0.81 to about 0.80 between three-gyro and two-gyro modes.

Example 2: SBC Objective Prism Spectrum of a UV Spectrophotometric Standard Star

What is the peak count rate using the PR110L prism in the SBC for the HST standard star HS2027+0651 (V=16.9), and will it exceed the SBC bright object limit?

Since the goal here is to check for bright-object issues, the three-gyro calculation given in the ACS Instrument Handbook is appropriate. It is possible that any given exposure will experience reduced jitter, and

therefore the normal three-gyro calculation should be used in these circumstances as stated in Section 7.5.

Example 3: WFC VIS Polarimetry of the Jet of M87

What signal to noise ratio is reached in three one orbit exposures (~2400s each) for M87, when using the WFC F555W filter for one orbit each in the three VIS polarizers? Assume `GAIN` = 2, the box size is 5x5 pixels, `CR-SPLIT`=2, and average sky values. The M87 jet region has μ_V=17 mag/square arcsec.

Since this is an extended source, the three-gyro calculation remains valid, and there is no change in going to two-gyro mode.

Example 4: SBC imaging of Jupiter's Aurora at Lyman-alpha

What signal to noise ratio is reached in a one orbit exposure (2000 sec) observing Jupiter's aurora in Lyα using the SBC and F122M filter? The surface brightness is 40kR = 1.22×10^{-12} erg cm^{-2} s^{-1} $arcsec^{-2}$.

Again, since this is an extended source, there is no change in going to two-gyro mode, even when the small 2x2 pixel resolution element is used.

Example 5: Coronagraphic Imaging of the Beta-Pictoris Disk

In the final example we shall consider the case where we are trying to determine the S/N achieved on the Beta Pictoris disk, assuming a disk surface brightness of R = 16 mag $arcsec^{-2}$ at a distance of 6 arcsec from the central star with V = 3.9, for an exposure time of 1000 seconds with the F435W filter. Assume that the star and disk have an A5V-type spectrum, and consider the case of the 3.0″ occulting mask.

Once again the disk is an extended target, so there is no change in going from the three-gyro to the two-gyro calculations. A more important question is whether PSF instability or pointing instability will corrupt our ability to accurately subtract the PSF. Further on-orbit testing is needed to evaluate those issues.

7.5 ACS SBC Bright Object Limits

The SBC detector can be damaged by over-exposure, so it is necessary to avoid count rates exceeding the established limits (see ACS Instrument Handbook Section 7.5). Since the SBC limits are specified as instantaneous count rates, there is effectively no change between the three-gyro and two-gyro cases. While pointing jitter in two-gyro mode may blur the PSF on most times scales, the instantaneous count rate on any given detector pixel is the same as in three-gyro mode.

The three-gyro calculation must be used when assessing brightness limitations for SBC observations.

7.6 ACS Observing Techniques

The primary difference between observing in three-gyro and two-gyro mode will be a reduction in the target visibility periods between occultations, with an attendant reduction in observing efficiency as discussed in Chapter 6. However, there may also be secondary impacts on observation planning. For example, there is some possibility that the HST pointing stability will be reduced for subsequent acquisitions of the same target. This might impact the strategy one uses for pointing offsets or dithers – if some dithers require high accuracy, it may be better to group these exposures together within one orbit, rather than allowing them to split across occultations.

We also expect the most severe pointing jitter will occur during brief disturbances lasting less than a minute and occurring perhaps a few times per orbit. For observations requiring the cleanest PSFs, it may be advantageous to break the exposure into shorter segments, so that data with bad jitter can be discarded. This does, however, cause a fairly severe penalty in terms of overhead time, and is probably not practical except for bright targets observed with the HRC or SBC.

There may also be some impact on data reduction methods. If indeed there is degraded pointing stability between exposures, it may become advantageous to use the **MultiDrizzle** software to combine exposures, as opposed to the simpler **CRREJ** method. The **MultiDrizzle** software is better able to cope with positional offsets between exposures, whereas the **CRREJ** method assumes accurate alignment of images.[3]

Guide star brightness may become a more important parameter than in the past. We expect that the pointing stability and the PSF will improve when bright guide stars are used.

3. Of course, it is possible to pre-align the images manually prior to running **CRREJ**. The SCALENOISE parameter in **CRREJ** can also be increased to cope with small positional offsets.

7.7 ACS Calibration Plans

A detailed set of on-orbit test observations in two-gyro mode is planned both in February 2005, and again in the event that gyro failures require permanent operation in two-gyro mode. The goal of these observations is to verify proper operation of HST in two-gyro mode, and to assess the data quality and success of typical observation strategies. The planned tests may be summarized as follows:

- Characterize the PSF in the HRC and WFC for a range of exposures from ~1 sec to ~1000 sec at ultraviolet and visible wavelengths.
- Characterize the PSF for a range of guide star brightnesses.
- Quantify the repeatability of the PSF between exposures for a range of exposure times.
- Measure the accuracy of pointing offsets and dithers both within a visibility period and across occultations.
- Test the functionality and repeatability of coronagraphic target acquisitions. Measure the accuracy of coronagraphic PSF subtractions.

7.8 References

- Biretta, J., et al., 2001, "WFPC2 Instrument Handbook"
- Krist, J. 2003, "ACS WFC & HRC Field-Dependent PSF Variations Due to Optical and Charge Diffusion Effects," Instrument Science Report ACS 2003-6

CHAPTER 8:

WFPC2 Performance in Two-Gyro Mode

In this chapter. . .

This chapter contains information about the performance of the Wide Field Planetary Camera 2 (WFPC2) when HST is guiding in two-gyro mode. Observers should use the information in this chapter to assess and justify the feasibility of their proposed WFPC2 observations. For information about the three-gyro performance of WFPC2 and planning observations in three-gyro mode, see the WFPC2 Instrument Handbook.

8.1 WFPC2 and Two-Gyro Mode

Two-gyro mode is expected to have relatively little impact on WFPC2 observations beyond those pertaining to scheduling. Little change is expected in the PSF because the pixel sizes in both the Planetary Camera (46 mas) and the Wide-Field Camera (100 mas), when combined with the Airy disk diameter, are similar in size to or larger than the jitter ellipse in two-gyro mode (30 x 10 mas RMS or 71 x 24 mas FWHM).

For both cameras there will be some reduction in the fraction of counts in the central pixel of the PSF, but the effect is modest. The largest reduction is for the WFPC2 Planetary Camera, which has a pixel size similar to the ACS WFC; the central pixel flux will be reduced by ~30%. This reduction is smaller than the factor of ~2 reduction in the PSF central pixel flux that occurs when a star falls on a pixel corner rather than a pixel

center; hence the increased size of the PSF is not expected to be a major issue. Rather than giving a detailed analysis of two-gyro PSF effects for the WFPC2 Planetary Camera, the reader is referred to material on the ACS WFC (Chapter 7), which will be affected similarly in two-gyro mode. The reduction in PSF central pixel flux for the WFPC2 Wide-Field camera in two-gyro mode is ~8%.

Other impacts might include changes in the pointing stability between exposures. On-orbit two-gyro tests are planned for WFPC2 that are similar to those outlined for ACS – see Chapter 7 for a discussion of these topics.

CHAPTER 9:

NICMOS Performance in Two-Gyro Mode

In this chapter . . .

This chapter contains information about the performance of the Near Infrared Camera and Multi-Object Spectrograph (NICMOS) when HST is guiding in two-gyro mode. Observers should use the information in this chapter to assess and justify the feasibility of their proposed NICMOS observations. For information about the three-gyro performance of NICMOS and planning observations in three-gyro mode, see the NICMOS Instrument Handbook.

9.1 NICMOS Imaging

NICMOS imaging is unlikely to be affected significantly by the switch to two-gyro mode because its PSF width is larger than the expected jitter. In the worst case scenario, we expect two-gyro mode operations to produce an elliptical jitter ellipse of 30 x 10 milli-arcseconds (mas). This can be compared to the pixel size of 43, 75 and 200 mas in NIC1, NIC2 and NIC3 respectively, and more importantly, to the FWHM of the PSF at 1 micron, which is 100 mas. At 1 micron the increased jitter in two-gyro mode would enlarge the PSF width by about 10%.

In the presence of jitter that causes the instantaneous center of the image to wander on time scales longer than the interval between MULTIACCUM reads, it may be possible to develop image reconstruction algorithms that take advantage of the information in each readout to reduce the blurring due to this secular jitter. Developing such algorithms will be considered after the fundamental two-gyro plan is put in place and after we gain a more detailed understanding of the telescope motion in two-gyro mode.

NICMOS grism spectroscopy is unlikely to be strongly affected by the switch to two-gyro mode. The pixel size in NIC3, the camera that must be used with the grism, is 200 mas, nearly seven times larger than worst case predictions for the long axis of the jitter ellipse.

9.2 NICMOS Coronagraphy

The transition from three-gyro mode to two-gyro mode will affect NICMOS coronagraphy substantially. Coronagraphic acquisition should be only modestly affected since the size of the two-gyro mode jitter ellipse (<30 mas RMS along the semi-major axis) will be about half the size of the NIC2 pixel (~75 mas). However, two-gyro mode operations will impact coronagraphic performance. Coronagraphic performance is dependent upon positioning light within the coronagraphic hole and the ability to obtain a second observation with a roll of the telescope within the same visibility period (see Chapter 5 in the NICMOS Instrument Handbook).

The strength of NICMOS coronagraphy is the ability to suppress the diffractive energy background in the close, circumstellar region of an occulted target. This ability is dependent upon the temporal and positional stability of the PSF (particularly at mid-spatial frequencies). The goal is to center the PSF of the occulted source to a precision of 1/6 pixel at a position offset slightly from the center of the hole, which is ~300 mas (~4 pixels) in radius. The “low scatter point” within the coronagraphic hole is offset from the hole photocenter by Δx=-0.75, Δy=-0.05 pixels. Small pointing excursions cause the edge of the coronagraphic hole to be illuminated by light from the first Airy ring or scatter off the hole edge, resulting in reduced brightness contrasts. An increase in the jitter to 15-30 mas would decrease rejection performance by factors of ~3-8 in a wavelength dependent manner. Artifacts introduced by the coronagraphic optics may reduce the diffractive suppression capabilities to a point where using this mode will no longer be more beneficial than direct imaging. Depending upon which gyro pair remains, the jitter ellipse semi-major axis will likely be offset from an image axis. It might be possible to adjust the flight software offset to center the jitter about the low scatter point and recover some of the coronagraphic performance.

The other strength of NICMOS coronagraphy is the current ability to image coronagraphically occulted targets at two field orientations (rolls) in a single visibility period (i.e., faster than the thermal time constant of the OTA), which mitigates in large part the PSF variability due to HST "breathing", and thus allows discrimination between optical instrumental artifacts and structures in an otherwise temporally variable PSF (see Section 5.1.3 in the NICMOS Instrument Handbook). It will not be possible to schedule observations at two different orientations within the same orbit because orientation changes such as these require new guide star acquisitions in two-gyro mode. It is very unlikely that there will be sufficient time available in a single two-gyro orbit to conduct the necessary acquisitions, observations, and roll maneuver. Scheduling such observations in successive orbits may be possible but will be harder in two-gyro mode than in three-gyro mode.

On-orbit tests will be conducted to verify and confirm the NICMOS coronagraphic performance.

9.3 NICMOS Calibration Plans

During the two-gyro on-orbit tests scheduled for early 2005, extensive testing will be done for the imaging, grism and coronagraphic modes of NICMOS. The imaging mode for all three cameras will be tested - both for bright stars, where individual MULTIACCUM images will be shifted and added to improve the PSF, and for relatively faint stars, for which the effects on the PSF due to the increased jitter in two-gyro mode will be measured. Dithering procedures and patterns will also be exercised. Grism observations will be performed to test the change in the spectral line spread function.

Coronagraphy will also be tested during the two-gyro on-orbit tests. The suppression of diffracted light from an occulted target depends on the stability of the PSF. Multiple observations of several H = 4.5 magnitude stars in two different orbits at two different roll angles each will be conducted to test the PSF stability.

CHAPTER 10:

STIS Performance in Two-Gyro Mode

In this chapter . . .

This chapter contains information about the performance of the Space Telescope Imaging Spectrograph (STIS) when HST is guiding in two-gyro mode. Observers should use the information in this chapter to assess and justify the feasibility of their proposed STIS observations. For information about the three-gyro performance of STIS and planning observations in three-gyro mode, see the STIS Instrument Handbook.

The Space Telescope Imaging Spectrograph suspended operations on 3 August 2004. At the present juncture it appears very unlikely that STIS will be available for scheduling in Cycle 14. Shortly before this Handbook was finalized, the HST Project at Goddard Space Flight Center assembled a Failure Review Board (FRB) to determine the cause of the STIS failure and to recommend further testing and potential recovery options. We expect this process to continue until after this Handbook is issued. Proposers should consult the STIS web page for the most recent information.

10.1 Overview

Of all the instruments on HST, STIS will likely show the largest degradation in overall performance when HST is operating with two gyros. The concerns fall into the following categories:

1. Loss of exposure time available for science observations, due to increased overheads.
2. Loss of spectral resolution, due to increased jitter in the dispersion direction.
3. Loss of aperture throughput, primarily due to increased jitter in the dispersion direction.
4. Loss of spatial resolution, both in imaging and in spatially-resolved-spectroscopy.

Under three-gyro operations, the jitter distribution is nearly spherical, with an RMS of about 5 mas in each direction, but under two-gyro operations, this distribution becomes an ellipsoid. According to current estimates, the dimensions of this ellipse projected onto the sky may be as large as 30x10 mas RMS (but will likely be smaller). The three-dimensional orientation of the ellipsoid long axis will depend upon the surviving gyro combination, but there is no combination for which the orientation will be aligned with either of the STIS detector axes. Furthermore, the projected size of this long axis onto the instrument focal plane depends upon the gyro combination. Assuming the worst gyro combination for spectroscopy (Gyros #1 and #6), approximately 80% of the increased jitter will project along the STIS dispersion direction (x-axis), and approximately 30% of the increased jitter will project along the STIS cross-dispersion direction (y-axis). Under the best gyro combination for spectroscopy (Gyros #2 and #6), approximately 10% of the increased jitter will project along the STIS dispersion direction, and approximately 60% of the increased jitter will project along the STIS cross-dispersion direction. The projection of the jitter ellipsoid along each of the STIS axes is given in Table 10.1 for each of the possible two-gyro combinations. Note that the long axis of the STIS slit is aligned with the y-axis of the STIS detector but rotated by 45 degrees with respect to the **V2**-**V3** vehicle frame of reference (**V1** is normal to the focal plane).

Table 10.1: Projection of Jitter Ellipse along the STIS Axes

Gyro Combination	X-axis	Y-axis
1-2	0.7	0.7
1-4	0.3	0.8
1-6	0.8	0.3
2-4	0.6	0.1
2-6	0.1	0.6
4-6	0.5	0.5

Given that we do not yet know how the telescope will perform under two-gyro operations, which combination of gyros will ultimately remain in two-gyro mode, or the functional shape of the increased jitter (e.g., Gaussian), it is difficult to predict accurately the degradation in STIS performance. However, in the text below, we note the broad issues and estimate the performance degradation possible, given reasonably conservative (i.e., fairly pessimistic) assumptions about the increased jitter under two-gyro operations. We caution observers that we will not know much about the STIS performance degradation until further tests are done, and a full characterization will not occur until HST is actually operating in two-gyro mode.

10.2 Additional Overhead Time

Overhead times for STIS science are detailed for three-gyro operations in Chapter 9 of the STIS Instrument Handbook. The first orbit of a visit usually entails an initial guide star acquisition followed by a STIS target acquisition. In subsequent orbits, the guide star re-acquisition is sufficiently accurate so that the STIS target acquisition is not repeated. However, if narrow slits are used, the pointing drift may require acquisition peak-ups in subsequent orbits (see Chapter 8 of the STIS Instrument Handbook). The STIS target acquisition must be repeated at the start of each new visit, following a new guide star acquisition.

When HST is operating in two-gyro mode, there will no longer be a guide star re-acquisition; every orbit will employ a guide star acquisition as done in the first orbit. Currently, guide star acquisitions take one minute longer than guide star re-acquisitions, so orbits beyond the first will have at least one additional minute of overhead in two-gyro mode. Furthermore, the duration of guide star acquisitions may be several minutes longer in two-gyro mode, incurring that additional overhead every orbit.

Fortunately, the STIS target acquisition will be required only following the initial guide star acquisition in the first orbit of a visit, even for

two-gyro operations. We recently tested flight software that saves the pointing information used in the first orbit and restores this information in subsequent orbits. The tests were successful and, if this software performs as expected when HST enters two-gyro mode, we do not anticipate additional overheads from repeats of the STIS target acquisition within a visit. However, if drift rates are increased, peak-ups may be required more frequently.

10.3 Loss of Spectral Resolution

Because STIS is an imaging spectrograph, movement of the source along the dispersion direction (x-axis) within the widest apertures (or in slitless mode) produces degradation of spectral resolution, but little loss of aperture throughput. Movement of the source along the dispersion direction within the narrowest apertures produces significant light loss, but little spectral degradation. Observations with slits in between these extremes will suffer a combination of these effects. Without knowing the magnitude of the jitter in the spectral direction or the functional form of that jitter, it is impossible to quantify exactly the resolution degradation, but users can refer to Chapter 13.3 of the STIS Instrument Handbook to obtain the plate scales of the different grating modes and thus estimate the blurring that might occur with a given grating. In most situations, we do not expect much degradation of the spectral resolution.

For example, consider observations with the E140M grating and the 0.2x0.2 arcsec slit. This is a wide photometric slit, so we expect the jitter will mainly affect spectral resolution, with little loss of aperture throughput. The plate scale in the dispersion direction of this grating is 36 mas/pixel. A resolution element is two pixels wide (i.e., the E140M mode is critically sampled). If the jitter in two-gyro mode increases to 30 mas along the long axis of the jitter ellipsoid, and if HST is using the worst combination of gyros for spectroscopy, 80% of this jitter (24 mas RMS) will be in the spectral direction. The movement will thus be 2/3 of a pixel RMS, and if the jitter is in a Gaussian distribution, the FWHM will be 1.5 pixels. Adding this in quadrature to the 2-pixel width of a resolution element implies a resolution element 2.5 pixels wide in two-gyro mode. This is just an example of how one might estimate the degradation of spectral resolution, but it relies upon several pessimistic assumptions that are poorly constrained at this time. Given that the overall jitter may be considerably smaller than 30 mas, and that HST might not use the gyro combination that most affects STIS spectroscopy, the actual resolution obtained in two-gyro mode might not be noticeably different from that in three-gyro mode.

The STIS “E” modes (echelle modes) are each critically sampled, so that a resolution element is two pixels wide across the entire wavelength range of the mode. A resolution element in the “G” modes (non-echelle gratings) is generally 2.5-3 pixels wide in the center of the wavelength range, but the exact sampling varies with wavelength. We summarize the plate scales of each grating in Table 10.2 so that users can conveniently calculate the jitter as a fraction of a pixel. Full information for each grating can be obtained from Chapter 13.3 of the STIS Instrument Handbook.

Table 10.2: STIS Plate Scales in the Dispersion Direction

Mode	Plate Scale (mas/pixel)
E140H	47
E140M	36
E230H	47
E230M	35
G140M	29
G140L	25
G230M	29
G230L	25
G230MB	50
G230LB	50
G430M	50
G430L	50
G750M	50
G750L	50

10.4 Loss of Aperture Throughput

Increased jitter in the dispersion direction has two effects: in the widest slits, the dominant effect will be degradation of spectral resolution, while in the narrowest slits, the dominant effect will be reduced aperture throughput. We can crudely estimate the loss of aperture throughput by taking a **TinyTIM** model of the STIS imaging PSF at the detector and assuming this is the shape of the STIS spectral PSF at the aperture. Within the uncertainties, these estimates show that the loss is not strongly dependent upon wavelength or detector. Table 10.3 gives the estimated loss

of light for varying amounts of jitter in the dispersion direction, given a range of aperture width.

Table 10.3: Throughput Loss (%) Relative to Three-Gyro Mode

Jitter (mas)	Slit Width (arcsec)			
	0.05	0.1	0.2	0.5
10	5	1	0	0
20	10	5	1	0
30	25	10	3	0

From these estimates, we expect that the loss of aperture transmission will only be significant for the narrowest slits and for large amounts of jitter in the dispersion direction. Pessimistic estimates of the two-gyro mode performance predict a jitter ellipsoid with a long axis of 30 mas RMS, of which 24 mas could potentially project into the STIS dispersion direction (given the worst combination of gyros remaining). In that situation, slit widths of approximately 0.05 arcsec may suffer about 20% loss of throughput, compared to the throughput in three-gyro mode.

Another factor is the reduction in aperture throughput due to the jitter component in the cross-dispersion direction, but this effect should be relatively small; most of the STIS slits are at least 0.2 arcsec in length. Even with large amounts of jitter projected into the cross-dispersion direction, Table 10.3 implies that there would be little loss of aperture throughput. However, there are several slits that are only 0.1 arcsec in length (in the cross-dispersion direction), such as the 0.1x0.03 and 0.1x0.09 apertures; these apertures could show significant loss of throughput regardless of the jitter orientation if the jitter is large.

10.5 Loss of Spatial Resolution

For imaging modes, the broader PSF in two-gyro mode means that less signal will appear within the central pixels of the PSF, compared to three-gyro performance. Except for observers using the coronographic wedges, most users will not be concerned with the orientation of the jitter ellipse projected on the STIS detector. However, the size of the jitter ellipse projected into the STIS plane varies with the combination of gyros remaining (see Table 10.1). If the long axis of the jitter ellipse is 30 mas RMS, the long axis of the jitter ellipse on the STIS detector will be 18-30 mas, depending upon the gyro combination. For the 1-2 gyro combination, the jitter projected into the STIS detector plane will be maximized, with

equal components along each axis (i.e., the angle between the long axis of the projected jitter ellipse and the detector axes will be 45 degrees). As an example, we show in Table 10.4 the flux within an extraction box of varying size, assuming 30 mas RMS of jitter and the 1-2 gyro combination, using the **TinyTIM** model of a PSF for a hot (O5) star.

Table 10.4: Extracted Signal in Two-Gyro Mode, Relative to Three-Gyro Mode

Detector	Extraction Box (pix)		
	1x1	3x3	5x5
FUV	0.48	0.82	0.95
NUV	0.40	0.82	0.94
CCD	0.67	0.94	0.99

The broader PSF in two-gyro mode will also reduce the amount of light within the standard spectral extraction boxes, which are either 7 or 11 pixels in height, depending upon the mode and detector. Users can increase the height of the extraction box to increase the signal within the extracted region, but this will also increase the background included, so it is worth estimating how much signal is lost due to increased jitter before increasing the extraction box height. Inspecting **TinyTIM** models as a function of wavelength and jitter in the spatial direction, we find that only a few percent of the light will be lost within the standard extraction boxes for any of the spectroscopic modes, even when there is 30 mas of jitter projected into the STIS spatial direction. In practice, the jitter ellipsoid may be as large as 30 mas RMS in one axis, but only 24 mas of that can project into the STIS spatial direction, given the worst combination of gyros remaining, and most gyro combinations project even less jitter into the cross-dispersion direction. So, although aperture transmission might be degraded in the smallest apertures, the light reaching the detector will not be significantly spread beyond the standard extraction box of each mode. For users specifying a narrow extraction box, the loss of signal within the box would be more significant. For example, a 3-pixel high spectral extraction could lose about 10% of the light in the FUV and NUV modes, and 5% of the light in the CCD modes, relative to three-gyro performance.

10.6 Summary

For most of the HST instruments, two-gyro operations will simply result in a slightly broader, elliptical PSF, but for STIS, the performance in both imaging and spectroscopic modes will depend upon the mode and gyro combination. Under a pessimistic assumption of the jitter in two-gyro mode, STIS should see a noticeable degradation in performance, but the degradation should not preclude most types of STIS observing programs. We will be better able to quantify the STIS performance in two-gyro mode once additional testing is done. The complete characterization of the STIS performance, along with a re-calibration of STIS to 1% spectrophotometric accuracy, will not occur until HST actually enters two-gyro operations.

CHAPTER 11:

FGS Performance in Two-Gyro Mode

In this chapter . . .

This chapter contains information about the performance of the Fine Guidance Sensors when HST is guiding in two-gyro mode. Observers should use the information in this chapter to assess and justify the feasibility of their proposed FGS observations. For information about the three-gyro performance of FGS and planning observations in three-gyro mode, see the FGS Instrument Handbook.

11.1 FGS Science

As a science instrument the FGS is used for high angular resolution observing in transfer (TRANS) mode and astrometry in positional (POS) mode. Spacecraft jitter and drift in three-gyro mode introduces a source of positional error that is typically much larger than the scientific measurement being pursued. For example, parallaxes can be measured to an accuracy of 0.2 milli-arcseconds (mas), while the drift of the FGS1r field of view during the course of an orbit can be as large as 20 mas. For both POS and TRANS mode data reduction, the FGS calibration pipeline uses the 40 Hz data from the guiding FGSs to model and remove jitter and drift over the time scales of a single POS mode exposure (typically 20 seconds) or single TRANS mode scan. Drift over times scales up to the duration of an orbit can be monitored, modeled, and eliminated during data analysis provided the proposer employs the appropriate “check star” strategy for POS mode observations. For TRANS mode, the cross

correlation of individual scans compensates for the drift. These observing strategies and data processing techniques are well documented in the FGS Instrument Handbook and the FGS Data Handbook.

During SM3B the HST solar panels were replaced, and afterwards a new pointing control law was activated. The control law contained an error which impressed a 0.5 Hz oscillation of 30 mas peak-to-peak on to the observatory pointing (the error was corrected within about 1 week). During this time FGS1r was used for both POS and TRANS mode observations. Application of routine jitter and drift removal tools in the FGS calibration pipeline effectively eliminated the pointing errors in the science data collected during that time period.

In two-gyro mode, the pointing jitter may have a characteristic periodicity, or time scale, that is similar to typical individual POS mode exposure times or the time it takes to sample the interference fringe of an object in a single TRANS mode scan. For stars brighter than about $m_V < 15$, this should introduce little additional error in the final measurements, as demonstrated by the post SM3B results. However, observations of fainter targets will be degraded somewhat. In POS mode, such stars need to be observed for about 1 minute to obtain the signal to noise ratio (SNR) necessary to centroid the star precisely enough to characterize the drift. Unlike observations of brighter stars, it is not possible to break such exposures into segments with adequate SNR that can be analyzed individually on shorter time scales. Likewise, in TRANS mode it is not possible to cross correlate individual scans of faint stars prior to co-addition due to their low intrinsic SNR. Thus, in two-gyro mode FGS1r is unlikely to be useful for determining the position of a faint ($m_V > 15$) star relative to bright field stars to better than several mas, or for resolving faint binary systems with separations less than about 20 mas.

11.2 Scheduling

The greatest impact to astrometry parallax programs in two-gyro mode, as shown in Figure 11.1 for an object at (α, δ) = (53°, -28°), will be the inability to schedule observations over an appreciable part of the object's parallactic ellipse, an effect which is more pronounced for low declination fields (see the general discussion of scheduling issues in Chapter 6). The inability to observe an object at both epochs of parallactic extremes in two-gyro mode will directly reduce the accuracy of the parallax measurement.

Figure 11.1: A Two-Gyro Mode Parallactic Ellipse

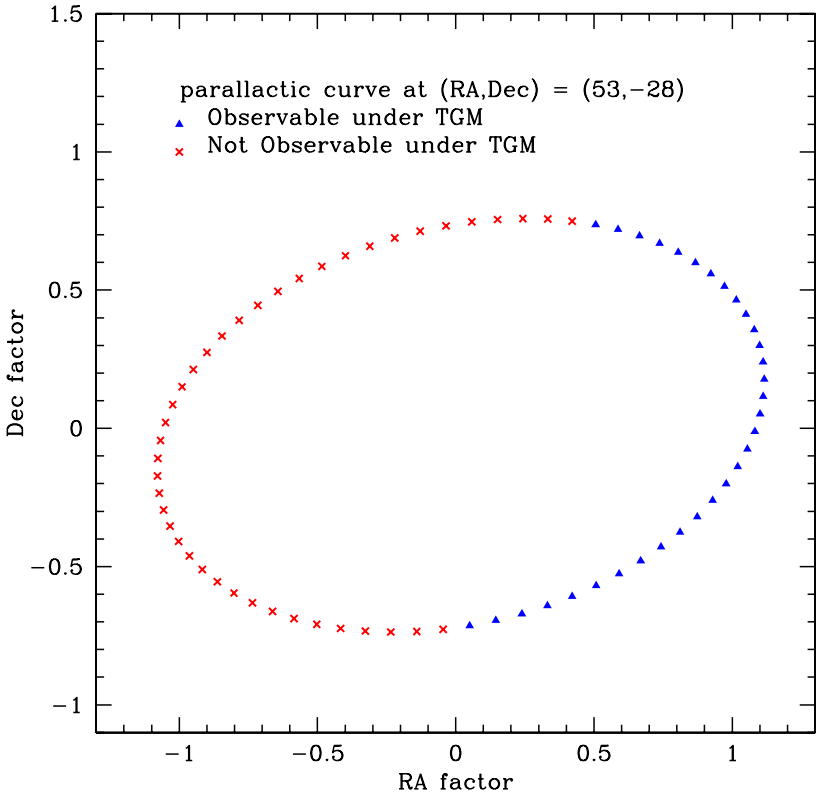

The above plot shows the schedulability (blue triangles) of observations in two-gyro mode for a target at (α, δ) = (53˚, -28˚) with observing windows of at least 30 minutes in length. Additional constraints may apply that would reduce the range of available roll angles, which in turn may preclude an observer from using an optimal set of reference field stars for positional astrometry.

PART IV:

Reference Material

The chapters in this part of the Handbook present more detailed information on FGS guide star brightnesses and the HST jitter simulations.

APPENDIX A:

Guide Star Magnitudes

In this chapter. . .

A.1 Guide Star Magnitude Tables

The following tables contain information about the brightness distributions of guide stars in the three Fine Guidance Sensors from January 2000 through August 2004. Both dominant and secondary guide stars are included. A small number of these guide stars resulted in failed acquisitions.

The magnitude distributions are based upon the predicted (catalog) magnitudes of the guide stars. The typical uncertainty in the magnitudes is 0.3-0.5 mag. Although it is possible to use guide stars fainter than $m_V = 14$, few such instances occur since brighter guide stars can usually be found.

Table A.1:HST FGS1r Guide Star Brightness Distribution (January 2000 - August 2004)

m_V	Percentage of Guide Stars Brighter than Listed Magnitude (8652 total, 5833 unique)				
	Y2000	**Y2001**	**Y2002**	**Y2003**	**Y2004**
9.5	1.2	2.0	2.5	1.6	1.9
10.0	3.5	6.8	8.6	6.0	5.9
10.5	6.3	13.3	15.0	10.8	10.5
11.0	11.0	21.4	22.4	17.8	17.1
11.5	17.7	34.2	36.5	25.5	27.6
12.0	26.4	47.7	52.0	43.1	39.9
12.5	39.2	61.1	64.7	57.1	54.6
13.0	55.9	74.5	76.5	75.0	68.7
13.5	75.8	88.1	88.0	87.7	84.1
14.0	99.8	99.7	99.5	99.3	99.9
14.5	100.0	100.0	100.0	100.0	100.0
Total	1652	1751	1645	2004	1600

Table A.2:HST FGS2 Guide Star Brightness Distribution (January 2000 - August 2004)

m_V	Percentage of Guide Stars Brighter than Listed Magnitude (8876 total, 6003 unique)				
	Y2000	**Y2001**	**Y2002**	**Y2003**	**Y2004**
9.5	1.1	3.4	2.4	2.0	1.8
10.0	4.2	8.6	7.4	5.9	5.2
10.5	8.2	15.5	13.8	11.6	10.5
11.0	12.7	25.0	23.5	19.1	17.3
11.5	18.4	34.5	35.4	28.9	24.8
12.0	27.5	49.4	49.8	42.9	38.0
12.5	41.9	63.3	64.2	54.1	52.4
13.0	58.3	77.2	76.9	71.5	68.7
13.5	76.7	89.9	87.4	84.4	84.5
14.0	99.6	100.0	99.9	99.7	99.9
14.5	100.0	100.0	100.0	100.0	100.0
Total	1135	1983	1886	2060	1812

Table A.3:HST FGS3 Guide Star Brightness Distribution (January 2000 - August 2004)

m_V	Percentage of Guide Stars Brighter than Listed Magnitude (8387 total, 5744 unique)				
	Y2000	**Y2001**	**Y2002**	**Y2003**	**Y2004**
9.5	1.2	2.3	2.8	2.5	5.0
10.0	3.3	7.2	7.5	6.1	6.8
10.5	7.2	12.8	13.7	11.4	12.6
11.0	11.7	20.8	23.6	24.8	16.6
11.5	18.2	31.7	33.5	34.4	25.4
12.0	27.9	46.2	48.3	46.6	35.9
12.5	41.7	59.9	62.1	61.5	47.3
13.0	58.7	75.8	76.5	75.3	64.5
13.5	76.1	89.4	87.2	88.6	80.6
14.0	100.0	99.9	99.6	99.7	99.9
14.5	100.0	100.0	100.0	100.0	100.0
Total	2050	2013	1769	1792	763

APPENDIX B:

Quiescent F2G-FL Jitter Predictions

In this chapter. . .

B.1 HSTSIM Quiescent Jitter Predictions

Estimates of the magnitude of the jitter in F2G-FL mode caused by rate gyro noise and FGS photomultiplier tube (PMT) noise are listed in Table B.1 for various combinations of guide star magnitudes (m_v = 9.58, 13.0, and 14.5) and possible gyro pairs. The jitter values listed are the maximum values expected for a 60 second exposure; they are only slightly larger than those predicted for the gyro noise in three-gyro mode. These "quiescent" simulations include only the jitter contributions from these two sources and do not include more prominent contributions from the on-orbit disturbances that contribute to the overall jitter budget discussed in Chapter 5.

Sample two-gyro jitter ellipses in the **V2**-**V3** plane caused by rate gyro noise and FGS PMT noise are shown in Figure B.1 for the 1-4 and 2-6 gyro pairs. No disturbances are included in these simulations; see Chapter 5 for a similar figure that includes disturbances. In the quiescent simulations, the shape of the jitter in the **V2**-**V3** plane depends strongly on the magnitude of the guide star used by the FGS to measure motions about the G_X axis. For bright guide stars, the FGS measures motions about the G_X axis very precisely, and the jitter is elongated in a direction corresponding to measurement of motions by the gyros (i.e., most of the jitter is contributed by gyro noise rather than FGS PMT noise – see the left panels in the figure). For faint guide stars, the jitter shape becomes more circular, with an increase in the magnitude of the jitter in the direction corresponding to

the measurement of motions about the G_X axis (i.e., PMT noise becomes more prominent – see right panels in the figure).

Table B.1:Quiescent Two-Gyro Jitter Predictions (No Disturbances)

Gyro Pair	Angle of G_X Axis on Plane of Sky[1]	Maximum F2G-FL Boresight Jitter (mas, 60-second RMS) [2]		
		m_V = 9.58	m_V = 13.0	m_V = 14.5
1-2	0.0	1.17	1.63	3.20
1-4	-22.7	1.28	1.78	3.42
1-6	22.7	1.29	1.85	3.42
2-4	55.6	2.70	2.88	3.89
2-6	-55.6	2.62	2.90	3.93
4-6	90.0	1.48	2.03	3.38

1. Angle is measured from the **V3** axis counterclockwise in the **V2-V3** (sky) plane (see Figure 5.2).
2. These values reflect only the jitter caused by rate gyro noise and FGS PMT noise.

Figure B.1: Jitter Ellipses Resulting from Rate Gyro Noise and FGS PMT Noise

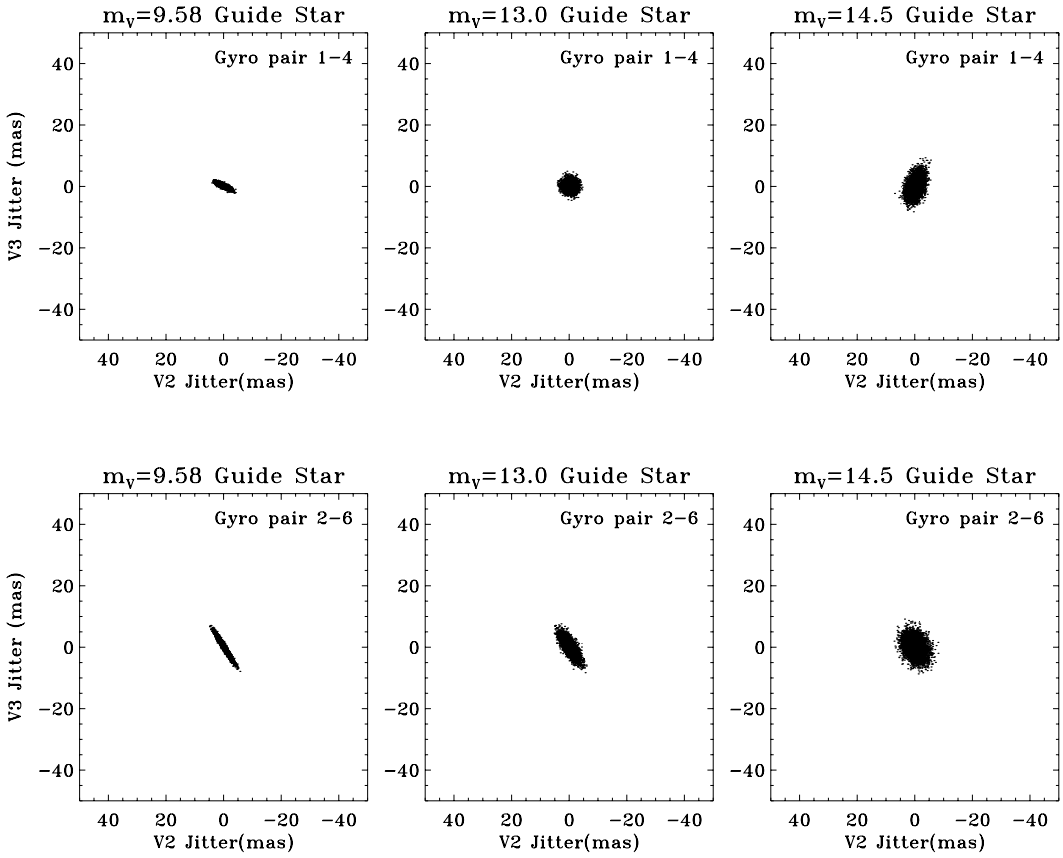

Glossary

The following terms and acronyms are used in this Handbook.

ACS: Advanced Camera for Surveys

ACS / HRC: ACS High-Resolution Channel

ACS / SBC: ACS Solar-Blind Channel

ACS / WFC: ACS Wide-Field Channel

APT: Astronomer's Proposal Tools

CP: Call for Proposals

CCD: Charge-coupled device

CVZ: Continuous viewing zone

ETC: Exposure time calculator.

F2G: Fine guidance sensor / two-gyro (mode)

FAQ: Frequently asked questions

FGS: Fine Guidance Sensor

FGS1r: Fine Guidance Sensor replacement for FGS1 (in SM2)

FRB: Failure Review Board

FHST: Fixed-head star tracker

GO: Guest Observer

HDF: Hubble Deep Field

HGA: High gain antenna

Help Desk: Facility for getting help on HST related topics via email. help@stsci.edu.

HST: Hubble Space Telescope

HUDF: Hubble Ultra-Deep Field

HV: High voltage

NICMOS: Near-Infrared Camera and Multi-Object Spectrograph

mas: milli-arcseconds

M2G: MSS / two-gyro (mode)

MSS: Magnetic Sensing System

OBAD: Onboard attitude determination

OTA: Optical Telescope Assembly

PCS: Pointing control system

Phase I proposal: A proposal for observing time on HST

Phase II program: An approved HST program; includes precise detail of how program is to be executed

PI: Principal Investigator

PMT: Photomultiplier tube

POS: POSitional (mode of FGS operation)

PSF: Point spread function

RA: Right Ascension (also denoted by "α")

RMS: Root-mean-square

RSU: Rate sensing unit

SA3: Solar arrays (third set installed during SM3B)

SAA: South Atlantic anomaly

SAZ: Solar avoidance zone

SM: Servicing Mission (as in SM1, SM2, SM3A, SM3B)

SMOV: Servicing Mission Observatory Verification

SNAP: SNAPshot (type of HST observation)

SNR: Signal-to-noise ratio

SSM: Support Systems Module

STIS: Space Telescope Imaging Spectrograph

STS: Space Transport System (Space Shuttle)

STScI: Space Telescope Science Institute

T2G: FHST / two-gyro (mode)

TAC: Time Allocation Committee

TDRSS: Tracking and Data Relay Satellite System

TGS: Two-Gyro Science

TOO: Target of opportunity

TRANS: TRANSfer (mode of FGS operation)

URL: Uniform resource locator

WFPC2: Wide Field Planetary Camera-2

WWW: World Wide Web

ZGSP: Zero-gyro sunpoint (safemode)

Index

J

M

N

P

S

T

U

W